STUDY ON SHEAR BEHAVIOR OF ULTRA-HIGH PERFORMANCE CONCRETE (UHPC) BEAMS

BY

SIFATULLAH BAHIJ

A Thesis Presented to the
DEANSHIP OF GRADUATE STUDIES

KING FAHD UNIVERSITY OF PETROLEUM & MINERALS

DHAHRAN, SAUDI ARABIA

In Partial Fulfillment of the
Requirements for the Degree of

MASTER OF SCIENCE

In

CIVIL ENGINEERING

DECEMBER 2016

KING FAHD UNIVERSITY OF PETROLEUM & MINERALS

DHAHRAN- 31261, SAUDI ARABIA

DEANSHIP OF GRADUATE STUDIES

This thesis, written by **SIFATULLAH BAHIJ** under the direction of his thesis advisor and approved by his thesis committee, has been presented and accepted by the Dean of Graduate Studies, in partial fulfillment of the requirements for the degree of **MASTER OF SCIENCE IN CIVIL ENGINEERING**.

Dr. Shamshad Ahmad
(Advisor)

Dr. Salah U. Al-Dulaijan
Department Chairman

Dr. Mohammad A. Al-Osta
(Co-Advisor)

Dr. Salam A. Zummo
Dean of Graduate Studies

عمادة الدراسات العليا
DEANSHIP OF GRADUATE STUDIES

Dr. Salah U. Al-Dulaijan
(Member)

24/1/17
Date

Dr. Ali Al-Gadhib
(Member)

Kalimur Rahman

Dr. Mohammad K. Rahman
(Member)

Dedicated

to

my beloved parents, sisters, brothers, and wife

for their love, sacrifices and prayers

ACKNOWLEDGMENTS

First, I would like to praise the Almighty Allah, for His Blessings; that He gave me the opportunity, health, strength, patience and endurance to go through all the stages and complete this research work.

My sincerest gratitude to King Fahd University of Petroleum & Minerals (KFUPM), Dhahran, Saudi Arabia for providing financial support and facilities through its well-equipped labs and well-trained staff. Such support is a rare affluence in a world of limited resources, and I am grateful to have received it. I would also sincerely like to acknowledge support of Yamama Construction Company, along with its team especially Engr. T.C. for supporting experimental phase of this research work.

I would like to express my deepest appreciation to my thesis advisor, Dr. Shamshad Ahmad and co-advisor, Dr. Mohammed A. Al-Osta, who have supported me throughout my research work with their patience, knowledge and personal involvement whilst allowing me the room to work in my own way. I learned a lot through my rich experience with them on the academic and professional grounds. Moreover, I acknowledge my gratitude to Dr. Mohammad K. Rahman, Dr. Salah U. Al-Dulaijan and Dr. Ali Al-Gadhib for their valuable contributions, guidance, moral support and encouragement. Their valuable suggestions greatly helped me to complete this research work.

I would like to express my hearty gratitude to the faculty members of the Civil & Environmental Engineering Department at KFUPM. I want to thanks lab technicians Engr. Omer, Engr. Syed Imran Ali and Engr. Khwaja Najam for their tireless efforts during experimental phase. I also want to thank PhD scholar in Civil & Environmental

Engineering department of KFUPM, Dr. Saheed Adekunle for his big contribution in my research work.

I would also like to extend my deepest gratitude to my friends Mohammad Umar Khan Hekmatullah Habibi, Bakhter Ihsan, Mohammad Hashim Ibrahimkhil, Mohammad Haroon and Mohammad Shoaib. Their care and support helped me a lot throughout my graduate studies.

Finally, this journey would not have been possible without sacrifice, encouragement and eternal love of my parents, sisters, brothers, wife and whole family who gave me an overwhelming support from cradle until today; I am forever indebted for their life-long efforts and struggle. Special words of thanks are due to my father Engr. Rahmatullah Zahid and my Uncle Engr. Ruhullah Zahidy for their encouragement, financial and unfailing support throughout these years of demanding studies.

TABLE OF CONTENTS

LIST OF TABLES

LIST OF FIGURES

LIST OF ABBREVIATIONS

UHPC	:	Ultra-High Performance Concrete
UHPFRC	:	Ultra-High Performance Fiber Reinforced Concrete
MS	:	Micro Silica
SP	:	Super Plasticizer
FEM	:	Finite Element Modeling
CDP	:	Concrete Damage Plasticity
ASTM	:	American Society for Testing and Materials
C-S-H	:	Calcium Silicate Hydrate
EXP	:	Experimental
ANOVA	:	Analysis of Variances
ACI	:	American Concrete Institute

ABSTRACT

Full Name : [Sifatullah Bahij]

Thesis Title : [Study on Shear Behavior of Ultra-High Performance Concrete (UHPC) Beams]

Major Field : [Civil Engineering]

Date of Degree : [December, 2016]

Recently, attempts are being made for utilizing a new concrete material, named ultra-high performance concrete (UHPC), in reinforced as well as in pre-stressed concrete beams. UHPC consisting of ultra-fine materials and steel fibers without coarse aggregate possesses very high compressive and tensile strengths, toughness, ductility, stiffness, and low permeability. The study of structural behavior of UHPC beams considering the simultaneous effects of key parameters is a great significance for optimum design of the beams prepared using UHPC and high-strength steel bars.

This research work was conducted to investigate the effects of key structural parameters on the shear behavior of non-prestressed ultra-high performance concrete (UHPC) beams passively reinforced with high strength steel bars (ASTM A722/A722M). The parameters studied were shear span to effective depth, *a/d* ratio, volume fraction of steel fibers, V_f, longitudinal reinforcement ratio, ρ, and stirrups spacing, *s*. Ten reinforced UHPC beam specimens with cross sectional dimensions of 150 mm × 225 mm were prepared and quasi-statically loaded to failure on a simple span length of 1.75 m, under a four-point loading configuration. The data pertaining to shear behavior (such as modes of failure, ultimate shear strength, mid-span deflection, strains in steel bars and concrete, etc.) were recorded for analysis.

Nonlinear 3-D finite element Modeling, using the concrete damage plasticity (CDP) model and material properties obtained from uniaxial compressive and tensile laboratory tests, was conducted to simulate UHPC beams using a commercial finite element software package ABAQUS 6.13. The developed model was validated with experimental results. Thereafter, a parametric study was conducted to further improve the understanding of shear behavior of UHPC beams and evaluate the contribution of the various levels of the variable parameters that were not included in the experimental program.

In addition, statistical analysis was conducted to quantify the real level of significance of the four key factors. The test response was the shear capacity of the beams, V_u. Using the experimental data generated under the present work, an attempt was made to best-fit an equation to predict shear capacity of UHPC beams in terms of *a/d* ratio, V_f, stirrups spacing, and ρ.

The results of the experimental study indicated that shear capacity and mid-span deflection increased with the increase in volume fraction of steel fibers, V_f, percentage of longitudinal reinforcement, ρ, and with the decrease in stirrups spacing and *a/d* ratio. Overall, finite element model was in good correlation with experimental results; therefore, it can be used in design and analysis. Statistical analysis of experimental data indicated that *a/d*, V_f, and stirrups spacing have significant effect on the shear capacity and failure behavior of beams, while the effects of ρ is quite insignificant. The experimental values of V_u and the values of V_u predicted using proposed shear capacity equation are validated and good agreement between the results was obtained. This indicates that the proposed equation can be used for shear design with a fair degree of accuracy for UHPC with compressive strength of around 150 MPa and in presence of shear stirrups.

ملخص الرسالة

الاسم الكامل: **صفت الله بهيج**

عنوان الرسالة: دراسة سلوك القص للكمرات الخرسانية عالية الأداء

التخصص: الهندسة المدنية

تاريخ الدرجة العلمية: ديسمبر 2016 م

المخلص:

تم الاستفادة حديثا من استخدام مادة خرسانية جديدة تدعى "الخرسانة عالية الأداء" (UHPC) وذلك لصب كمرات مسلحة بحديد عادي المقاومة وحديد مسبق الإجهاد. تتكون الخرسانة عالية الأداء من مواد متناهية الصغر وألياف حديدية كما انها لا تحتوي على الحصى الخشن، وتتميز هذه الخرسانة بمقاومة عالية للضغط والشد والمتانة والصلابة بالاضافة الى المسامية المنخفضه. تعتبر دراسة السلوك الانشائي للكمرة المنشأه من الخرسانة عالية الأداء مع الأخذ بعين الإعتبار التأثيرات المجتمعة للعوامل الإنشائية الرئيسية ذات أهمية كبيرة لتصميم مثل هذه الكمرات والمصنوعة من الخرسانة عالية الأداء (UHPC) والمسلحة بحديد تسليح ذو مقاومة عالية.

تم إجراء هذا العمل البحثي لدراسة تأثير العوامل الإنشائية الرئيسية على سلوك الكمرة الغير مسبقة الإجهاد والمسلحة بحديد ذو مقاومة عالية حسب المواصفات (ASTM A722/A722 M) تحت تأثيرقوى القص. تم دراسة العوامل التالية: نسبة طول الكمرة المعرضة لقوى القص الى العمق الفعال لها (a/d)، كمية المشغول من الألياف الحديديه (V_f)، نسبة حديد التسليح الطولي (ρ)، والمسافة بين الكانات (s). تم تحضير عشر كمرات من الخرسانة المسلحة عالية الأداء (UHPC) بأبعاد ذات مقطع عرضي 150 mm * 225 mm وطول 1.75 m وتم تحميلها بمعدل شبه ثابت (quasi – statically) والمعروف بالتحميل تحت أربع نقاط حتى الإنهيار. تم تسجيل كل البيانات المتعلقة بالسلوك تحت القص مثل (نمط الانهيار، قوة القص القصوى، واقصى ازاحة في منتصف طول التحميل، الإنفعالات في حديد التسليح والخرسانة،...إلخ) وذلك لغرض التحليل.

تم إجراء نمذجة عددية ثلاثية الأبعاد لمحاكاة الكمرات باستعمال نموذج لدونة تشوه الخرسانة (CDP) و باستخدام خواص المواد التي تم الحصول عليها من اختبارات الضغط المحوري وكذلك اختبارات مقاومة الشد المعملية. تم

إجراء المحاكاة لسلوك القص للكمرات المنشأة من الخرسانة عالية الأداء وذلك باستخدام برنامج ABAQUS اصدار 6.13 . بعد ذلك تم التحقق من دقة النموذج عن طريق مقارنة النتائج التي تم الحصول عليها من النموذج والتجارب المعملية. بعد ذلك، تم إجراء دراسة حدودية (parametric study) للمساعدة أكثر في فهم السلوك القصي للكمرة المنشأة من الخرسانة عالية الأداء من ناحية، ولتقييم مساهمة مستويات العوامل الأخرى والغير متضمنة في التجارب المعملية من ناحية أخرى.

بالإضافة إلى ما تقدم، تم أيضا إجراء تحليل إحصائي لتحديد مستوى الأهمية للعوامل الأربعة الرئيسية المشار إليهما أعلاه. تم أخذ قوة القص للكمرة (V_u) كإستجابة للاختبار (test response). وبعد ذلك تم استخدام البيانات التي تم الحصول عليها معمليا في هذا العمل لمحاولة الحصول على معادلة بأفضل مستوى ثقة لحساب قوة القص للكمرة المنشأة من الخرسانة عالية الأداء وذلك باستخدام النسبة (a/d) و (V_f) المشار إليهما أعلاه وكذلك المسافة بين الكانات (s) بالإضافة إلى نسبة حديد التسليح الطولي (ρ).

وضحت نتائج التجارب إلى أن كل من قوة القص والتشوه في منتصف الكمرة تزداد وذلك بزيادة كمية ألياف الحديد (V_f)، ونسبة التسليح الطولي (ρ) وبنقصان كلا من المسافة بين الكانات ونسبة (a/d). الجدير بالذكر، أن النمذجة العددية تتفق مع النتائج المعملية وبالتالي يمكن استعمالها في التحليل والتصميم. على الصعيد الآخر، أشار التحليل الإحصائي إلى أن كل من النسبة (a/d)، (V_f) والمسافة بين الكانات له تأثير كبير على قوة القص ونمط الإنهيار الخاص بالكمرة بينما كان تأثير (ρ) غير مهم. تم المقارنة بين النتائج المعملية لقوة القص V_u مع تلك المتحصل عليها من المعادلة المقترحة. أظهرت المقارنة اتفاق كبير بين القيم مما يشير إلى إمكانية إستعمال المعادلة المقترحة لتصميم الكمرات الخرسانية عالية الأداء ذات مقاومة ضغط تصل الى حوالي 150 MPa وبإستعمال الكانات لقوى القص بدرجة جيدة من الدقة.

درجة الماجستير في العلوم

جامعة الملك فهد للبترول والمعادن

الظهران 31261

المملكة العربية السعودية

CHAPTER 1

INTRODUCTION

1.1. General

New construction materials and methods are being developed to extend the lifespan of concrete structures, gradually changing the design and construction practices [1]. Development of ultra-high performance concrete (UHPC) during the recent years is one of the examples. UHPC consists of ultra-fine materials such as fine quartz sand, quartz powder, silica fume, and cement and does not contain coarse aggregate. The water-cement ratio is kept at very low level (less than 0.20 by mass) that requires a high dosage of an efficient superplasticizer. UHPC also consists of steel fibers for its improved performance [2]. This concrete is characterized by a very high strength (compressive strength above 150 MPa), high ductility, and very less effect of environmental exposures on durability because of its very dense microstructure. Use of UHPC allows designers to select thinner sections and longer spans for structural members [3, 4]. Insertion of steel fibers into UHPC improves mechanical properties of concrete, reduce the brittleness of concrete and alter the cracking pattern [5]. Research works on evaluation of constructability, mechanical properties, and durability of UHPC are widely reported in literature [6, 7]. With increasing demand for high-rise buildings and large-span concrete members, the demand for UHPC is also increasing. In such scenario, the need for research on studying the behavior of UHPC structural members in subjected to different actions such as shear and flexure is growing.

Beams are designed to make them safe against shear and flexural actions. The shear and flexural behaviors of normal concrete beams have been well established for long time. However, there is limited information available regarding shear and flexural behaviors for beams made using UHPC. In case of normal concrete beams, shear reinforcement in the form of stirrups take most of the shear and a small part of shear force is taken by the concrete. However, the usage of closely spaced stirrups is expensive, time consuming, and caused overcrowding at beam-column joints. The UHPC with very high strength and containing steel fibers may take a larger share of the shear force and therefore, its application might greatly reduce the requirement of shear reinforcement.

Experimental study on shear strength of UHPC beams without stirrups showed that with the increasing in compressive strength and amount of steel fibers, shear capacity increased and modes of failure changed from shear-tension to shear-compression [8]. The research work on steel fibers as shear reinforcement in high strength concrete (HSC) beams shows that the shear strength of HCS beams improved by adding steel fibers to the HSC [9]. A study on shear strength of fibrous concrete beams without shear stirrups considering several parameters (amount of steel fibers, compressive strength of concrete, percentage of longitudinal reinforcement and *a/d* ratio) is reported by Mansur et al. [10]. They found that the shear capacity increased with the increase in the, amount of steel fibers, longitudinal reinforcement ratio and with the decrease in the *a/d* ratio [10].

Finite element Modeling (FEM) is considered to be a substitute of experimental investigations for studying the behaviors of the structural members that saves the time and expenses [11]. FEM was conducted for shear behavior of bridge girders made of normal and ultra-high performance fiber reinforced concrete (UHPFRC) beams using the ANSYS

software package with the variable parameters such as cross-section height, amount of steel fibers and stirrups spacing. Good correlations were observed between FEM and experimental data [12]. Numerical simulation was carried out to study the structural performances of an AASHTO Type II girder and a 2nd-generation Pi-girder. The concrete damaged plasticity (CDP) model was primarily employed to model the constitutive behaviors of UHPC and it was observed that CDP models can capture both linear and nonlinear behaviors of the I-girders and pi-girders reasonably well [13, 14]. The effect of pozzolanic admixture and volume fraction of fibers were numerically investigated with the uses of ANSYS software. It demonstrated that the FEM solution is in good agreement with the experimental results. A relatively softer numerical response is noticed at stages closer to the ultimate load [15].

1.2. Needs for Research

Although the information on effects of various factors on shear capacity of beams made using high-strength concrete is available in literature, however, most of the researcher who studied the shear behavior of UHPC beams considered the key factors individually. However, simultaneous effects of the key factors on shear behavior need to be established, to develop an equation for shear capacity in terms of the key factors. Such an equation for shear capacity could be utilized for an optimum design in shear. Furthermore, although many aspects of UHPC beams have been studied, a limited number of numerical studies pertaining to the shear behavior of UHPC beams exist in the literature.

In order to fulfill the need for study of shear behavior considering the effects of key factors simultaneously, the present research work considered the combinations of the key variables, a/d ratio, V_f, ρ, and s were selected and beam specimens were prepared using

UHPC made of local available materials in Saudi Arabia. The beams were tested by applying the load to record the shear capacity, mid-span deflection, and cracking pattern, etc. In addition, the numerical modeling of the shear behavior of UHPC beams was carried out which enabled to develop a 3-D finite element model incorporating nonlinear material properties. The 3-D finite element model was validated with the experimental test data. Parametric study was conducted to study the effects of the key variables; *a/d* ratio, V_f, ρ, and *s* on shear behavior of UHPC beams. Finally, an equation for shear capacity of UHPC beams was obtained in terms of the key factors.

1.3. Objectives

The main objective of this research work was to study shear behavior of UHPC beams considering the effects of key parameters (V_f, *a/d* ratio, ρ, and *s*).

The specific objectives of this study were the following:

1. To design, prepare and test the UHPC beam specimens considering the experimental variables and ensuring the failure of beams in pure shear.
2. To evaluate the simultaneous effect of, V_f, *a/d* ratio, ρ, and *s* on shear behavior of beams (initial cracking, modes of failure, ultimate shear capacity and mid-span deflection, strains in concrete, and strain in longitudinal reinforcement and stirrups).
3. To conduct FEM of shear behavior of beams and validating the numerical model with experimental data.
4. To conduct parametric study using the numerical model to study the effects of key variables on shear behavior of beams considering the levels of the key variables outside the experimental range.

5. To conduct statistical analysis and develop shear capacity equation and verify with previous experimental results.

CHAPTER 2

LITERATURE REVIEW

In order to extract relevant information from the previous works conducted to study the shear behavior of UHPC beams, literature review was carried out and presented as follows.

2.1. Ultra-High Performance Concrete (UHPC)

Ultra-high performance concrete (UHPC) is the outcome of recently research in concrete development. UHPC is one of the cement composite materials and has been characterized by fine steel fibers (2.0% to 10.0% by volume), no coarse aggregate, high amount of cementitious paste, high amount of fine aggregates and high-range water reducing admixture (superplasticizer) with very low water-cement ratio [16]. UHPC possesses high compressive strength (above 150 MPa), split tensile strength above (8 MPa), high elastic limit, high strain hardening, high toughness, low permeability, greater frost and deicing salt resistance, low rate of carbonation, greater chloride resistance, self-compacting property during pouring and high durability property due to its dense micro structure. UHPC has been successfully used in many civil engineering projects (such as several bridges in Canada, Korea, Japan, roof structures in France and Netherland, cooling tower of power station in France, etc.) [2, 17].

Compared with normal concrete, UHPC permits to decrease dimensions for cross-sections of structure members, to decrease shear reinforcement for confinement of longitudinal reinforcement in beams. Constructions made of UHPC have lower maintenance and repair costs in the future than normal concrete [17]. UHPC became more useful around 2000 in

USA. The Federal Highway Administration (FHWA) started research on the use of UHPC for highway infrastructure in 2001; this research has led to the use of UHPC in many applications such as bridge, precast and pre-stressed girders, and precast waffle panels for bridge decks. In Canada, bridge was constructed with the UHPC for the first time in 1997, and finally 26 bridges were constructed using UHPC. In Germany, 12-million-euro research works just completed which were started in 2005 and this program was sponsored by the German Research Foundation. In 2002, the first recommendation (mechanical properties, structural design and durability behavior) in UHPC structures was published in Franc. After 2002, several bridges were constructed in France using UHPC. Other countries such as Australia, Austria, Italy, Japan, Malaysia, Netherlands, New Zealand, South Korea and Switzerland have used UHPC in bridges structures, almost more than 90 projects related to UHPC have been completed in these countries. In 2009, two bridges with cast in place UHPC for deck-level connection between precast concrete elements were constructed in New York. In one bridge UHPC was used for transverse connections of precast deck panels and in other bridge for longitudinal connections of top flanges of deck-bulb-tee girders as shown in Figure 2.1 [18].

Figure 2.1: Wapello County, Iowa structure, first UHPC Bridge constructed in USA [18]

2.2. UHPC Mixture

Formulations for UHPC mix design show; combination of Portland cement, fine sand, micro silica, and high range water reducer admixture, water and steel fibers. Different types and combinations of the mentioned materials can be used to provide appropriate mix design for UHPC. According to ASTM C 230/C 230M standard, with the increasing silica fume in the range of (0-25) %, compressive strength of concrete increases up to 160 MPa. Replacement of (20-30) % of cement with glass powder resulted compressive strength up to 240 MPa. Research shows that with the increasing, V_f, within specific range increases tensile strength, and twisted or hooked steel fibers increases tensile strength and tensile strain more than straight fibers [18].

Important information regarding the ingredients of UHPC are presented in the following sub-sections.

2.2.1. Cement

To produce UHPC, cement is the key factor and binder to hold the aggregates together and react with mineral materials to get hardening. The characteristics of UHPC depend to the quantities and qualities of its ingredients. Fineness of the cement is the most important property for selecting the quality of cement in UHPC. Cement has the largest unit cost, therefore, its selection is important to obtain the cheapest UHPC mixture [19].

Decreasing the amount of sand is the best method to increase the amount of cement and it allows for unchanged content of the ingredients. According to DIN EN 196 standards, low alkali Portland cement (Type-I) is better than high sulfate resistance (Type-V) and low heat of hydration (Type-IV). Water requirement should be according to cement selection, because of the flow behavior and amount of superplasticizer [20].

2.2.2. Micro Silica (MS)

Micro silica is one of the best material in high-strength concrete and UHPC to combine with superplasticizer. According to its outstanding properties, such as; filling ability, increase of rheological characteristics by lubrication and production of secondary hydrates (C-S-H) by pozzolanic reaction, therefore, it is possible to produce concrete with the best properties. Micro silica is ultra-fine powder, 50 to 100 times finer than cement; and considered as the best filler for concrete. Its particles size is 0.1 μm and spherical shapes, 85 to 96 percent of its microstructure is made by silicon dioxide (SiO_2). It gives dark color to the concrete, because of unburnt coal contamination. Its microstructure is free of pores and impermeable [19-21].

2.2.3. Superplasticizer

Superplasticizer according to ASTM C494 specification have different types such as, A, B, D, and G. Addition of superplasticizer shows strong plasticizing effect and improves the characteristics of fresh and hardened concrete such as; increase workability, reduction in w/c ratio, delay the initial and final setting time, better slump retention and etc. To increase the workability of the concrete matrix, normal dosage of the liquid superplasticizers (containing about 40% of active material) is between (1-3) liters/m^3 of concrete. To reduce the w/c ratio of the mix, normal dosage of the liquid superplasticizers (containing about 40% of active material) is between (5-20) liters/m^3 of concrete [20, 22]. Currently different types of superplasticizer are available commercially; selection of them should be according to the binders and w/c ratio used in the concrete mix.

Superplasticizer, which can de-agglomerate both the cement and other fine materials, can be used for UHPC with high amount of micro silica. Glenium 51, a polycarboxylic ether

(PCE) based superplasticizer with 65% water content by weight that does not contain chlorides and complies with ASTM C494 Types A and F, is reported to be suitable for use in UHPC.

2.2.4. Water

Water is one of the important constituent of concrete. It chemically reacts with binders to produce hydration products. Almost any natural water, which is drinkable and has no pronounced taste or odor, can be used in concrete mix design for preparation of concrete. However, questionable water, which cannot be used for drinking, is also suitable for preparation of concrete. Questionable water also can be used which satisfy (ASTM C 94) specifications and has 7 days' strength equal to 90% strength of concrete made with drinkable water [22].

2.2.5. Fine aggregates

Fine aggregate is the inexpensive, strong filler material in UHPC. Aggregate can be selected according to its gradation, maximum size and strength. Large size aggregate is not desirable for UHPC because of decreasing the workability. Before mixing, it is important to ensure that aggregate is clean, because silt or clay layer on aggregate surface will decrease bond strength between aggregate and cement, and it increases water demand [18]. The shape and surface texture of fine aggregate have a significant effect on the water demand, because of the large surface area of fine aggregate. For a given workability and cement content, the strength of concrete increases with increasing aggregate size, because of low w/c ratio [22].

2.2.6. Steel Fibers

Concrete is brittle; when load exceeds the maximum load capacity it will cause sudden failure. Steel fibers improve the post fracture property of concrete and the post fracture property is governed by the type and quantity of steel fibers. Addition of long fibers instead of short fibers decreases the amount of required steel fibers. Wille and Naaman (2011) suggested a limit of $\frac{l_f}{d_f} \times V_f = 2$ for the steel fibers to get suitable workability, where, l_f is the length of fibers, d_f is the diameter of fibers and V_f is the volume fraction of steel fiber. Steel fibers with maximum 0.2 mm diameter and length of 9 to 17 mm having 2000 MPa tensile strength are suitably used in UHPC. In corrosive environments, stainless steel fibers can be used [18, 20].

2.3. Preparation of UHPC Mixture

2.3.1. Mixing

Most of the operations for conventional concrete are common for UHPC. Any mixer for conventional concrete such as twin shaft batch mixer, pan mixer and planetary mixer can be used for UHPC. However, UHPC needs more energy for mixing because of high amount of ultrafine materials and the need for wetting the particles completely with water and superplasticizer. Therefore, mixing time for UHPC is more than normal concrete. Mixing time for UHPC ranges from 7 to 18 minutes, which is longer than conventional concrete. This time can be reduced by optimization of the particle size distribution, replacement of cement with micro silica and increase in the mixer speed [20].

2.3.2. Placing

Method of placing affects the orientation and dispersion of steel fibers. The orientation of the fibers does not affect first cracking but it affects the ultimate tensile strength in bending. Internal vibration cannot be used for UHPC because of steel fibers, but less external vibration is recommended to release the entrapped air in concrete. Fiber reinforcement tends to align with the direction of flow during casting. Research program conducted on the tensile and compressive behaviors of UHPC when loaded parallel to and perpendicular to the direction of flow during casting. The results from cube compression test show no significant effect of fiber alignment on compressive strength and modulus of elasticity of UHPC. However, the three-point flexure test results show that the flexural strength of the UHPC prisms decreased more than three times when the fibers were preferentially aligned perpendicular to the principal flexural tensile forces [14, 23].

2.3.3. Curing

Since very low amount of water is used in UHPC, its surface dries and become dense immediately after its casting. Therefore, curing of UHPC should start shortly after casting the members. To prevent UHPC from early dry, its surface can be covered with an impermeable layer, such as metal, plastic or plastic-coated wood materials immediately after concreting. The most efficient way of curing is to spray water over the whole surface of the concrete or putting specimens in water. Precast components made of UHPC are heat treated at a temperature between 80 to 90 °C. At a high temperature, micro silica reacts with the calcium hydroxide and makes (C-S-H) gel, which causes high compressive strength, high flexural strength, dense microstructure and less shrinkage. In heat curing,

specimens cover with plastic sheets for 24 hours before heating for 48 hours and it is important to allow the specimen to cool slowly after the heat treatment [2].

2.4. Mechanical Properties of UHPC

In general, test procedures for evaluation of mechanical properties of conventional concrete are also applicable to UHPC. Some tests need modified procedure to obtain true properties of the UHPC. For example, compression test of UHPC needs smaller specimens, different shapes of specimens and high capacity machine than conventional concrete [14].

2.4.1. Compressive Strength

Compressive strength is the most important behavior of concrete for the design of each concrete structure. Cylinder and cube compression test methods are also applicable for UHPC as used for conventional concrete. Research was conducted by Graybeal [2] on the compressive strength of about 1000 different shapes and size specimens, cured under different curing regime. The summary of this research work is as follow:

- Compressive strength was higher for the specimens which were cured under 90 ºC steam and 95% relatively humidity for 48 hours than specimens which were cured under laboratory condition (23 ºC and ambient humidity).
- Compressive strength slightly increases as the density increased.
- Cubes specimens had 5.0% more compressive strength than cylinders specimens.
- Loading rates between 0.24 to 1.7 MPa/s had no noticeable effect on compressive strength, modulus of elasticity and Poisson's ratio.
- Irregularities in the loaded surface caused more decrease in UHPC compressive strength than conventional concrete.

2.4.2. Tensile Strength

Tensile strength of UHPC is higher than conventional concrete, and it will extend after first cracking. Tensile strength testing procedure used for conventional concrete can be used for UHPC as well. The ASTM C78 standard test method can be used for flexural tensile strength and ASTM C496 standard test method can be used for splitting tensile strength of UHPC [2]. Four-point or three-point bending setup on un-notched specimens can be used to obtain the flexural tensile strength of UHPC. Both tensile and flexural tensile capacity for UHPC depend on the distribution, orientation of steel fibers in concrete and preparation of the specimens [20].

Graybeal [2] has found the uniaxial tensile stress-strain behavior curve for UHPC, as shown in Figure 2.2. This behavior is divided into four parts. Part 1 is elastic behavior. Part 2 starts when multiple tightly spaced cracks form. Part 3 starts at the strain level when additional cracks form with existing cracks. Part 4 starts at the strain level when individual cracks begin to pull out the fibers from concrete mix.

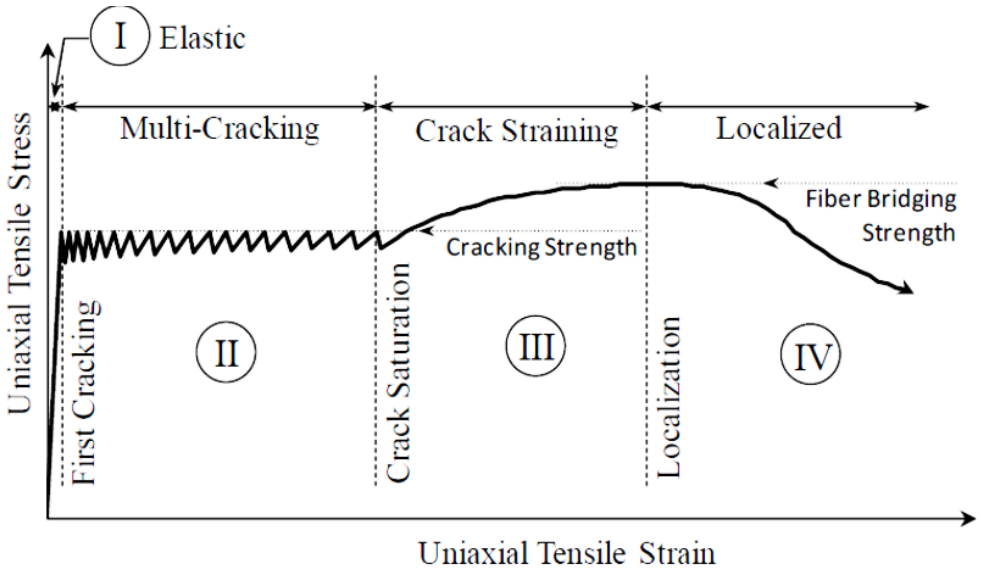

Figure 2.2: Uniaxial tensile strain-stress behavior [2]

2.4.3. Modulus of Elasticity

Modulus of elasticity is the concrete behavior, which depends on material characteristics and often explained using stress-stress relationship. According to ASTM C469 standard, the value of modulus of elasticity of concrete refers to the slope of elastic part of the compressive stress-strain curve up to 40% of ultimate compressive strength.

Graybeal [2] measured modulus of elasticity in compression according to ASTM C469 standard at different curing regime. In addition, six cylinders' specimens for each curing regime were tested. The estimated values after 28 days curing were, for steam-cured cylinders 50 GPa and for cylinders cured under standard laboratory condition 42.7 GPa. The modulus of elasticity estimated in direct tension (steam cured 51.9 GPa and standard laboratory condition 47.6 GPa) was slightly higher than estimated in compression.

2.4.4. Poisson's Ratio

Poisson's ratio (v) is the relationship between transverse strain ($\varepsilon_{transverse}$) and the longitudinal strain ($\varepsilon_{longitudinal}$).

$$v = \frac{\varepsilon_{transverse}}{\varepsilon_{longitudinal}}$$

Poisson's ratios of UHPC reported by different researchers are presented in Table 2.1 [2]:

Table 2.1: Values of Poison's ratio of UHPC [2]

Reference (First Author)	Poisson's Ratio
Simon	0.20
Joh	0.16
Ahlborn	0.21
Bonneau	0.19
Graybeal	0.18
Ozyildirim	0.18

2.5. Experimental Study on Shear Behavior of Concrete Beams

Shear behavior of UHPC structural elements is an important aspect. Design of beams in shear is mainly based of experimentally derived equations for shear capacity of beams made using normal concrete. Such equations may not be suitable for beams made of UHPC [2]. Addition of steel fibers in UHPC increases the strength, stiffness, ductility, ultimate failure load and shear capacity of the beams. Type of steel fibers and its dimensions are the important factors for the assessment of shear performance of UHPC beams. Steel fibers having 6 mm length and 0.15 mm diameter are the most effective fibers especially for small beams. However, short steel fibers are found unable to contribute to the shear resistance of large beam specimens, resulting in a complete pull-out of all the fibers at an early stage of loading [9].

Gustafsson et al [9] conducted research work on steel fibers as shear reinforcement in high strength concrete beams. Twenty beams were prepared and tested considering variable parameters that included: with and without shear stirrups, combined steel fibers with shear

reinforcement, and steel fibers with different shapes and dimensions (Table 2.2). Furthermore, the beams contained a substantial amount of longitudinal reinforcement to avoid flexural failure. The concrete mix proportion was prepared to get 120 MPa cube compressive strength at 28 days. Longitudinal reinforcement with yield strength of 590 MPa, and 8 or 10 mm diameter stirrups having 400 MPa yield strength were used.

Table 2.2: Material and geometrical data of steel fibers [9]

Types of steel fibers	Geometrical configuration	Aspect ratio (L_f/D_f)	f_y (MPa)
Dramix® 6/0.15	—	40	2600
Dramix® 30/0.6		50	1100
Dramix® 60/0.7	D_f L_f	86	2600

Small beams were subjected to midpoint loading and large beams to two-point loading because of keeping constant a/d = 3.0 ratio. Load was applied with deflection ratio of 0.02 mm per second. Numbers of strain gauges were attached to each beam specimen to measure the strains at different points of beams. During the loading process, cracks were observed and marked on the beam sides. The results of this study showed that the shear strength of the beam specimens improved with addition of steel fibers. The beams with short steel fibers failed with lower load than beams with other type of steel fibers. The elastic modulus and tensile strength were also improved, because of the fact that the steel fibers acted as an active material at early stage and prevented the micro-cracks. Ultimate shear strength was increased by 42% with addition of 1.0% steel fibers as compared to an increase of just 12% by using shear stirrups. Beams with short steel fibers collapsed in lower load; therefore, long steel fibers were needed for the large size beams. Failure of shorter beam specimens was more ductile than longer beam specimens. The large numbers of diagonal cracks were

observed on the side face of small beam specimens; it indicates failure ductility of beam specimens. However, single large diagonal crack was observed on the largest beam specimens indicating that the residual strength of the steel fibers was not enough to resist large impulse load. Beams having long or hooked steel fibers had more ductility than beams having short or straight steel fibers.

Mansur et al. [10] studied shear strength of fibrous concrete beams without stirrups. Twenty-four beams were prepared considering variable parameters that included amount of steel fibers, compressive strength of concrete, percentage of longitudinal reinforcement, and *a/d* ratio. All the tested beams had a rectangular cross-section (150 × 225) mm and a length of 2.0 m. The V_f, was varied from 0 to 1.0 % and *a/d* ratio was varied from 2.0 to 4.4. All the beams were subjected to four-point loading setup. Highly yield deformed steel reinforcement bars were used as longitudinal reinforcement, as shown in Figure 2.3:

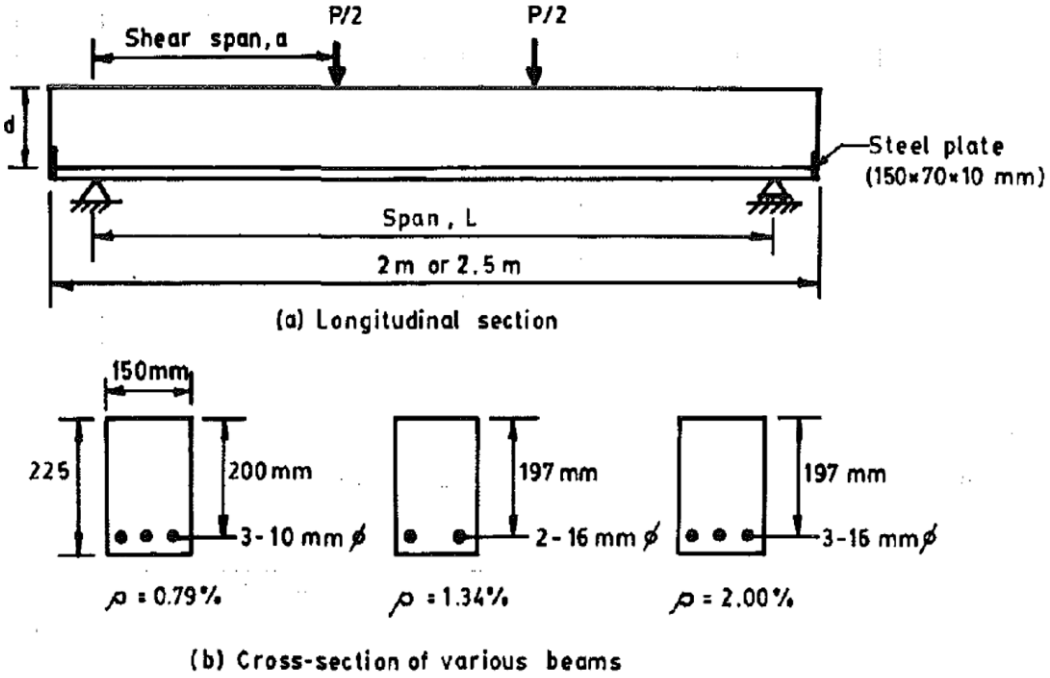

Figure 2.3: Details of the tested beam specimens [10]

They captured four modes of failure (proper shear, shear compression, diagonal tension and flexure) during four-point loading test. Shear capacity increased with the increasing, V_f, simultaneously modes of failure changed from shear to flexure. Shear capacity increased with the decreasing *a/d* ratio, increasing percentage of longitudinal reinforcement (ρ), increasing fiber content, and increasing compressive strength of concrete (f'_C) as shown in Figure 2.4.

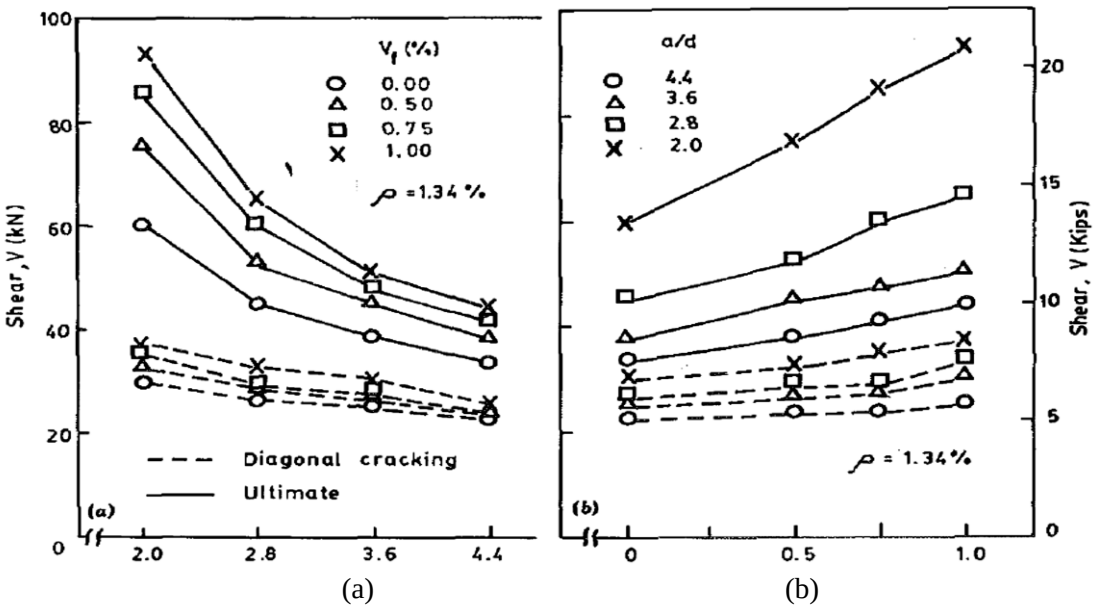

(a) (b)

Figure 2.4: Effect of key factors on shear behavior of the beams: a) V_f and; b) *a/d* ratio[10]

Research was carried out at the University of Kassal [20] to study shear capacity of UHPC beams. The study was conducted on rectangular beams with and without stirrups and having different value of longitudinal reinforcement. Four-point loading setup was used for all the beam specimens. The results showed that the UHPC beams with steel fibers had much higher shear capacity than beams without steel fibers, and for all the tested beams ductile behavior was observed. Shear capacity increased while steel fibers added and increased more for beams having steel fibers plus stirrups. For the UHPC beams without

steel fibers, cracks occurred within large spacing but with bigger widths. However, cracks occurred within closer spacing and with smaller widths in beams with steel fibers [20].

Son et al. [24] conducted experimental study on shear strength for UHPC beams without shear reinforcement. Three beams having (200 × 350 × 1600) mm dimensions and a constant *a/d* ratio of 2.0 were considered. The first beam had no fibers (V_f=0) and made of UHPC having a compressive strength of 200 MPa, second V_f = 2.0% and a compressive strength of 100 MPa, and third V_f =2.0% and a compressive strength of 200 MPa. Steel fibers had a circular cross-section with a diameter of 0.15 mm, length of 6 mm, and ultimate tensile strength of 2600 MPa. The results show that with the increasing compressive strength and, V_f, cracking pattern changed from shear-tension to shear-compression. Initial cracking load increased about three times with the addition of steel fibers. Loads at initial cracking, diagonal cracking and ultimate strength also increased with the increasing both V_f, and compressive strength of concrete. Mid-span deflection increased with the presence of steel fibers and increasing compressive strength as shown in Figure 2.5.

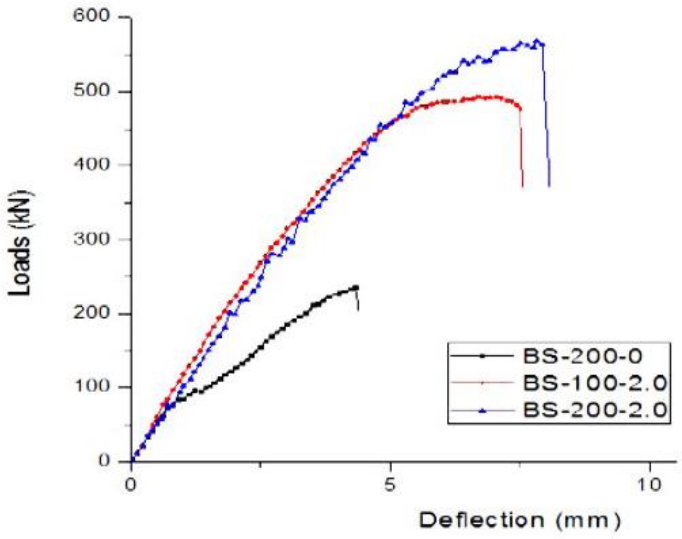

Figure 2.5: Load-mid-span deflection curves [24]

Baby et al. [25] conducted experimental work on shear resistance of UHPC beams with and without stirrups, passive and active longitudinal reinforcement. In this study, nine beams were tested and all the tested beams had 2.0 m span, 380 mm depth and 270 mm width. Steel fibers having length of 20 mm length and 0.3 mm diameter were used in two volume fractions of 2.0 and 2.5%. All the beam specimens were subjected to four-point loading setup and *a/d* ratio was kept constant at 2.5 in all the beam specimens. The results demonstrated that the participation of stirrups to control cracking is significant at the stage of serviceability. Shear capacity increased with the increasing V_f, and stirrups for both pre-stressed and reinforced beams.

Research was conducted at RWTH Aachen University [26] to investigate the shear behavior of UHPC beam specimens considering different scenarios such as: no stirrups, with stirrups, steel fibers, and combination of steel fibers and stirrups. All the steel fibers were plain, without hooks and had tensile strength more than 2000 MPa. The results of this study show that the beams with the combination of steel fibers and stirrups had the maximum shear strength. While beams without steel fibers and stirrups had the minimum shear strength as shown in Figure 2.6. Addition of 0.9% steel fibers increased 80% of shear capacity and 2.5% increased 177% shear capacity of UHPC beams. Ultimate shear force for beam having a/d=4.4 was 15% lower than that for the beam with a/d=3.8, which indicates that with the increasing *a/d* ratio, ultimate shear capacity decreased [26].

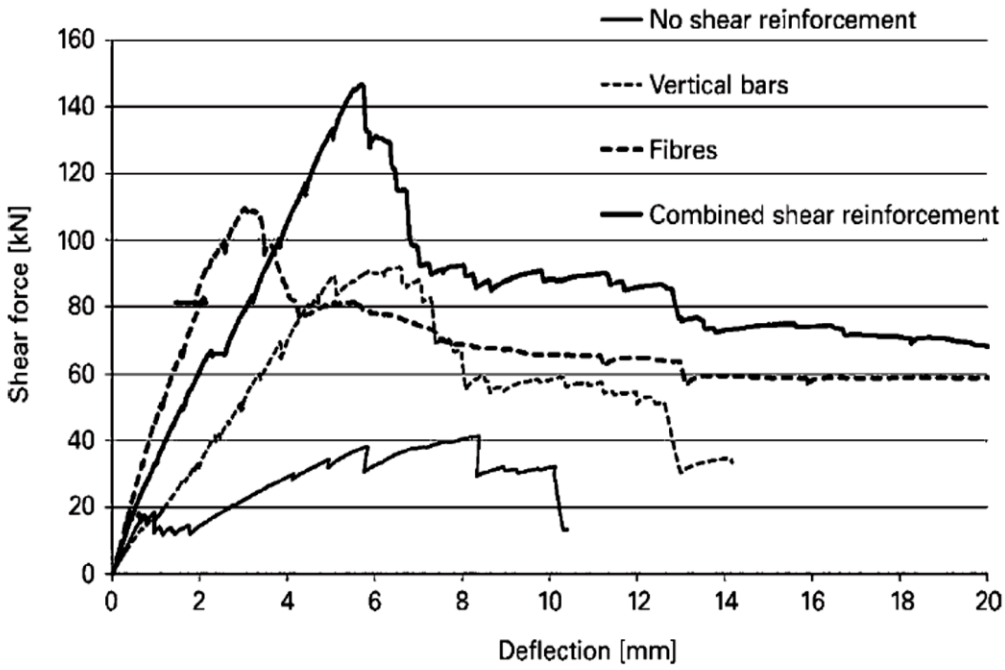

Figure 2.6: Shear load-deflection behavior of the beam specimens [26]

Yen et al. [27] investigated the shear strength of steel fiber reinforced UHPC beams without stirrups. The variable parameters were amount of steel fibers and *a/d* ratio. All the tested beams had 8.6 m length, 8.0 m span, 650 mm depth and 500 mm wide flange. High-energy ribbon blender mixer was used to produce UHPC. The used steel fibers had a diameter of 0.2 mm, three different lengths (Type-I with 15 mm, Type-II with 20 mm and Type-III with 25 mm), and 2300 MPa tensile strength. Two fiber contents (1.0 and 1.5%) were used. The results show that the beams with same steel fibers but with low *a/d* ratio (1.8) failed at higher load than beams with same steel fibers but with high *a/d* ratio (>1.8). Shear capacity increased with the increasing, V_f. All the cracks initiated at webs of shear span and propagated toward the top flange.

Many other researchers, for example [28-31], studied shear behavior of UHPC beams. They also considered the above-mentioned variable parameters. The results show that the shear behavior of UHPC beams was significantly affected by the key parameters.

2.6. Numerical Modeling of the Shear Behavior of Concrete Beams

Many empirical equations derived from experimental works are able to predict the behavior of concrete beams but have some limitations and they cannot provide serviceability requirements such as structural deformation and cracking. Strut and tie model based on equilibrium solution provides safe design, but cannot provide non-linear material behavior and serviceability requirements. Cracking of concrete, yielding of steel, ultimate load capacity and service behavior of concrete must be taken in account. Therefore, finite element Modeling (FEM) is the powerful tools to study the linear and non-linear behavior of reinforced concrete beams. In the last three decades, many studies have been conducted to develop models representing shear behavior of reinforced concrete beams [32].

FEM and parametric studies were conducted on structural performance of an AASHTO Type II girder and a 2nd-generation Pi-girder constructed from UHPC. The concrete damaged plasticity (CDP) model was primarily employed to model the constitutive behaviors of UHPC. The results show that CDP models can capture both linear and nonlinear behaviors of the I-girders and pi-girders reasonably well [14, 33].

Numerical and parametric studies were carried out on shear behavior of bridge girders made of normal concrete and UHPFRC using the ANSYS software package with the variable parameters that included cross-section height, amount of steel fibers (V_f), and stirrups spacing. The results show a good agreement between FEM and experimental results. Shear capacity increased with the increasing cross-section height, V_f, and decreasing stirrups spacing [12].

FEM and parametric studies were conducted on structural performance of second-generation UHPC pi-girders using the ABAQUS software. The results show that the FEM predicted symmetrical behavior of the girder even though the experiment setup may not have ensured perfectly symmetrical behavior. The structural behavior of beams was in good agreement with the experimental results [34].

Effect of pozzolanic admixture and, V_f, was investigated with the uses of ANSYS software. The results show that the FEM simulation is in good agreement with the experimental results. A relatively softer numerical response is noticed at stages closer to the ultimate load [15].

Experimental and analytical investigations were conducted on shear behavior of reinforced geopolymer concrete beams. ANSYS software package was used for numerical simulation. Shear capacity increased with the increasing compressive strength but decreased with the increasing *a/d* ratio. The ANSYS model was able to simulate the nonlinear and load-deflection behavior of the beams. Shear cracks for both GPC and OPCC derived from FEM were in good agreement with the experimental results [35].

FEM were carried out on the shear capacity of GFRP-reinforced concrete short beams. The tested beams were prepared considering *a/d* ratio and longitudinal reinforcement ratio, ρ, as variable parameters. FEM was developed using the ABAQUS commercial software to simulate the shear behavior of beams subjected to four-point loadings. The results showed that the FEM is capable of studying the shear behavior such in terms of modes of failure, maximum load and load-deflection relationship of the deep and short beams. Shear capacity increased with the increasing ρ but decreased with the increasing *a/d* ratio [36].

2.7. Summary of the Literature Review

From the review of both experimental and numerical studies reported in literature, following points can be summarized:

1. Common factors affecting shear behavior of UHPC beams are the volume fraction of steel fibers V_f, percentage of longitudinal reinforcement ρ, stirrups spacing, s, a/d ratio, beam size and compressive strength.
2. Shear capacity increased with the increasing in, V_f, ρ, compressive strength and with the decreasing in stirrups spacing, and a/d ratio.
3. However, hardly anybody reported any experimental or numerical Modeling work on the simultaneous effects of all the key four factors on the shear capacity of the UHPC beams.

CHAPTER 3

RESEARCH METHODOLOGY

3.1. General

This chapter describes the experimental program conducted to meet out the objectives of the present work. The test program mainly composed of casting and testing of ten UHPC beam specimens having 150 mm width, 225 mm depth, and 2000 mm length. The focus of the test program was to generate the qualitative and quantitative data required to study the effects of four key factors (*a/d* ratio, volume fraction of steel fibers, V_f, percentage of longitudinal reinforcement, ρ, and stirrups spacing, *s*) on shear behavior of UHPC beams. The experimental work was followed by the finite element Modeling including parametric study. Finally, the statistical analysis of the experimental data was carried out and an equation for shear capacity of the UHPC beams was derived in terms of the four key parameters.

The work was carried out in the following steps:

- Design of UHPC beam specimens
- Design of UHPC mixture for preparation of the beam specimens
- Preparation of the beam specimens
- Test setup and procedure
- Mechanical properties
- Results and discussions
- Finite element modeling and parametric study

- Statistical analysis and development of the new shear design equation

3.2. Design of UHPC Beam Specimens

3.2.1. Experimental Variables

Four experimental variables namely shear span to effective depth ratio, *a/d*, volume fraction of steel fibers, V_f, percentage of longitudinal reinforcement, ρ, and stirrups spacing, *s*, were considered to study their effects on shear behavior of the beams. As shown in Table 3.1, two levels of each of the four variables were considered as follows: *a/d* ratio-1.8 and 2.6; V_f-1.0 and 2.0%; ρ-1.935 and 3.226%; *s*- 200 and 370 mm. The selection of the levels of variables was made to ensure the failure of all the UHPC beam specimens in pure shear.

3.2.2. Geometrical Details of the Beam Specimens

As shown in Table 3.1, ten UHPC beam specimens were considered to study the effects of four variables. All beam specimens had a rectangular cross section (150 mm width and 225 mm depth) and a length of 2000 mm. Since depth of all the beam specimens was kept constant at 225 mm, the *a/d* ratio varied by changing only the shear span, *a*, during testing.

In all the beam specimens, 15 mm diameter PSB 1080 steel bars, conforming to ASTM A722/A722M specifications, were used as longitudinal reinforcements. In addition, 2-legged stirrups, made with Grade 60 steel bars of 10 mm diameter, conforming to ASTM A615 specifications, were utilized as stirrups in all the beam specimens. Two samples from each types of rebar were tested in direct uniaxial tension. The yield and ultimate strengths of the PSB 1080 bars were 1320 MPa and 1600 MPa, respectively, while those for Grade

60 bars were 420 MPa and 500MPa, respectively. Figure 3.1 shows the details of the beam specimens, which are divided into five series, designated as A to E (Table 3.1).

Table 3.1: Details of variables used in the beam specimens

Series	No	Beam	*a/d*	ρ (%)	V_f (%)	Spacing of 10 mm two-legged stirrups
A	1	A-1	1.8	1.935	1	200 mm
	2	A-2	1.8	1.935	2	
B	3	B-1	1.8	1.935	1	370 mm
	4	B-2	1.8	1.935	2	
C	5	C-1	1.8	3.226	1	
	6	C-2	1.8	3.226	2	
D	7	D-1	2.6	1.935	1	
	8	D-2	2.6	3.226	1	
E	9	E-1	2.6	1.935	2	
	10	E-2	2.6	3.226	2	

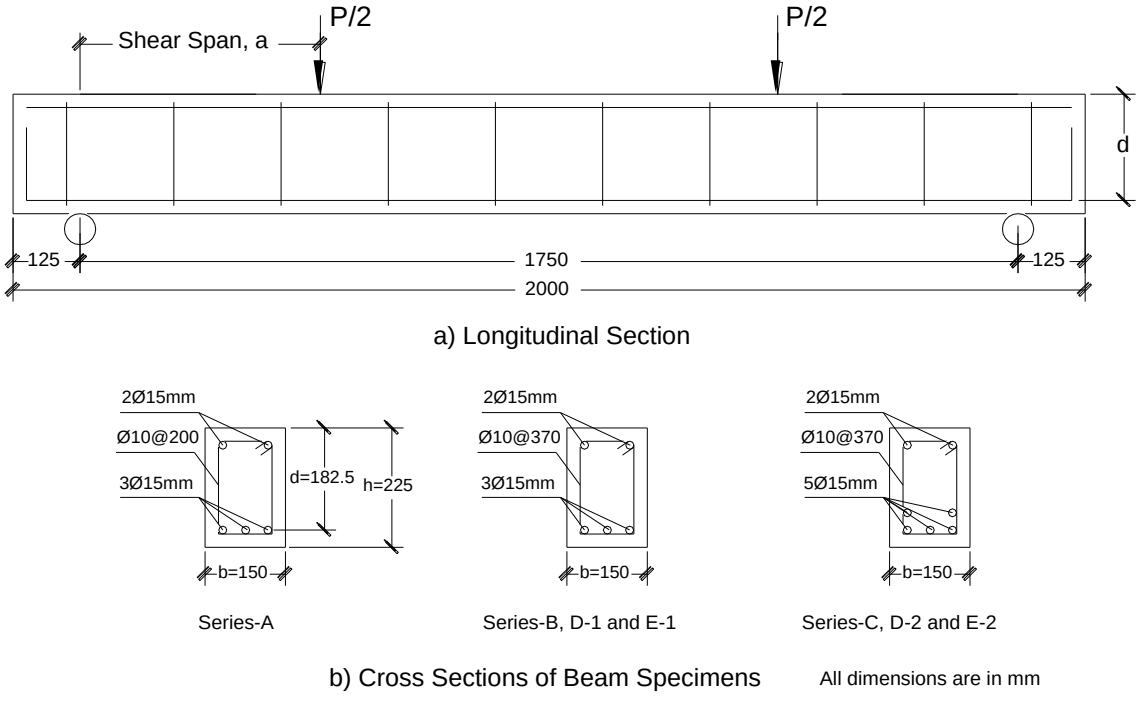

Figure 3.1: Details of the beam specimens

3.2.3. Design of the Beam Specimens

Before casting, all the beam specimens were designed to ensure failure in pure shear. Many researchers generated equations for predicting shear capacity of fiber-reinforced concrete beams based on their experimental studies. In the present work, Narayan's analytical equation [37], as follows, was used to design UHPC beam specimens:

$$V_c = \left[0.24 \cdot \left(\frac{f_c}{20 - \sqrt{F_f}} + 0.7 + \sqrt{F_f} \right) + 80\rho \frac{d}{a} + 1.7F_f \right] \cdot b \cdot h \tag{3.1}$$

Where:

V_c = shear force in concrete, f_c = compressive strength of concrete,

$$F_f = \frac{l_f}{d_f} \cdot V_f \cdot \alpha \tag{3.2}$$

l_f = length of steel fibers, d_f = diameter of steel fibers, V_f = volume fraction of steel fibers in percentage, α = bond factor (for straight steel fibers = 0.5), d = effective depth of the beam, a = shear span, ρ = ratio of longitudinal reinforcement.

The ultimate shear capacity of concrete beam specimens with shear stirrups was calculated as follows:

$$V_u = V_c + V_s \tag{3.3}$$

V_u = ultimate shear force, V_c = shear force in concrete, V_s = shear force in stirrups.

$$V_s = \frac{A_s \cdot f_y \cdot d}{s} \tag{3.4}$$

A_s = cross sectional area of two-legged stirrups, f_y = yield stress of stirrups, S = stirrups spacing.

To ensure failure of the beam specimens in pure shear, flexural capacity of the beams was kept greater than moment caused by the applied shear loads. The flexural capacity of the UHPC beam specimens was calculated using the following equation for nominal moment capacity for a singly reinforced UHPC beam [38]:

$$M_n = A_s \cdot f_y\left(d - \frac{a}{2}\right) + \sigma_t \cdot b(h-c)\left(\frac{h+c-a}{2}\right) \tag{3.5}$$

Where:

A_s = cross-sectional area of longitudinal reinforcement, σ_t = post cracking strength of fiber reinforced composite.

$$\sigma_t = 0.85 \cdot V_f \cdot \tau_f \cdot \frac{l_f}{d_f} \tag{3.6}$$

τ_f = frictional bond strength fiber matrix and is given by; $\tau_f = 0.66\sqrt{f_c}$ (MPa), b = width of beam, h = complete depth of beam, C = natural axis depth and is given by; $c = \frac{a}{\beta_1}$, a = depth of the equivalent compressive block and is given as:

$$a = \frac{A_s \cdot f_y + \sigma_t \cdot b \cdot h}{\eta \cdot f_c \cdot b + \sigma_t \cdot b} \tag{3.7}$$

η = concrete stress block parameter (equal to 0.86 for $f_c' \geq 55MPa$), β_1 = concrete stress block parameter (equal to 0.65 for $f_c' \geq 55MPa$).

As a sample, the design of beam A-1 (1.0% steel fibers, *a/d*=1.8 ρ =1.935% and *s* = 200 mm) using Narayan's analytical Eq. 3.1 is given as follows:

Given data:

Diameter of longitudinal reinforcement = 15 mm

Diameter of shear reinforcement (stirrups) = 10 mm

$l_f = 13$ mm

$d_f = 0.2$ mm

$f_c' = 140$ MPa

$V_f = 0.01$ (1.0%)

$h = 225$ mm

d = h – (cover + stirrups diameter + ½ diameter of longitudinal bar) = 225 - (25 + 10 +0.5 ×15) = 182.5 mm

$a = 1.8 \cdot d = 1.8 \times 182.5 = 328.5$ mm

$b = 150$ mm

Step-1: Ultimate shear force in UHPC beam is given as:

$$V_u = V_c + V_s$$

$$V_c = 0.24 \cdot \left(\frac{f_c}{20 - \sqrt{F_f}} + 0.7 + \sqrt{F_f} \right) + 80\rho \frac{d}{a} + 1.7F_f$$

$$F_f = \frac{l_f}{d_f} \cdot V_f \cdot \alpha = \frac{13}{0.2} \cdot 0.01 \cdot 0.5 = 0.325$$

$$V_c = 0.24 \cdot \left(\frac{140}{20 - \sqrt{0.325}} + 0.7 + \sqrt{0.325} \right) + 80 \cdot 0.01935 \cdot \frac{182.5}{328.5} + 1.7 \cdot 0.325 = 3.446 MPa$$

$$V_c(Force) = 3.446 \cdot 150 \cdot 225 = 116302\, N = 116.302 kN$$

$$V_s = \frac{A_s \cdot f_y \cdot d}{s}$$

$$V_s = \frac{2 \cdot \frac{3.14 \cdot 10^2}{4} \cdot 430 \cdot 182.5}{200} = 61603\, N = 61.603 kN$$

$$V_u = 116.302 + 61.603 = 177.905 \text{ kN}$$

Step-2: Maximum bending moment due to applied load (Figure 3.2):

$$\frac{P}{2} = V_u$$

$$M = \frac{P}{2} \cdot a = 177.905 \cdot 328.5 = 58451.7 kN \cdot mm$$

$$M = 58.451 \text{ kN} \cdot \text{m}$$

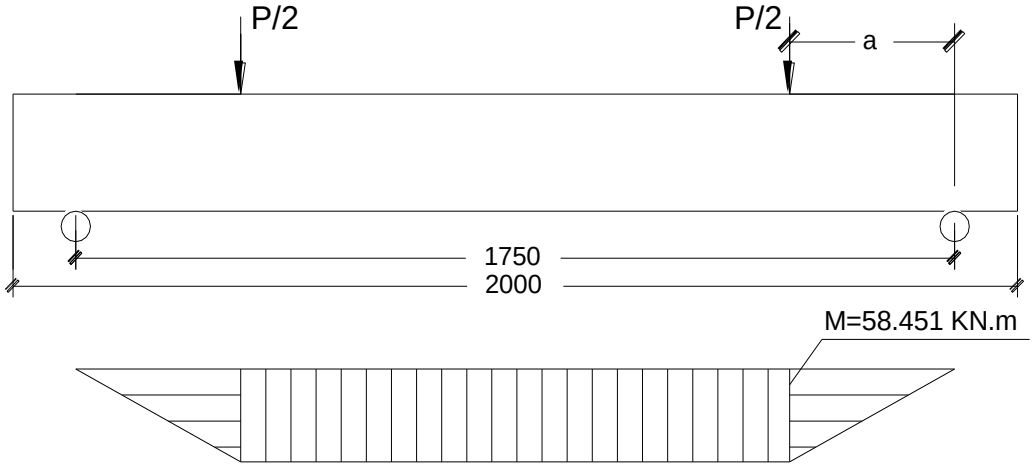

Figure 3.2: Bending moment diagram for beam A-1

Step-3: Nominal moment capacity of the beam specimen using Eq. 3.5:

$$M_n = A_s \cdot f_y \left(d - \frac{a}{2} \right) + \sigma_t \cdot b(h - c) \left(\frac{h + c - a}{2} \right)$$

$$a = \frac{A_s \cdot f_y + \sigma_t \cdot b \cdot h}{\lambda \cdot f_c \cdot b + \sigma_t \cdot b} = \frac{3 \cdot \frac{3.14 \cdot 15^2}{4} \cdot 1320 + 4.314 \cdot 150 \cdot 225}{1 \cdot 140 \cdot 150 + 4.314 \cdot 150} = 39.038 mm$$

$$\sigma_t = 0.85 \cdot V_f \cdot \tau_f \cdot \frac{l_f}{d_f} = 0.85 \cdot 0.01 \cdot 7.809 \cdot \frac{13}{0.2} = 4.314 MPa$$

$$\tau_f = 0.66\sqrt{f_c'} = 0.66\sqrt{140} = 7.809 MPa$$

$$c = \frac{a}{\beta_1} = \frac{39.038}{0.65} = 60.057 mm$$

$$M_n = 529.875 \cdot 1320\left(182.5 - \frac{39.038}{2}\right) + 4.314 \cdot 150(225 - 60.057)\left(\frac{225 + 60.057 - 39.038}{2}\right)$$

$$= 127125000\, N \cdot mm = 127.125\ \text{kN} \cdot \text{m}$$

Since the nominal moment capacity of the beam, M_n, is more than the maximum bending moment, M, that will be resulted due to shear load, P, that beam (A-1) would fail in pure shear, not in flexure.

Step-4: Safety percentage of shear failure:

$$\text{Safety percentage} = \frac{127.125 - 58.451}{127.125} \cdot 100 = 54.02\%$$

Step-5: Shear load at maximum flexural capacity:

If applied load exceeds that maximum flexural capacity, beam will cause flexural failure rather than shear failure.

$$V_u = \frac{M_n}{a} = \frac{58.451 \cdot 1000}{328.5} = 387 KN$$

The values of V_u for shear and flexural failures for all the beam specimens are shown in Table 3.2.

Table 3.2: The values of V_u for shear and flexural failures of the beam specimens

Beam	V_u at shear failure (kN)	V_u at flexural failure (kN)	Intended mode of failure
A-1	177.94	386.99	Pure shear
A-2	199.21	418.09	
B-1	149.63	386.99	
B-2	170.91	418.09	
C-1	168.99	573.59	
C-2	190.27	595.47	
D-1	140.70	267.92	
D-2	154.10	397.10	
E-1	161.98	289.44	
E-2	175.38	412.25	

3.3. Design of UHPC Mixture used for Preparation of the Beam Specimens

3.3.1. Ingredients of the UHPC Mixture

Ordinary Portland cement (Type I), polycarboxylic-based ether hyperplasticizer, micro silica, fine dune sand and potable laboratory water, and plain high strength steel fibers were used to produce UHPC mixture for casting the beam specimens. Proportions of these constituent materials have been chosen carefully in order to optimize the packing density of the mixture.

3.3.1.1. Cement

Ordinary Portland cement (Type-I) conforming to ASTM C150 specifications, manufactured by Saudi Cement Company, was used. Figure 3.3 shows the sample of the cement used. The chemical composition of the cement is shown in Table 3.3.

Figure 3.3: Ordinary Portland cement (Type-I)

Table 3.3: Chemical composition of ordinary Portland cement (Type- I)

Component	Weight (%)
CaO	64.35
SiO_2	22.00
Al_2O_3	5.64
Fe_2O_3	3.80
K_2O	0.36
MgO	2.11
N_2O	0.19
Equivalent alkalis	0.33
SO_3	2.10
Loss on ignition	0.70
C_3S	55.00
C_2S	19.00
C_3A	10.00
C_4AF	7.00

3.3.1.2. Micro Silica

Micro silica used in the present study was obtained from a local ready mixed company. As shown in Figure 3.4, it had a dark color. Chemical composition of the micro silica is shown in Table 3.4.

Figure 3.4: Micro Silica

Table 3.4: Chemical composition of micro silica

Constituent	**Weight (%)**
SiO_2	92.5
Al_2O_3	0.72
Fe_2O_3	0.96
CaO	0.48
MgO	1.78
SO_3	-
K_2O	0.84
Na_2O	0.5
Loss on ignition	1.55

3.3.1.3. Superplasticizer

Superplasticizer used in this research work was a new generation of polycarboxylic-based ether hyperplasticizer, as shown in Figure 3.5. It was sourced from a local supplier in Saudi Arabia.

Figure 3.5: Superplasticizer

3.3.1.4. Water

Drinkable water was used for mixing and curing.

3.3.1.5. Fine aggregates

Fine dune sand, as shown in Figure 3.6, available in Saudi Arabia was used as fine aggregate. The specific gravity and absorption of fine aggregate were 2.56 and 0.4%, respectively.

Figure 3.6: Dune sand used as fine aggregate

The grading of dune sand is shown in Table 3.5:

Table 3.5: Grading of dune sand used as fine aggregate

ASTM Sieve #	Size (mm)	% Passing
4	4.75 mm	100
8	2.36 mm	100
16	1.18 mm	100
30	600 µm	76
50	300 µm	10
100	150 µm	4

3.3.1.6. Steel Fibers

Steel fibers used in this study are shown in Figure 3.7. The steel fibers had a diameter of 0.2 mm and a length of 13 mm and made of high strength steel.

Figure 3.7: Steel fibers

3.3.1.7. Longitudinal and Shear Reinforcement Bars

Two types of steel reinforcement bars were used in this study. High-strength steel reinforcement (PSB 1080, ASTM A722/A722M) of 15 mm diameter was used as the

longitudinal reinforcement in both tension and compression zones. Grade 60 steel bars (ASTM A615) of 10 mm diameter were used as stirrups in the beam specimens as shown in Figure 3.8a and Figure 3.8b. High-strength steel bars were imported from China and normal strength steel reinforcement bars were provided by a local company inside KSA.

(a)

(b)

Figure 3.8: a) High-strength main steel bar; and b) Normal-strength shear steel bar

3.3.2. Mix Design

Mixture proportions of UHPC with two-volume fraction of steel fibers (1.0 and 2.0% by mass of steel) are shown in Table 3.6. The steel fibers content is calculated taking density of steel fibers as 7850 kg/m^3. For example, 1.0% fibers content by mass of steel fibers is taken as 1×7850/100 = 78.5 kg for 1.0 m^3 of UHPC.

Table 3.6: Proportions of UHPC mixture with two steel fibers contents

Ingredient	**Quantity of ingredients for 1.0 m^3 of UHPC mixture (kg)**	
	V_f =1.0%	**V_f =2.0%**
Cement	900	900
Micro silica	220	220
Water	162	162
Superplasticizer	40	40
Steel fibers	79	157
Dune sand	1030	1005

3.4. Preparation of the Beam Specimens

3.4.1. Cutting, Bending and Tying of Steel Reinforcement Bars

For casting the UHPC beams, the longitudinal rebars and shear stirrups were cut, bent and tied together, as shown in Figure 3.9. As mentioned earlier, high-strength steel reinforcement bars used as longitudinal reinforcements in both tension and compression zone. Steel bars at tension zone were hooked with 90 degrees.

Figure 3.9: Bending and tying of steel reinforcement bars

To prepare beam specimens with different percentage of longitudinal reinforcement in tension zone and to maintain two different stirrups spacing, three types of reinforcement cages were prepared as follow:

1. Reinforcement cage with (3ϕ15mm) longitudinal reinforcements in tension zone to have ρ=1.935%, (2ϕ15mm) longitudinal reinforcements in compression zone, and 10 mm diameter two-legged stirrups at a spacing of 200 mm center to center as shear reinforcement, as shown in Figure 3.10.

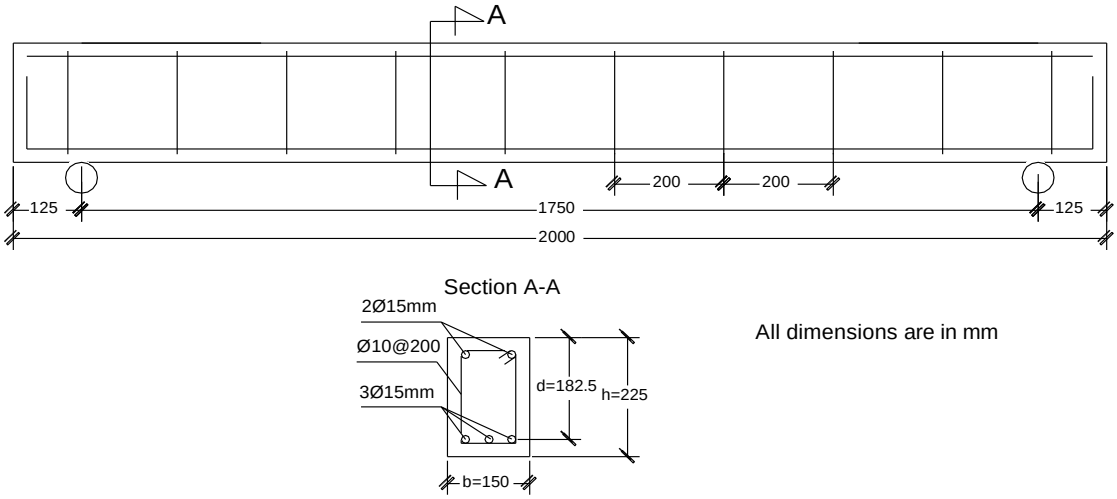

Figure 3.10: Steel bars cage for beams with ρ =1.935% and s = 200 mm

2. Reinforcement cage with (3ϕ15mm) longitudinal reinforcements in tension zone to have ρ=1.935%, (2ϕ15mm) longitudinal reinforcements in compression zone, and 10 mm diameter two-legged stirrups at a spacing of 370 mm center to center as shear reinforcement, as shown in Figure 3.11.

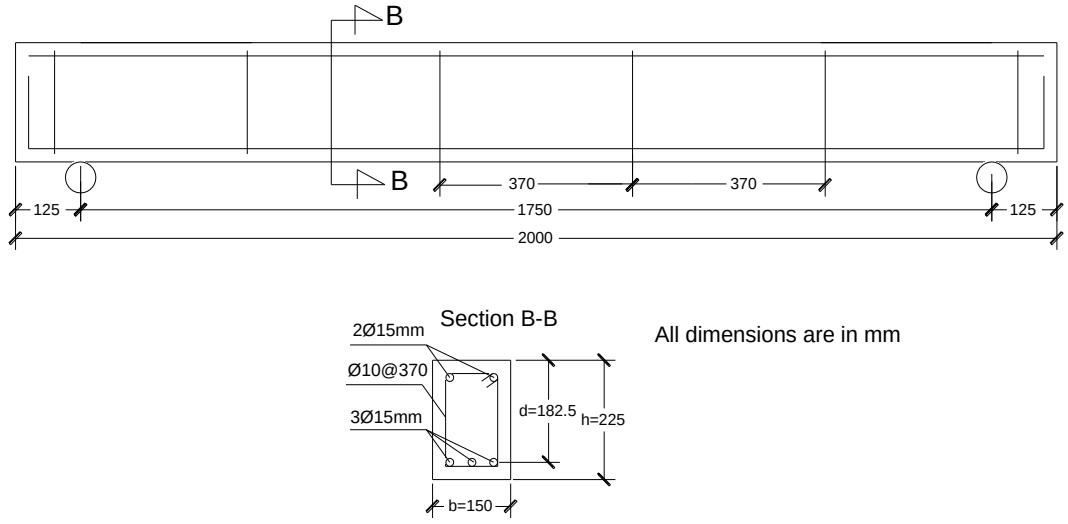

Figure 3.11: Steel bars cage for beams with ρ =1.935% and s = 370 mm

3. Reinforcement cage with (5ϕ15mm) longitudinal reinforcements in tension zone to have ρ=3.226%, (2ϕ15mm) longitudinal reinforcements in compression zone, and 10

mm diameter two-legged stirrups at a spacing of 370 mm center to center as shear reinforcement, as shown in Figure 3.12.

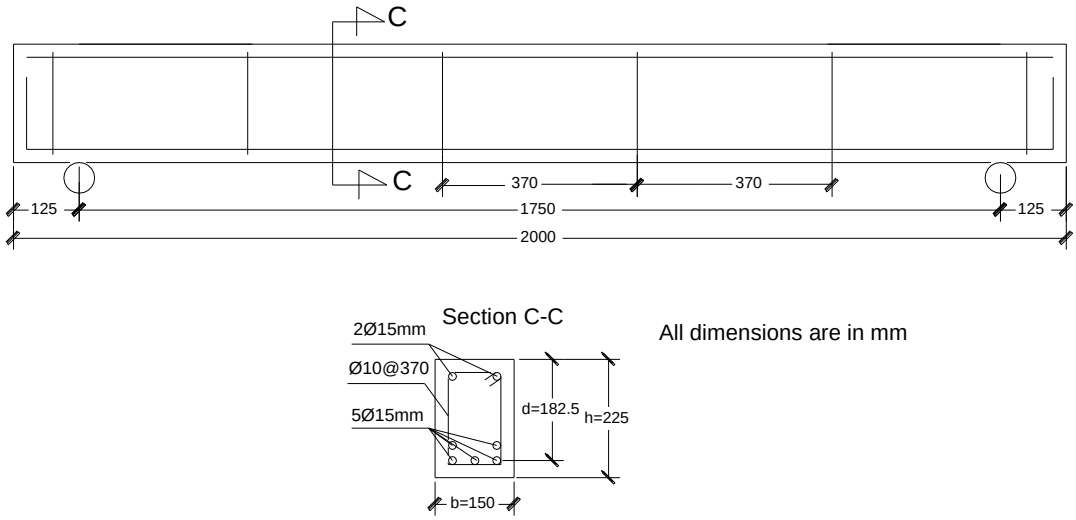

Figure 3.12: Steel bars cage for beams with ρ =3.226% and s = 370 mm

After completion of the bending and tying of steel reinforcement bars, steel strain gauges were attached to the longitudinal rebars and shear stirrups, as shown in Figure 3.13.

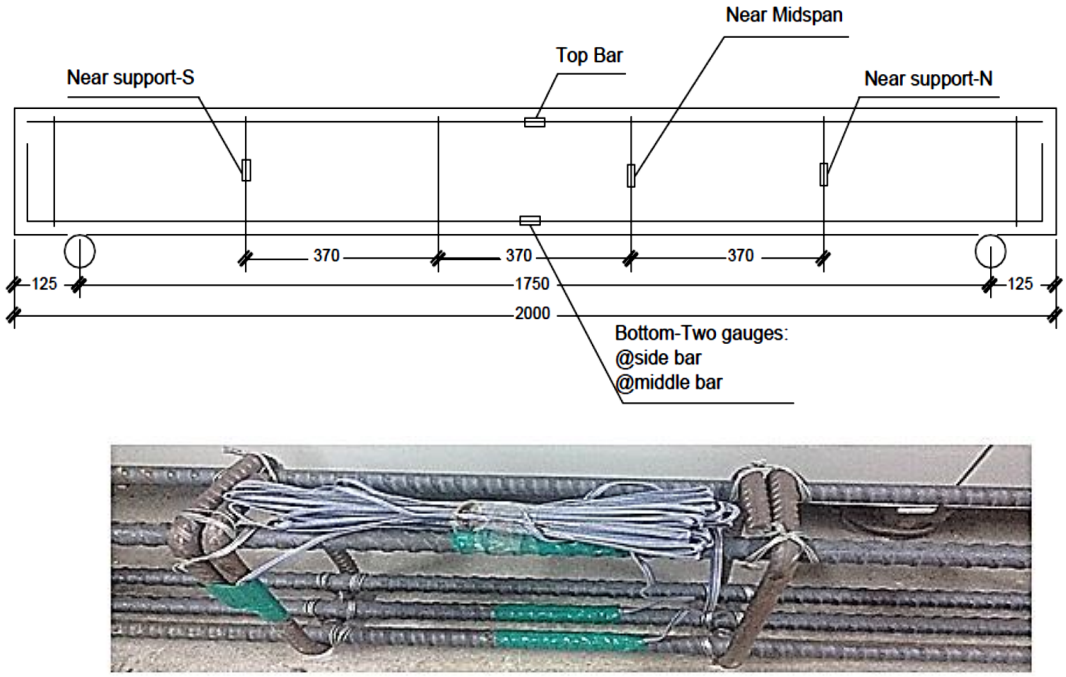

Figure 3.13: Details of the stain gauges attached to the longitudinal rebars and stirrups

3.4.2. Mixing

Ingredients of UHPC were mixed in a twin-shaft batch mixer in the following steps:

1. The quantity of all needed materials was weighed according to the mix design, as shown in Figure 3.14.

Figure 3.14: The weighed ingredients of UHPC mixture

2. 30 minutes before mixing, water and superplasticizer were mixed together, as shown in Figure 3.15.

Figure 3.15: Mixed superplasticizer and water

3. Cement and micro silica were put into mixer and were mixed for 5 minutes, as shown in Figure 3.16.

Figure 3.16: Cement and micro silica inside mixer

4. Mixture of water, superplasticizer and dune sand were added gradually to mixer, as shown in Figure 3.17.

Figure 3.17: Addition of water, superplasticizer and dune sand into mixer

5. Steel fibers were added separately to mixer and mixing continued until a homogeneous matrix of UHPC was obtained, as shown in Figure 3.18.

Figure 3.18: Addition of steel fibers into mixer

3.4.3. Casting

For casting the UHPC beams, all sides of the formwork were oiled for easy demolding. After mixing, the concrete mixture was poured into plastic buckets and covered with plastic sheets to prevent surface dryness. Then plastic buckets were moved to the molds. Concrete was poured at one end of the mold and allowed to flow under its own weight and fill the mold completely, following the recommended practice as shown in Figure 3.19.

Figure 3.19: Concrete pouring in plastic buckets and mold

To maintain an equal width of the beam (150mm), mold was tightened at top and bottom, as shown in Figure 3.20.

Figure 3.20: Mold taken by strengthener at top and bottom

Along with each beam specimen, six cylindrical specimens of size 75 × 150 mm and six prism specimens of size 40 × 40 × 160 mm were cast to conduct the compression and flexural tests, according to ASTM C 39 and ASTM C1018, respectively. In addition, with each beam specimens, six 50 mm cubes and 2 dog-bone specimens were cast to conduct the compression and direct tensile stress-strain behavior tests, respectively, as shown in Figure 3.21:

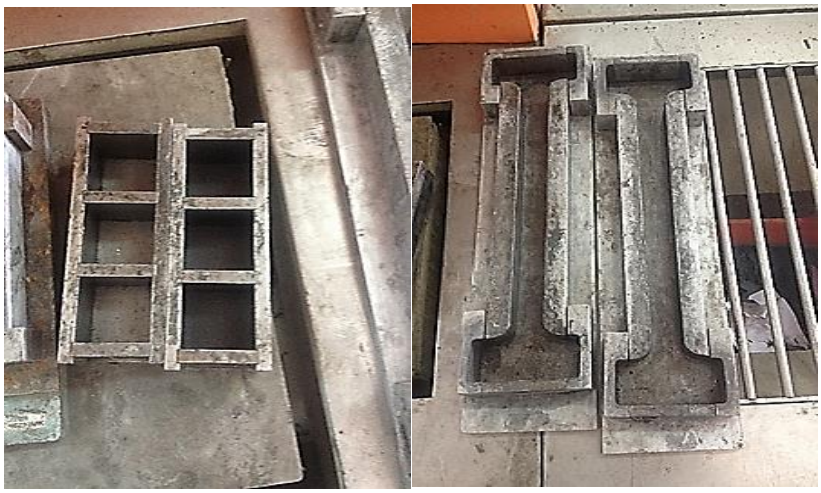

Figure 3.21: Molds for cylindrical, prism, cube and dog bone specimens

3.4.4. Curing

Immediately after casting, the surfaces of the beams were covered with plastic sheet. After 24 hours in mold, the beams were demolded and transported to the curing tank and cured at an average temperature of 22 °C for 28 days, as shown in Figure 3.22.

After completion of curing, concrete strain gauges were attached to the surface of beams at different locations, as shown in Figure 3.23, to record strains in concrete during testing the beam specimens.

(a)

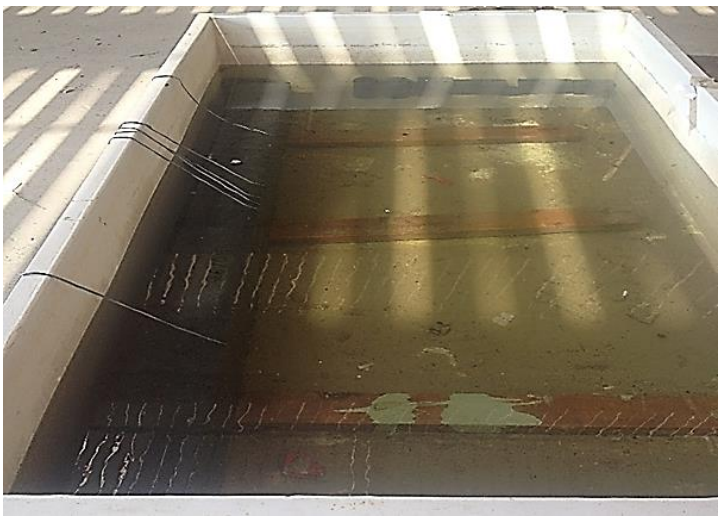

(b)

Figure 3.22: a) Beam covered with plastic sheet after casting; and b) beam in curing tank

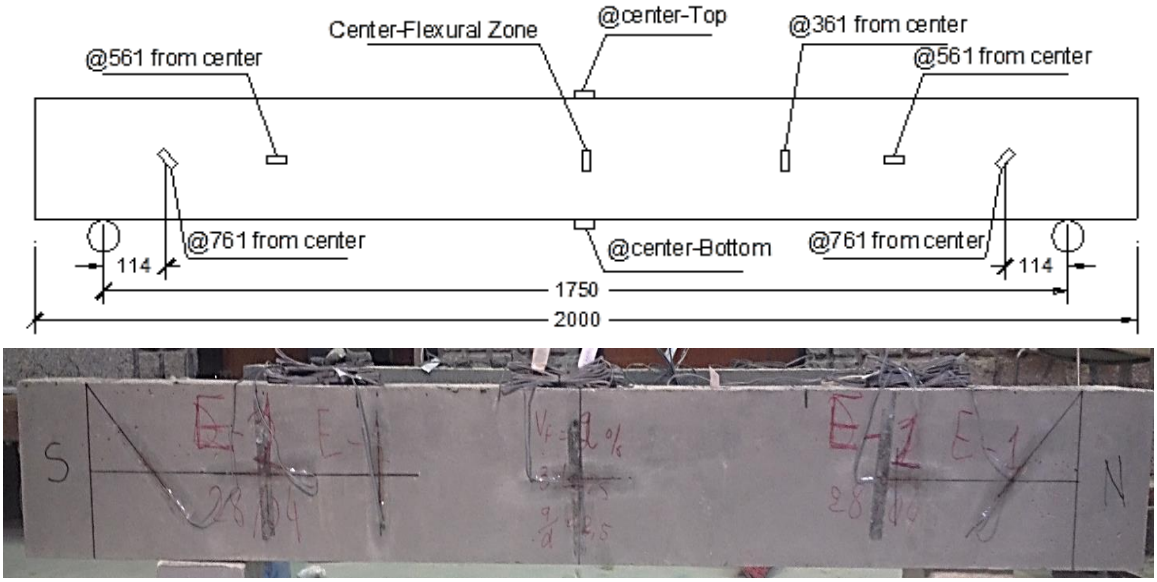

Figure 3.23: Details of the stain gauges attached to the beam for recording strains in concrete

3.5. Test Setup and Procedure

After 28 days curing, beam specimens were dried for one day in the air. The beam specimens were subjected to four-point loading, as shown in Figure 3.24. The spacing between two point loads were changed to maintain different values of shear span ratio (*a/d*) as shown in Figure 3.25.

Figure 3.24: Four-point load test setup

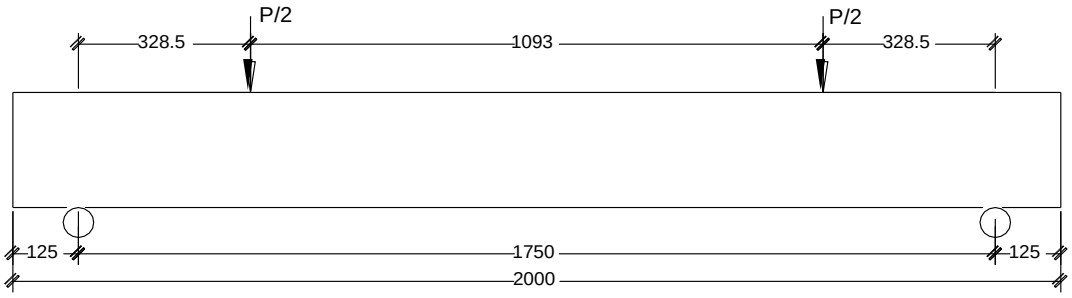

a) *a/d*=1.8

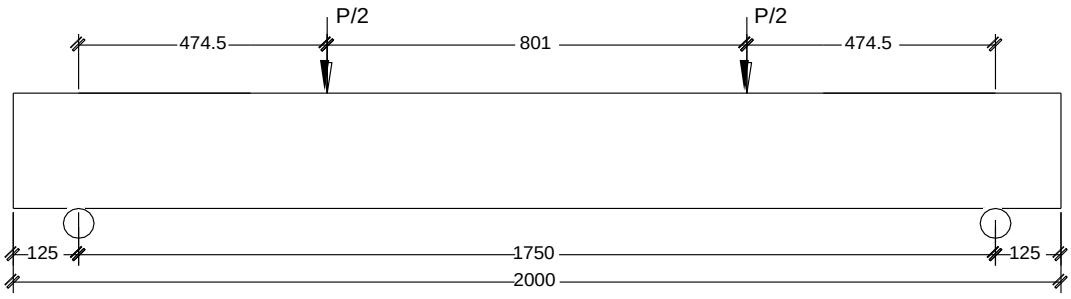

b) *a/d*=2.6

Figure 3.25: Four-point load test setup details for beams: a) *a/d* = 1.8 and b) *a/d* = 2.6

One LVDT was placed below the beam at mid-span to measure deflection of the beam at middle and two LVDTs were placed above the beam at the locations of both supports of

the beams to measure any rotation, as shown in Figure 3.26. The load was applied at a deflection rate of 0.05 mm/s. The duration of a single test was approximately 20 minutes. During the entire loading process, deflection and strain data were recorded using a data logger. In addition, cracks were observed and marked out on the beam surfaces.

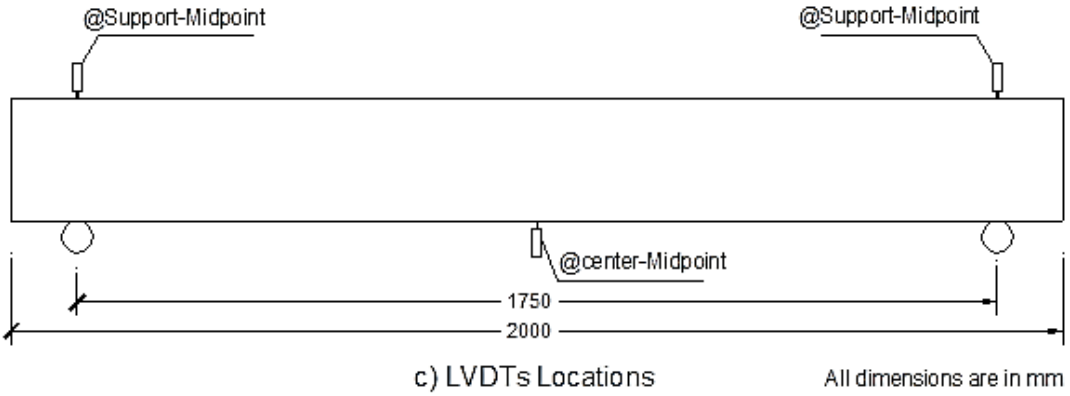

Figure 3.26: Locations of LVDTs

3.6. Mechanical Properties of UHPC Mixture and Steel Reinforcement

This part describes the mechanical behavior of UHPC mixture and longitudinal and shear reinforcement. The mechanical properties of UHPC mixture and steel reinforcement determined under the present work were utilized in the analytical and finite element modeling of the shear behavior of the UHPC beam specimens.

3.6.1. Mechanical Properties of the UHPC Mixture

3.6.1.1. Compressive Strength

Compressive strength of UHPC mixture was obtained by testing the 50 mm cube and 75 × 150 mm cylindrical specimens after 28 days of water curing. Cube compression test conducted with the compression test machine available in Concrete Lab at KFUPM, as shown in Figure 3.27.

Figure 3.27: Compression test machine inside KFUPM lab

Cube compressive strength test results for the UHPC mixtures with 1.0 and 2.0% of fibers (after 28 days of water curing) are shown in Table 3.7 and 3.8, respectively.

Table 3.7: Cube compressive strength test results for 1.0% steel fibers

Cube No	**28-d compressive Strength (MPa)**
1	155.8
2	151.56
3	144.8
4	151.2
5	152.3
Average	**151.13**

Table 3.8: Cube compressive strength test results for 2.0% steel fibers

Cube No	28-d compressive Strength (MPa)
1	163.56
2	158.68
3	155.72
4	157.2
5	158.76
Average	**158.78**

Compression test on cylindrical specimens was conducted according to ASTM C 39 [39]. The same compression test machine, which was used for cube specimens, was used to test the cylinder specimens. One end of the cylinder specimens cut before testing because of rough surface, and their final lengths were approximately 1.95 times their diameter. Two LVDTs and a load cell were used and connected to data logger to record deformation at both sides of cylindrical specimens, and applied load on the specimen, respectively, as shown in Figure 3.28. The applied loading rate was 1.0 kN/s. Finally, stresses and strains were determined as load/cross-sectional area of the specimen and deformations from LVDT/spacing between two rings that was 90 mm, respectively.

Figure 3.28: Test setup for compression stress-strain behavior of concrete

The stress-strain data obtained through compression test conducted on cylindrical specimens cast along with the beam using UHPC with 1.0 and 2.0% steel fibers were plotted, as shown in Figure 3.29. From Figure 3.29, the ultimate cylindrical compressive strengths were found to be around 140 MPa and 150 MPa for the UHPC mixtures with 1.0 and 2.0% steel fibers, respectively. The strains at peak loading were found to be 0.0033 and 0.0035 for the UHPC mixtures with 1.0 and 2.0% steel fibers, respectively.

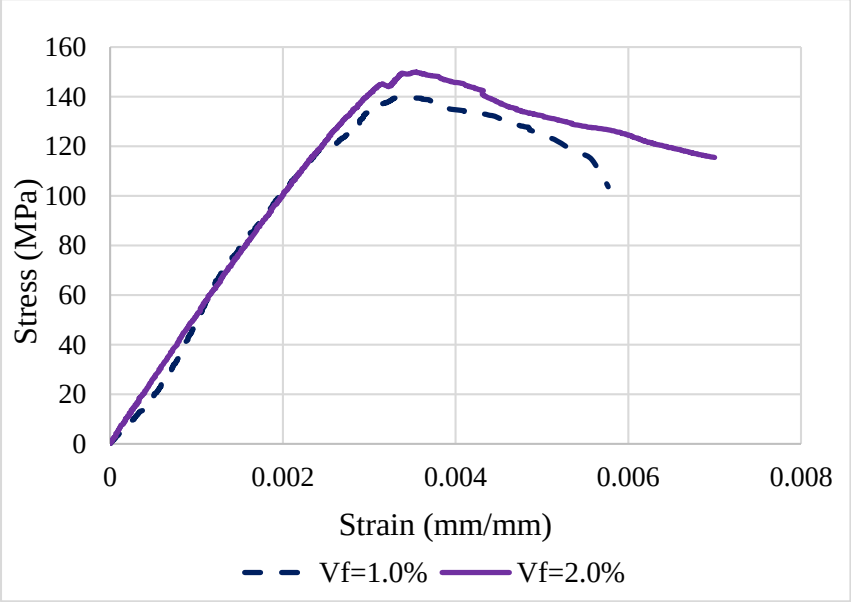

Figure 3.29: Stress-strain curves for cylindrical specimens tested under compression

3.6.1.2. Modulus of Elasticity

Test for modulus of elasticity of concrete was conducted according to ASTM C469 [40]. As specified in ASTM C 469 standard test method, the slope of elastic portion of the compressive stress-strain curve (between origin and a point on the curve corresponding to 40 percent of the ultimate compressive strength) was taken as modulus of elasticity, as shown in Figure 3.29.

Modulus of elasticity for UHPC mixture having 1.0% steel fibers:

$$E = \frac{\sigma_2 - \sigma_1}{\varepsilon_2 - \varepsilon_1} = \frac{125 - 50}{0.002533 - 0.000933} = 46990\,MPa = 47GPa$$

Modulus of elasticity for UHPC mixture having 2.0% steel fibers:

$$E = \frac{\sigma_2 - \sigma_1}{\varepsilon_2 - \varepsilon_1} = \frac{130 - 40}{0.002711 - 0.000778} = 46919\,MPa = 46.91GPa \approx 47GPa$$

3.6.1.3. Direct Tensile Strength

Direct tensile test was conducted on dog-bone specimens cast along with the beam specimens using UHPC with 1.0 and 2.0% steel fibers. This test was conducted with the tensile test machine available in Structural Engineering Lab at KFUPM, as shown in Figure 3.30.

Figure 3.30: Direct tensile test setup

Before testing, a 5 mm deep notch was created at the middle of the specimens to force the breaking point towards the notch. A 40 mm extensometer was used and connected to data logger to calculate deformation at both sides of the notch. Finally, stresses and strains were

determined as loads/cross-sectional area of dog-bone specimens around the notch and deformations from extensometer/40 mm, respectively. The tensile stress-strain data obtained through dog-bone specimens for the UHPC mixtures with 1.0 and 2.0% steel fibers, respectively, were plotted, as shown in Figure 3.31.

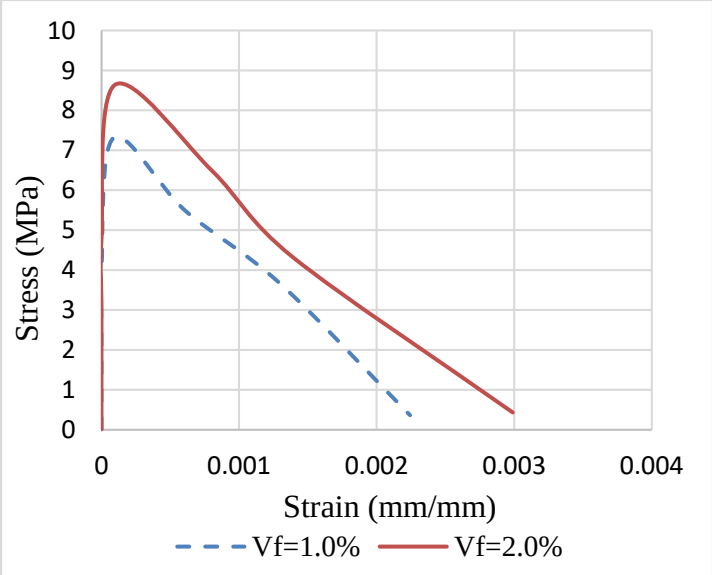

Figure 3.31: Stress-strain curves for dog-bone specimens tested under direct tension

Compressive stress-strain, modulus of elasticity, and tensile stress-strain behaviors of UHPC mixture were used for simulation of beam specimens in ABAQUS software for studying the shear behavior of the UHPC beam specimens.

3.6.1.4. Flexural Strength

Test for flexural behavior of UHPC mixture was conducted according to ASTM C 1018 [41] using 40 × 40 × 160 mm prisms. Four-point loading setup was used. One LVDT was placed below the prism at mid-span to measure deflection of the prism at middle. During the test, loads and deflections of the prisms were monitored by a data logger. Flexural tests

conducted using the equipment available in Structural Engineering Lab at KFUPM, as shown in Figure 3.32.

Figure 3.32: Flexural test setup

The stress-mid-span deflection data obtained through prism specimens for the UHPC mixtures with 1.0 and 2.0% steel fibers, respectively, were plotted as shown in Figure 3.33.

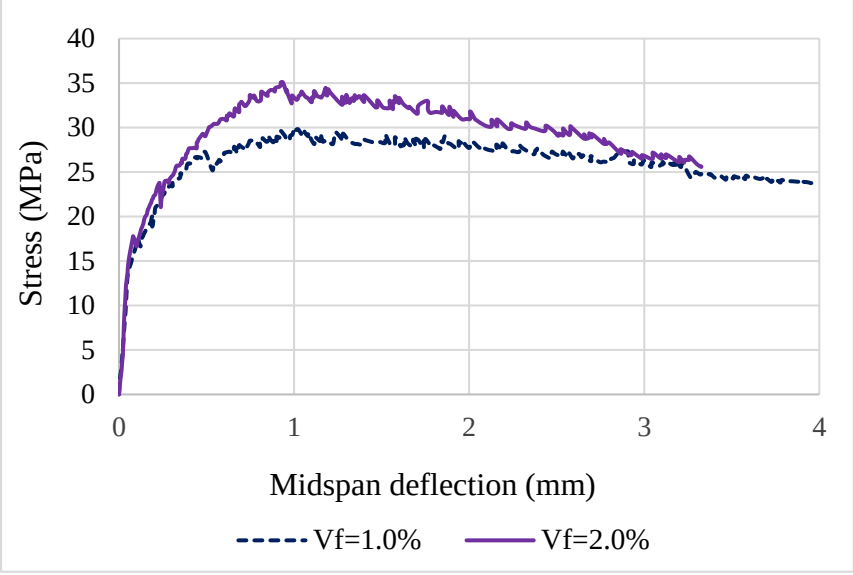

Figure 3.33: Stress-mid-span deflection curves for prism specimens tested under flexure

It can be noted from Figures 3.29, 3.31 and 3.33 that the UHPC is softening after reaching to the peak load, indicating its ductile nature. Slightly higher compressive strength, tensile strength, flexural strength, and strain were found with increase in the fiber content from 1.0 to 2.0%.

3.6.2. Tensile Stress-Strain Behavior of Steel Reinforcement Rebars

Two samples from each rebar types were tested in direct uniaxial tension. The yield and ultimate strengths of the PSB 1080 bars were found to be 1320 MPa and 1600 MPa, respectively, while those for Grade 60 steel bars were 420 MPa and 500MPa, respectively. Both types of rebars were tested to obtain tensile stress-strain behavior inside Structural Engineering Lab at KFUPM, as shown in Figure 3.34.

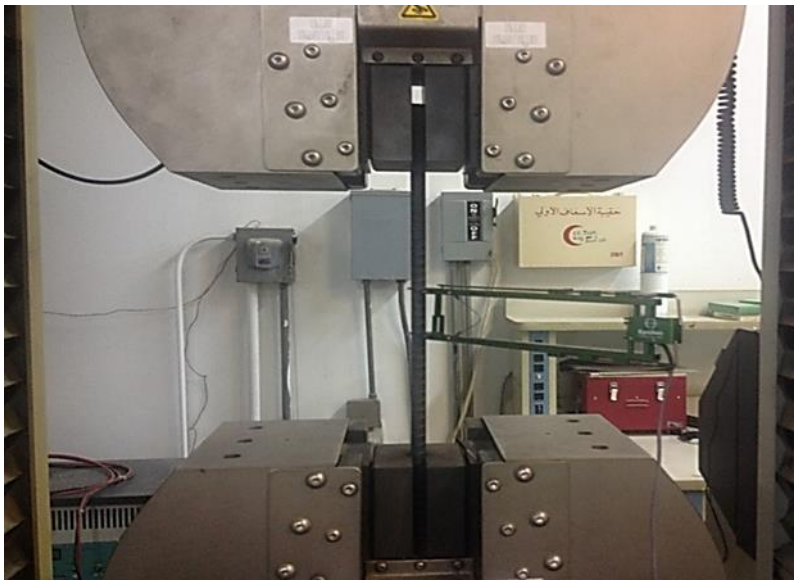

Figure 3.34: Steel rebars testing setup

The stress-strain data obtained through direct tensile test for the high-strength steel rebars (PSB 1080), and normal strength steel rebars (Grade 60), respectively, were plotted as shown in Figures 3.35 and 3.36.

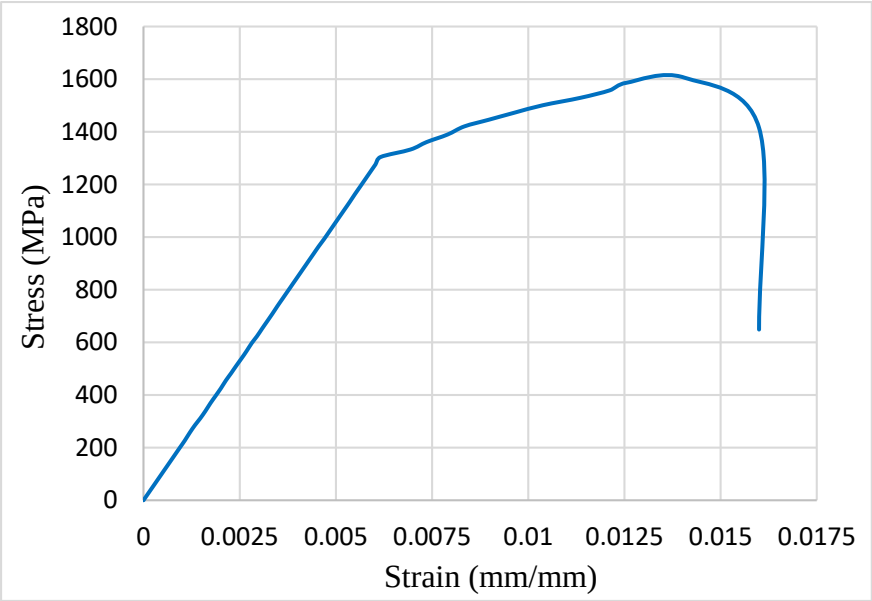

Figure 3.35: Stress-strain curve for high-strength rebars tested under direct tensile test

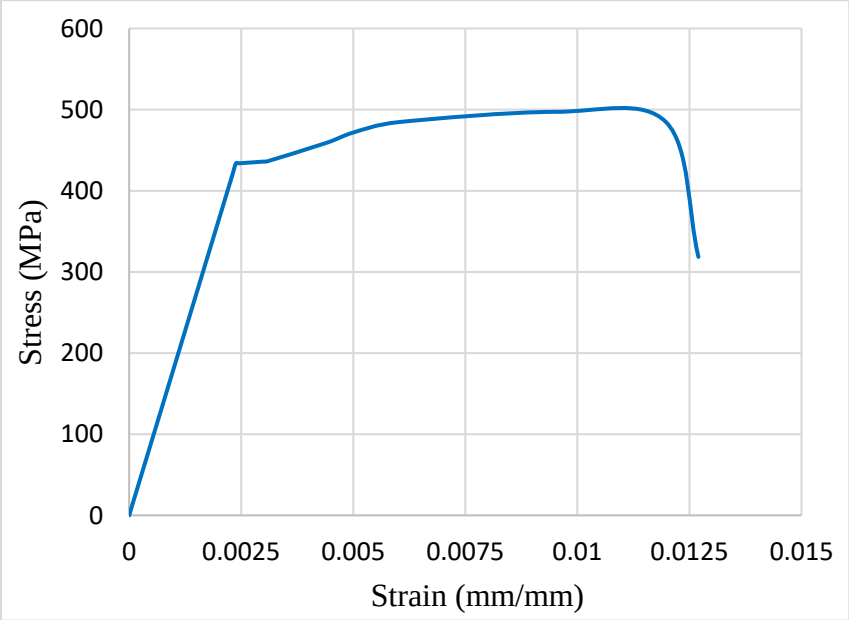

Figure 3.36: Stress-strain curve for normal-strength rebars tested under direct tensile test

CHAPTER 4

RESULTS AND DISCUSSIONS

4.1. General

This chapter describes the results of experimental work and the discussions related to the shear behavior of the beam specimens. The discussions based on the experimental data mainly focused on the structural behavior of the beams under shear load application. Important observations were made based on the shear load-mid-span deflection curves, photographs showing cracking patterns, and strains measured in concrete and steel bars of all the ten beam specimens. Furthermore, the effects of all four key parameters on shear behavior of the beams are separately discussed.

4.2. Structural Behavior of Beam Specimens Subjected to Shear Loading

In the four-point loading test of the beam specimens, the applied shear load, *V*, was taken as *P/2*, where *P* represents the total applied load. The cracks developed during testing of all ten-beam specimens were marked, shear load versus mid-span deflection data were recorded, shear loads at different stages of cracking (occurrence of first crack, diagonal crack and ultimate shear load capacity) were recorded, and strains in concrete and shear and longitudinal reinforcement bars were obtained and photographs were taken after occurrence of failure. The structural behavior of the beams is discussed below using the respective photographs showing crack patterns and shear load versus mid-span deflection curves.

4.2.1. Beam A-1

Beam A-1 cast with 1.0% steel fibers, 3ϕ15 mm longitudinal reinforcements in tension zone (ρ=1.935%), 2ϕ15 mm longitudinal reinforcements in compression zone, 10 mm @200 mm shear reinforcement center-to-center, and *a/d* ratio =1.8.

The first crack detected in flexural zone at shear load of 24 kN corresponding to a displacement of 1.08 mm. With the increasing load, hairline cracks increased and diagonal cracks appeared in shear zones at 59 kN corresponding to a displacement of 5.1 mm and propagated to compression zone till failure and beam failed in pure shear at an ultimate shear load of 172.5 kN corresponding to 21.14 mm mid-span deflection. Shear load versus mid-span deflection response is shown in Figure 4.1.

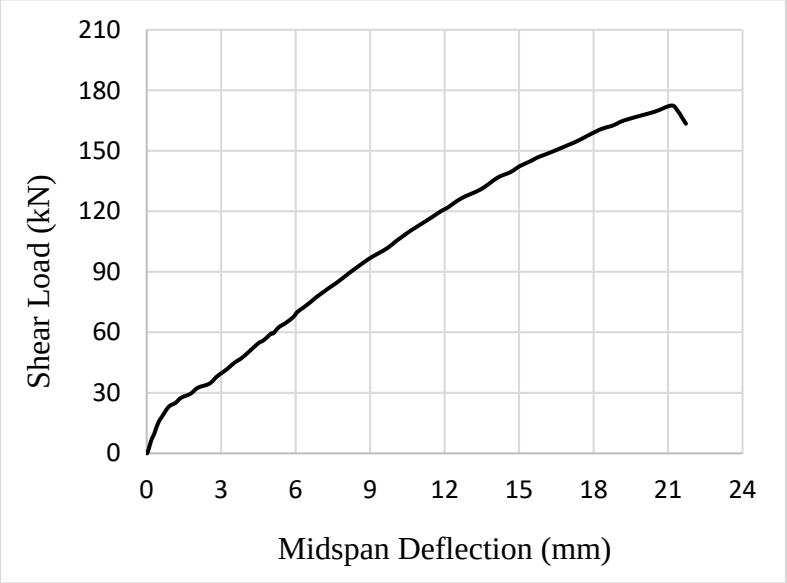

Figure 4.1: Shear load-mid-span deflection curve for beam A-1

It can be observed from Figures 4.2 that the minor hairline cracks start developing in flexural zone at initial stage of loading followed by the development of diagonal cracks in the shear zone of the beam. The beam specimen failed in pure shear with the development

of wide diagonal cracks near supports. This can be attributed to the fact that the beam A-1 had more shear reinforcement than the other eight beams except beam A-2. Due to more shear reinforcement in beam, the load is distributed over a smaller area that resulted into wider and single crack.

Figure 4.2: Mode of failure for beam A-1

Figure 4.3 shows the plots of strains in concrete measured during load testing of beam A-1 with the help of strain gauges attached at different locations. Concrete strain at the top of the beam was 0.0023 at the time of failure that is less than crushing strain (0.0033) of the UHPC mixture (1.0% fiber content) obtained from compression stress-strain behavior. This indicates that no crushing of concrete occurred at the top of the beam when beam failed in pure shear diagonally near the support, as shown in Figure 4.2.

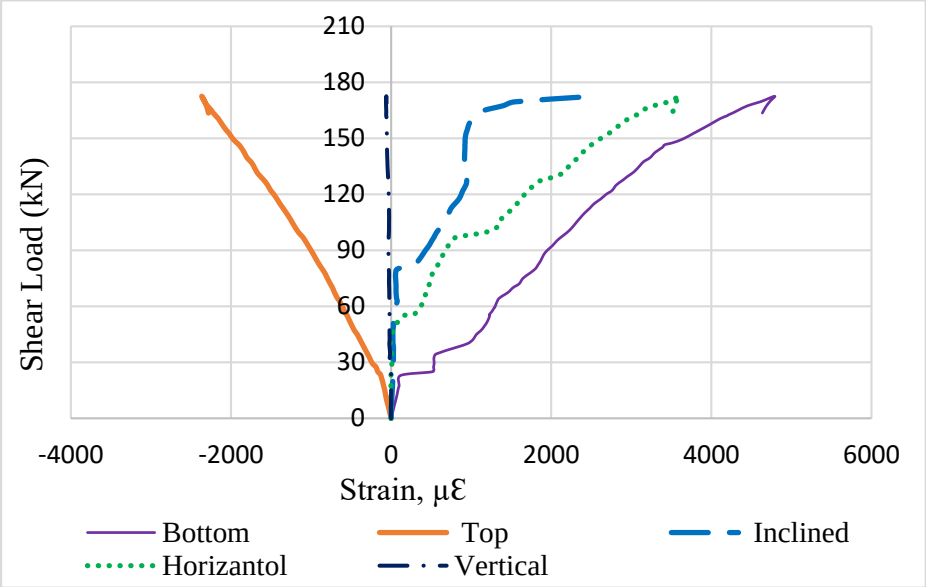

Figure 4.3: Strains in concrete at different locations on the surface of beam A-1

Figure 4.4 shows the plots of strains in longitudinal steel bars at the time of failure. The top and bottom bars had a strain of 0.003 and 0.0046, respectively. Strains in the longitudinal bars were less than the yielding strain of 0.00694 (for PSB 1080 bars) indicating that they did not yield at the time of shear failure. However, a strain of 0.0044 in stirrups that is more than the yielding strain of 0.0023 (for Grade 60 steel bars) indicated that the stirrups yielded during the shear failure.

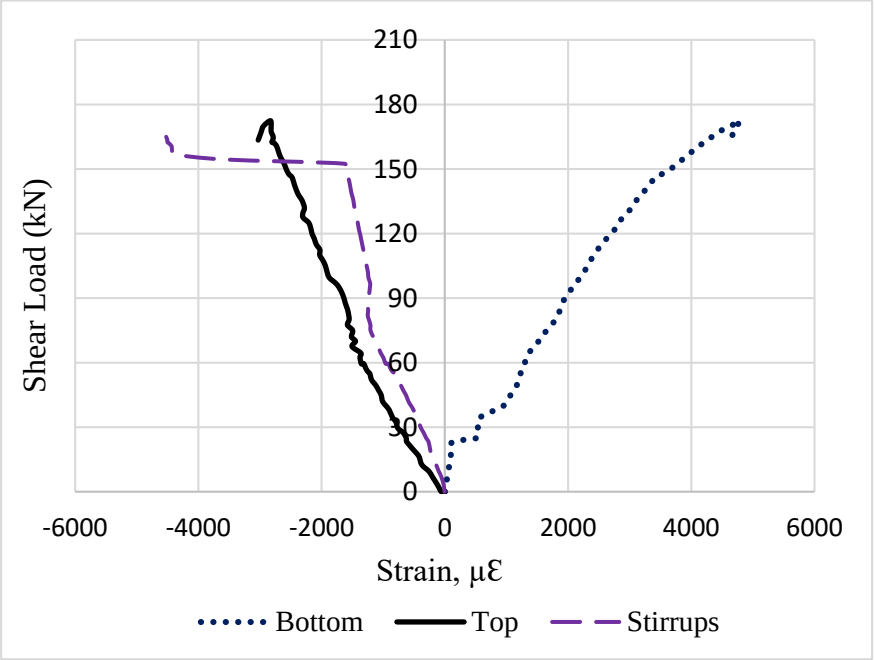

Figure 4.4: Strains in top and bottom longitudinal rebars and in stirrups of beam A-1

4.2.2. Beam A-2

Beam A-2 cast with 2.0% steel fibers, 3ϕ15mm longitudinal reinforcements in tension zone (ρ=1.935%), 2ϕ15mm longitudinal reinforcements in compression zone, 10 mm @ 200 mm shear reinforcement center-to-center and *a/d* ratio =1.8.

The first crack detected in flexural zone at shear load of 28 kN corresponding to a displacement of 2.08 mm. With increasing load, hairline cracks increased and diagonal cracks appeared in shear zones at 78 kN corresponding to a displacement of 7.46 mm and

propagated to compression zone till failure and beam failed in pure shear at an ultimate shear load of 186 kN corresponding to a mid-span deflection of 23.3 mm. Shear load-mid-span deflection response is shown in Figure 4.5.

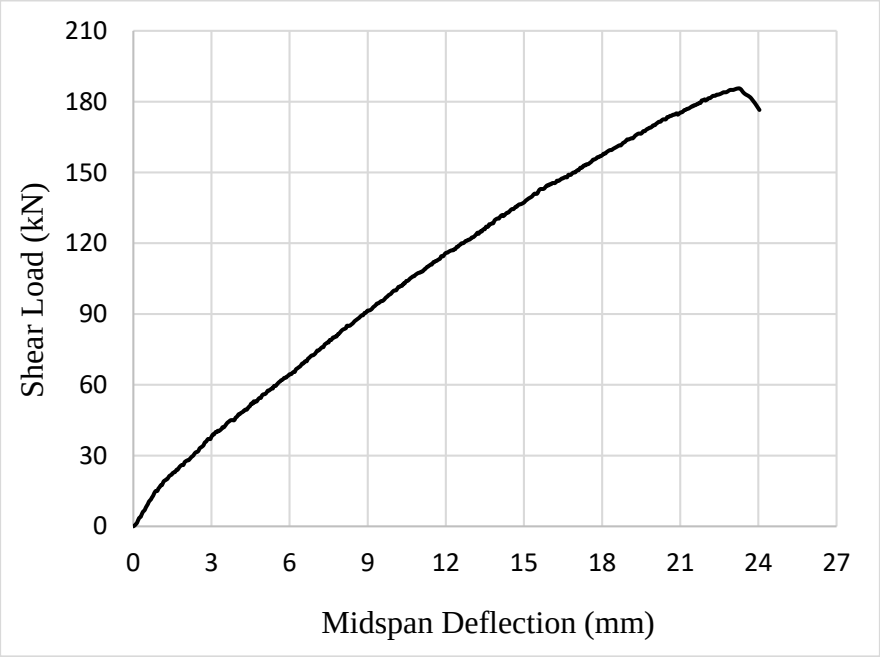

Figure 4.5: Shear load-mid-span deflection curve for beam A-2

Similar to beam A-1, it can be observed from Figures 4.6 that the minor hairline cracks start developing in flexural zone at initial stage of loading followed by the development of diagonal cracks in the shear zone of the beam. The beam specimen failed in pure shear with the development of wide diagonal cracks near supports. This can be attributed to the fact that the beam A-2 had more shear reinforcement than the other eight beams. Due to more shear reinforcement in beam, the load is distributed over a smaller area that resulted into wider and single crack.

Figure 4.6: Mode of failure for beam A-2

Figure 4.7 shows the plots of strains in concrete measured during load testing of beam A-2 with the help of strain gauges attached at different locations. Concrete strain at the top of the beam was 0.0028 at the time of failure that is less than crushing strain (0.0035) of the UHPC mixture (2.0% fiber content) obtained from compression stress-strain behavior. This indicates that no crushing of concrete occurred at the top of the beam when beam failed in pure shear diagonally near the support, as shown in Figure 4.6.

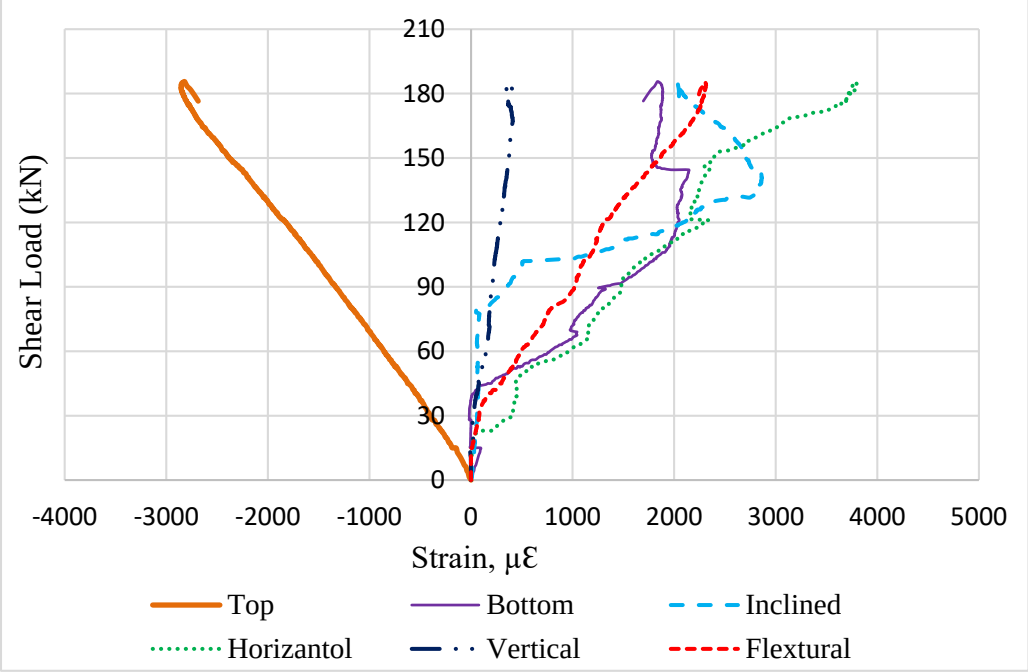

Figure 4.7: Strains in concrete at different locations on the surface of beam A-2

Figure 4.8 shows the plots of strains in longitudinal steel bars and shear stirrups at the time of failure. The top and bottom bars had a strain of 0.0028 and 0.0057, respectively. Strains in the longitudinal bars were less than the yielding strain of 0.00694 (for PSB 1080 bars)

indicating that they did not yield at the time of shear failure. However, a strain of 0.0056 in stirrups that is more than the yielding strain of 0.0023 (for Grade 60 steel bars) indicated that the stirrups yielded during the shear failure.

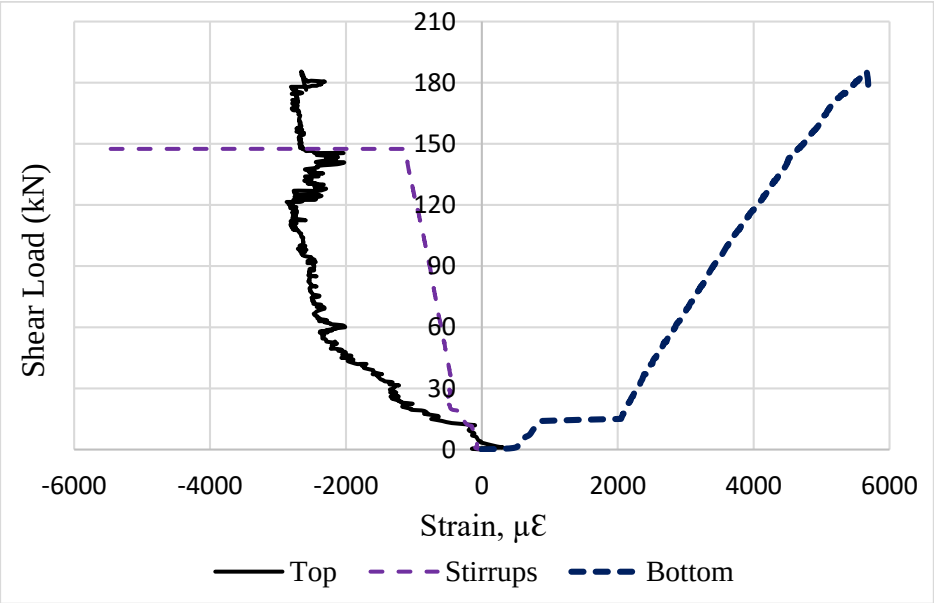

Figure 4.8: Strains in top and bottom longitudinal rebars and in stirrups of beam A-2

4.2.3. Beam B-1

Beam B-1 cast with 1.0% steel fibers, 3ϕ15mm longitudinal reinforcements in tension zone (ρ=1.935%), 2ϕ15mm longitudinal reinforcements in compression zone, 10 mm @ 370 mm shear reinforcement center-to-center and *a/d* ratio =1.8.

The first crack detected in flexural zone at shear load of 19 kN corresponding to a displacement of 1.0 mm. With the increasing load, hairline cracks increased and diagonal cracks appeared in shear zones at 54.5 kN corresponding to a displacement of 4.16 mm and propagated to compression zone till failure and beam failed in pure shear at an ultimate shear load of 147.5 kN corresponding a 16.1 mm mid-span deflection. Shear load-mid-span deflection response is shown in Figure 4.9.

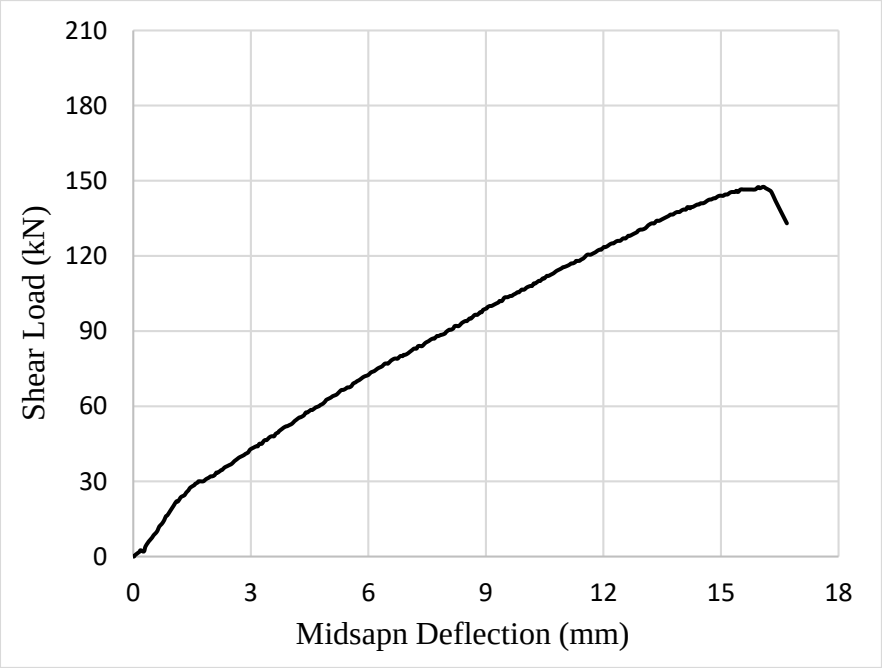

Figure 4.9: Shear load-mid-span deflection curve for beam B-1

It can be observed from Figures 4.10 that the minor hairline cracks start developing in flexural zone at initial stage of loading followed by the development of diagonal cracks in the shear zone of the beam. The beam specimen failed in pure shear with the development of lesser wide but multiple diagonal cracks near supports. The reason behind multiple and lesser wide cracks, as compared to beams A-1 and A-2, is the distribution of the load to concrete over a wider area due to lesser shear reinforcement.

Figure 4.10: Mode of failure for beams B-1

Figure 4.11 shows the plots of strains in concrete measured during load testing of beam B-1 with the help of strain gauges attached at different locations. Concrete strain at the top of

the beam was 0.0018 at the time of failure that is less than crushing strain (0.0033) of the UHPC mixture (1.0% fiber content) obtained from compression stress-strain behavior. This indicates that no crushing of concrete occurred at the top of the beam when beam failed in pure shear diagonally near the support, as shown in Figure 4.10.

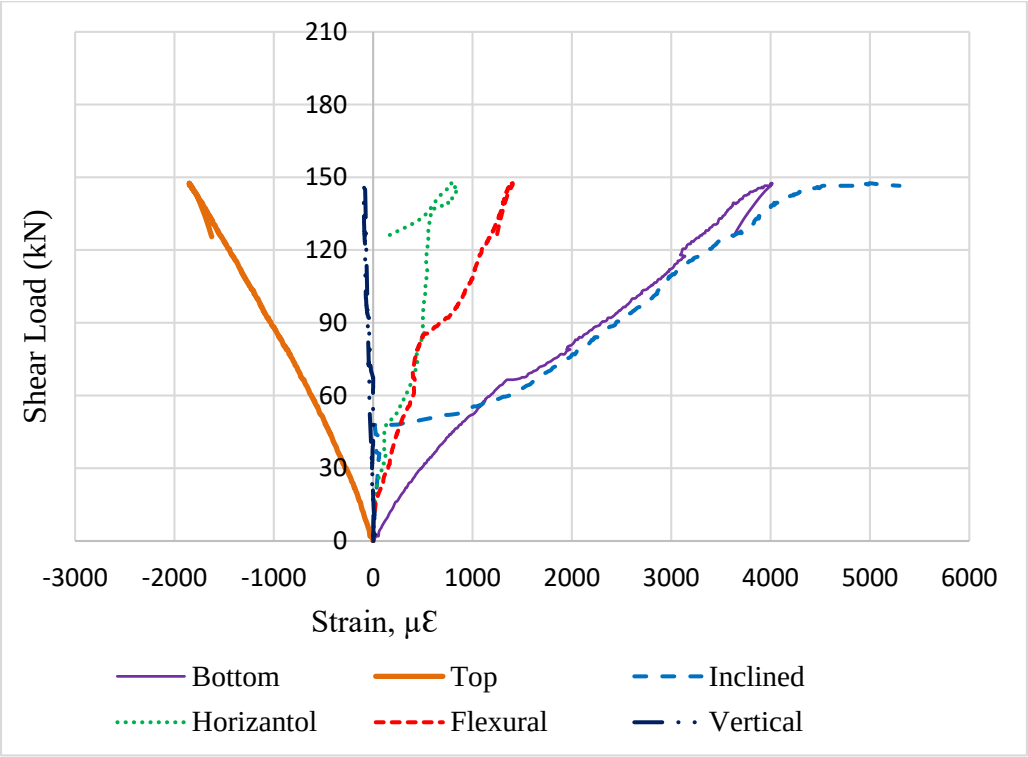

Figure 4.11: Strains in concrete at different locations on the surface of beam B-1

Figure 4.12 shows the plots of strains in longitudinal steel bars at the time of failure. The top and bottom bars had a strain of 0.0055 and 0.0057, respectively. Strains in the longitudinal bars were less than the yielding strain of 0.00694 (for PSB 1080 bars) indicating that they did not yield at the time of shear failure. However, a strain of 0.0064 in stirrups that is more than the yielding strain of 0.0023 (for Grade 60 bars) indicated that the stirrups yielded during the shear failure.

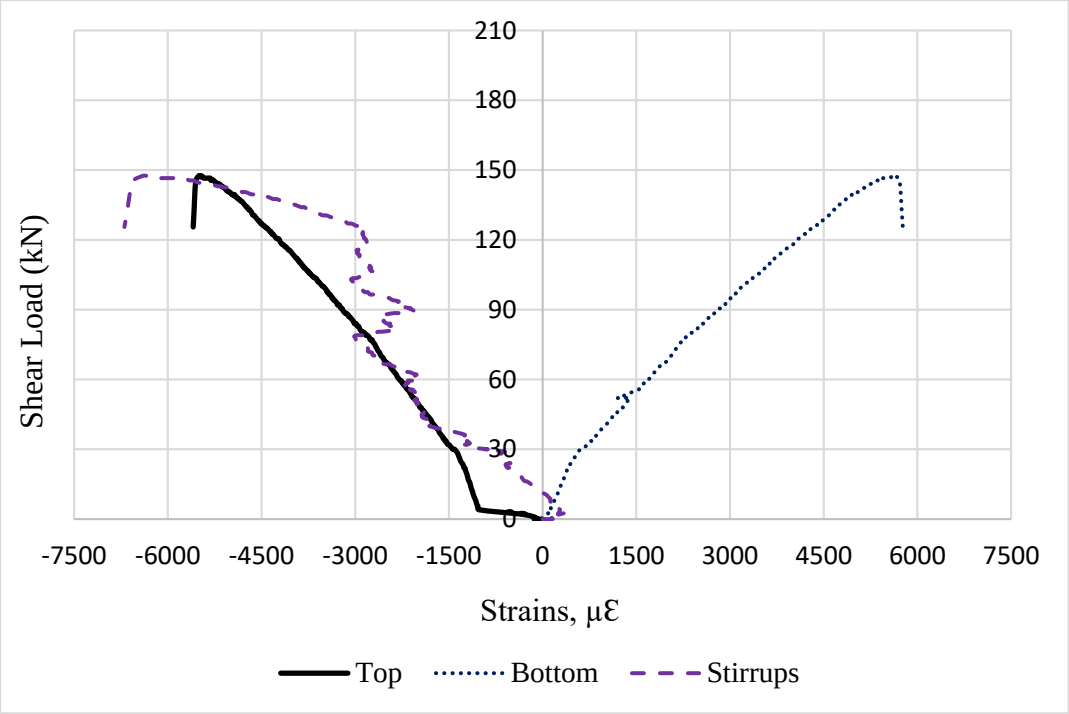

Figure 4.12: Strains in top and bottom longitudinal rebars and in stirrups of beam B-1

4.2.4. Beam B-2

Beam B-2 cast with 2.0% steel fibers, 3ϕ15mm longitudinal reinforcements in tension zone (ρ=1.935%), 2ϕ15mm longitudinal reinforcements in compression zone, 10 mm @ 370 mm shear reinforcement center-to-center and *a/d* =1.8.

The first crack detected in flexural zone at shear load of 21.5 kN corresponding to a displacement of 1.3 mm. With the increasing load, hairline cracks increased and diagonal cracks appeared at shear zones. Diagonal cracks started at 57.5 kN corresponding to a displacement of 4.93 mm and propagated to compression zone till failure and beam failed in pure shear at an ultimate shear load of 176 kN corresponding to a mid-span deflection of 18.06 mm. Shear load-mid-span deflection response is shown in Figure 4.13.

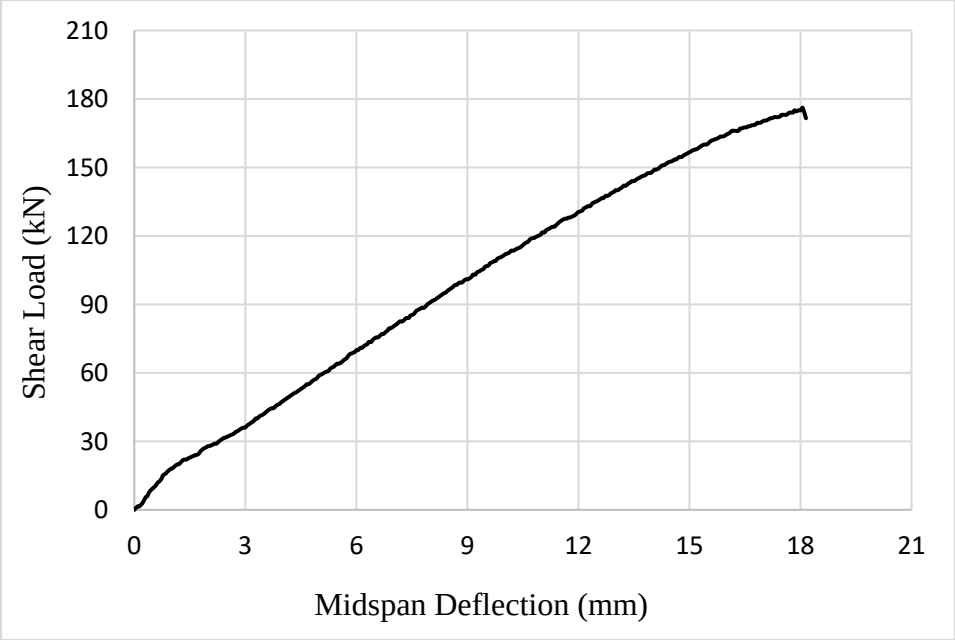

Figure 4.13: Shear load-mid-span deflection curve for beam B-2

Similar to the beam B-1, it can be observed from Figures 4.14 that the minor hairline cracks start developing in flexural zone at initial stage of loading followed by the development of diagonal cracks in the shear zone of the beam. The beam specimen failed in pure shear with the development of lesser wide but multiple diagonal cracks near supports. The reason behind multiple and lesser wide cracks is the distribution of the load to concrete over a wider area due to lesser shear reinforcement.

Figure 4.14: Mode of failure for beams B-2

Figure 4.15 shows the plots of strains in concrete measured during load testing of beam B-2 with the help of strain gauges attached at different locations. Concrete strain at the top of the beam was 0.0022 at the time of failure that is less than crushing strain (0.0035) of the

UHPC mixture (2.0% fiber content) obtained from compression stress-strain behavior. This indicates that no crushing of concrete occurred at the top of the beam when beam failed in pure shear diagonally near the support, as shown in Figure 4.14.

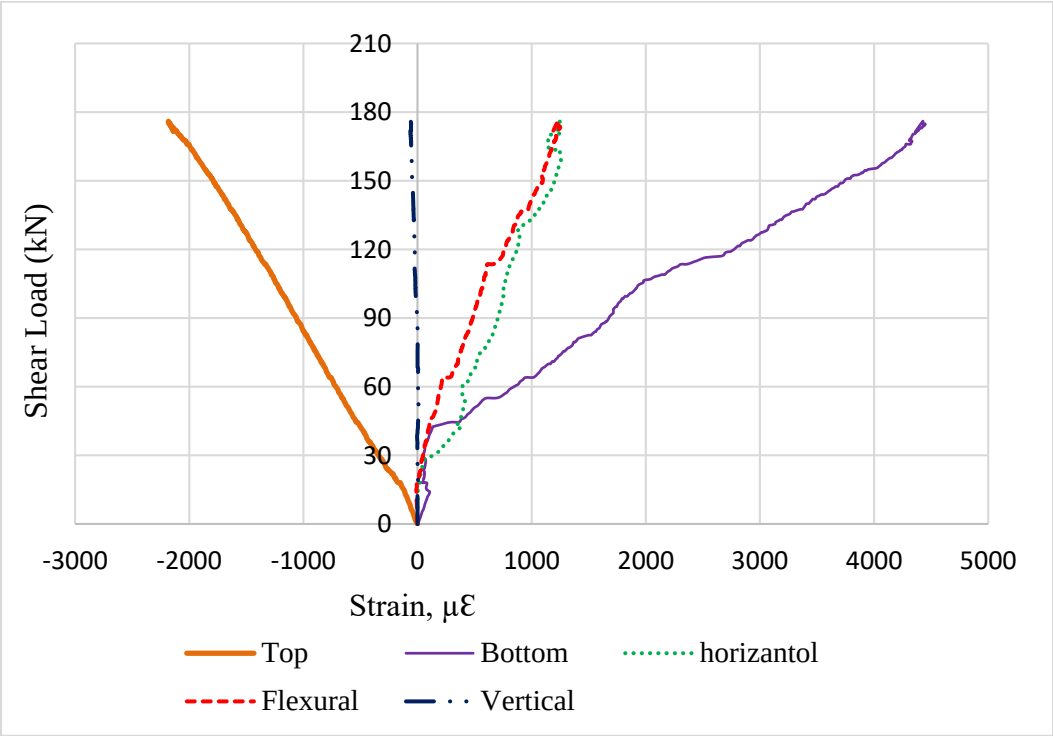

Figure 4.15: Strains in concrete at different locations on the surface of beam B-2

4.2.5. Beam C-1

Beam C-1 cast with 1.0% steel fibers, 5ϕ15mm longitudinal reinforcements in tension zone (ρ=3.226%), 2ϕ15mm longitudinal reinforcements in compression zone, 10 mm @ 370 mm shear reinforcement center-to-center and *a/d* ratio =1.8.

The first crack was detected in flexural zone at a shear load of 20 kN corresponding to a displacement of 1.46 mm. With the increasing load, hairline cracks increased and diagonal cracks appeared at shear zones. Diagonal cracks started at 60 kN corresponding to a displacement of 5.71 mm and propagated to compression zone till failure took place in pure

shear at an ultimate shear load of 155.5 kN corresponding to a mid-span deflection of 17.58 mm. Shear load-mid-span deflection response is shown in Figure 4.16.

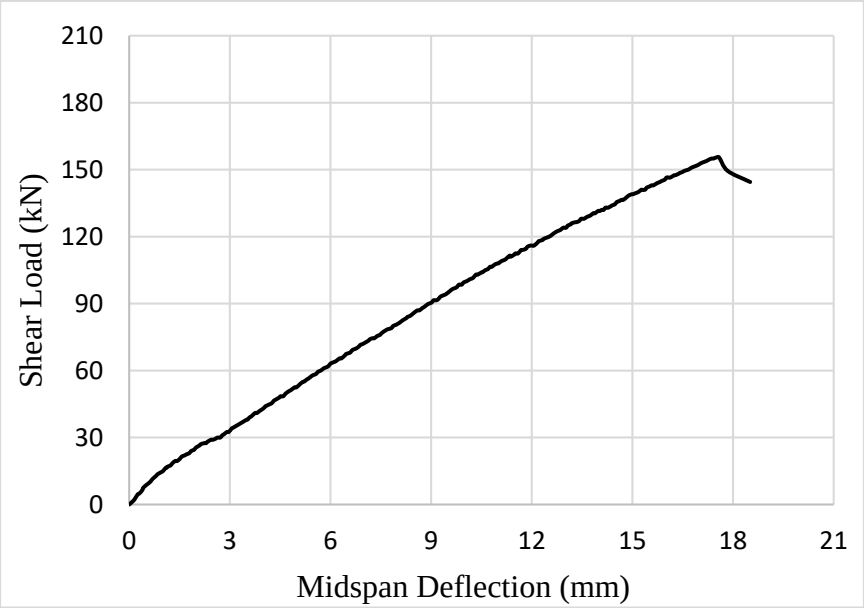

Figure 4.16: Shear load-mid-span deflection curve for beam C-1

It can be observed from Figures 4.17 that the minor hairline cracks start developing in flexural zone at initial stage of loading followed by the development of diagonal cracks in the shear zone of the beam. The beam specimen failed in pure shear with the development of lesser flexural cracks in the flexural zone. The reason behind less flexural cracks is the high percentage of longitudinal reinforcement.

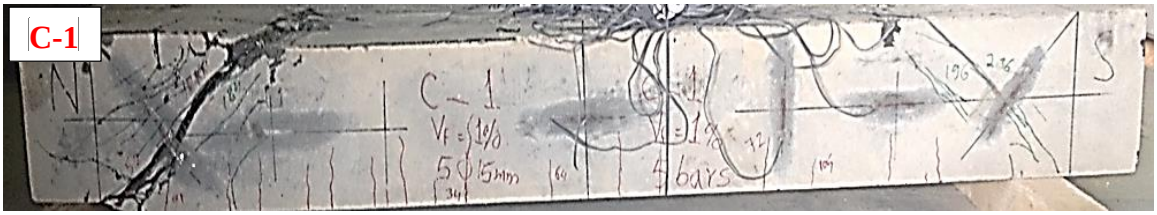

Figure 4.17: Mode of failure for beam C-1

Figure 4.18 shows the plots of strains in concrete measured during load testing of beam C-1 with the help of strain gauges attached at different locations. Concrete strain at the top of

the beam was 0.0018 at the time of failure that is less than crushing strain (0.0033) of the UHPC mixture (1.0% fiber content) obtained from compression stress-strain behavior. This indicates that no crushing of concrete occurred at the top of the beam when beam failed in pure shear diagonally near the support, as shown in Figure 4.17.

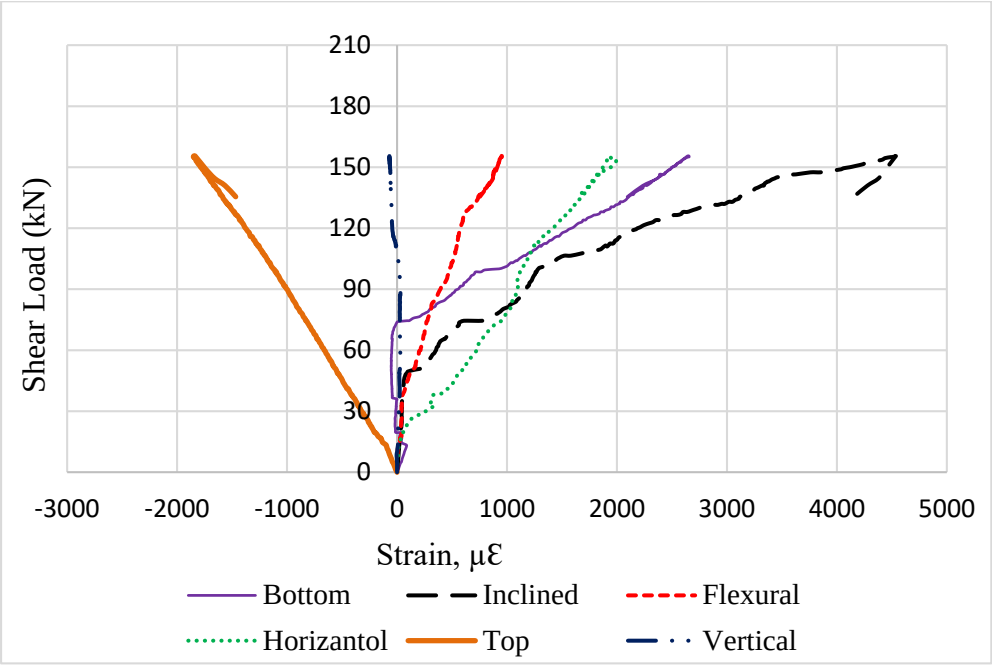

Figure 4.18: Strains in concrete at different locations on the surface of beam C-1

Figure 4.19 shows the plots of strains in longitudinal steel bars at the time of failure. The top and bottom bars had a strain of 0.0022 and 0.0052, respectively. Strains in the longitudinal bars were less than the yielding strain of 0.00694 (for PSB 1080 bars) indicating that they did not yield at the time of shear failure. However, a strain of 0.0045 in stirrups that is more than the yielding strain of 0.0023 (for Grade 60 steel bars) indicated that the stirrups yielded during the shear failure.

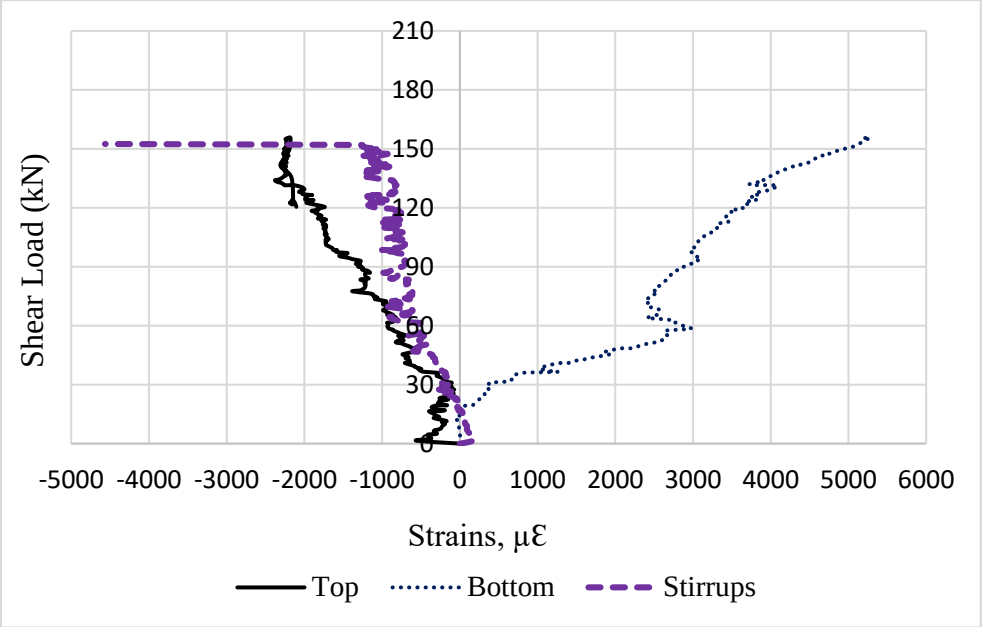

Figure 4.19: Strains in top and bottom longitudinal rebars and in stirrups of beam C-1

4.2.6. Beam C-2

Beam C-2 cast with 2.0% steel fibers, 5ϕ15mm longitudinal reinforcements in tension zone (ρ=3.226%), 2ϕ15mm longitudinal reinforcements in compression zone, 10 mm @ 370 mm shear reinforcement center-to-center and *a/d* ratio =1.8.

The first crack detected in flexural zone at a shear load of 22.5 kN corresponding to a displacement of 2.85 mm. With the increasing load, hairline cracks increased and diagonal cracks appeared at shear zones. Diagonal cracks started at 67.5 kN corresponding to a displacement of 6.71 mm and propagated to compression zone till failure and beam failed in pure shear at an ultimate shear load of 182.5 kN corresponding to a mid-span deflection of 19.86 mm. Shear load-mid-span deflection response is shown in Figure 4.20.

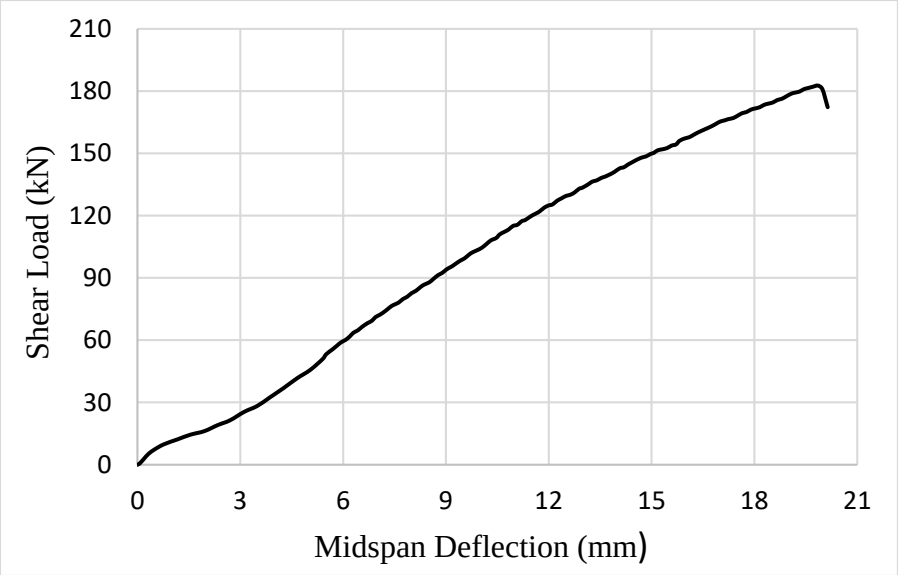

Figure 4.20: Shear load-mid-span deflection curve for beam C-2

It can be observed from Figures 4.21 that the minor hairline cracks start developing in flexural zone at initial stage of loading followed by the development of diagonal cracks in the shear zone of the beam. The beam specimen failed in pure shear with the development of lesser flexural cracks in the flexural zone. The reason behind less flexural cracks is the high percentage of longitudinal reinforcement. In addition, these flexural cracks were lesser than beam C-1 because of higher fiber content.

Figure 4.21: Mode of failure for beam C-2

4.2.7. Beam D-1

Beam D-1 cast with 1.0% steel fibers, 3ϕ15mm longitudinal reinforcements in tension zone (ρ=1.935%), 2ϕ15 mm longitudinal reinforcements in compression zone, 10 mm @ 370 mm shear reinforcement center-to-center and *a/d* ratio =2.6.

The first crack detected in flexural zone at a shear load of 15 kN corresponding to a displacement of 0.84 mm. With the increasing load, hairline cracks increased and diagonal cracks appeared at shear zones. Diagonal cracks started at a load of 41 kN corresponding to a displacement of 4.56 mm and propagated to compression zone till failure and beam failed in pure shear at an ultimate shear load of 104 kN corresponding to a mid-span deflection of 14.19 mm. Shear load-mid-span deflection response is shown in Figure 4.22.

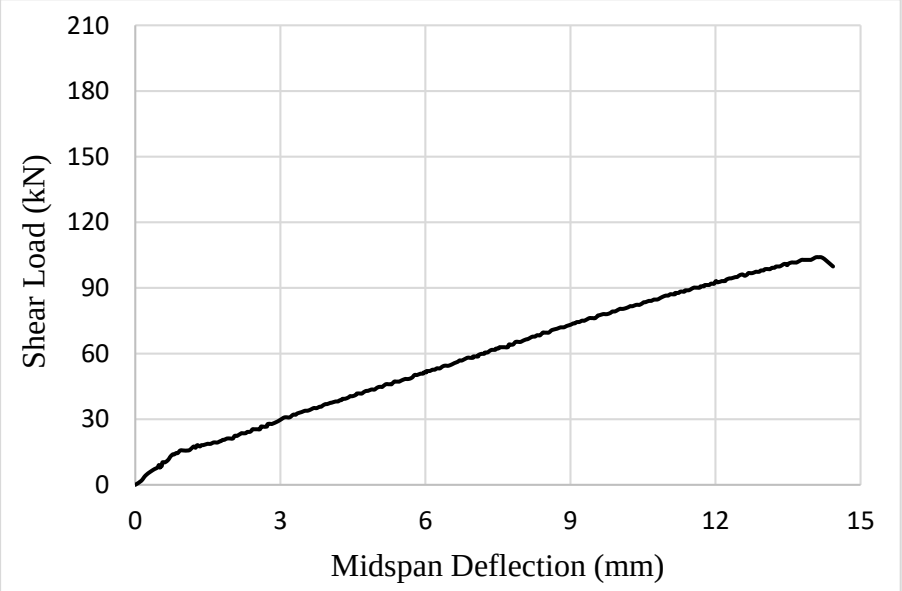

Figure 4.22: Shear load-mid-span deflection curve for beam D-1

It can be observed from Figures 4.23 that the minor hairline cracks start developing in flexural zone at initial stage of loading followed by the development of diagonal cracks in the shear zone of the beam. The beam specimen failed in pure shear with the development of more flexural cracks in the flexural zone. The reason behind more flexural cracks is the higher *a/d* ratio =2.6.

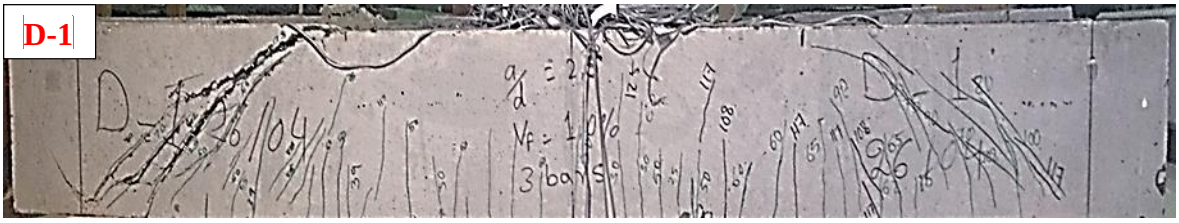

Figure 4.23: Mode of failure for beam D-1

Figure 4.24 shows the plots of strains in concrete measured during load testing of beam D-1 with the help of strain gauges attached at different locations. Concrete strain at the top of the beam was 0.0021 at the time of failure that is less than crushing strain (0.0033) of the UHPC mixture (1.0% fiber content) obtained from compression stress-strain behavior. This indicates that no crushing of concrete occurred at the top of the beam when beam failed in pure shear diagonally near the support, as shown in Figure 4.23.

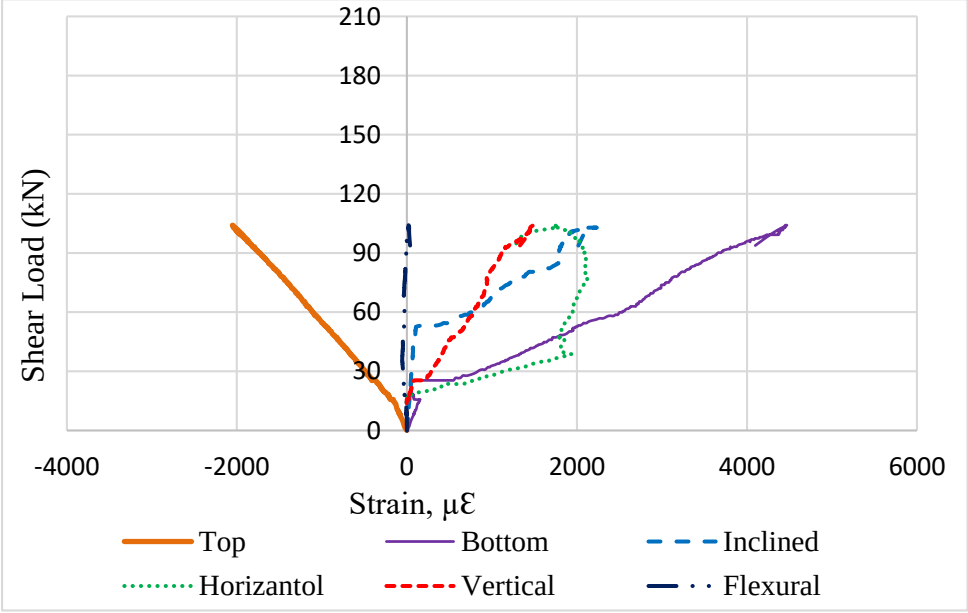

Figure 4.24: Strains in concrete at different locations on the surface of beam D-1

4.2.8. Beam D-2

Beam D-2 cast with 1.0% steel fibers, 5ϕ15mm longitudinal reinforcements in tension zone (ρ=3.226%), 2ϕ15 mm longitudinal reinforcements in compression zone, 10mm @ 370mm shear reinforcement center-to-center and *a/d* ratio =2.6.

The first crack detected in flexural zone at a shear load of 18 kN corresponding to a displacement of 0.92 mm. With the increasing load, hairline cracks increased and diagonal cracks appeared at shear zones. Diagonal cracks started at a load of 43.5 kN corresponding to a displacement of 3.54 mm and propagated to compression zone till failure and beam failed in pure shear at an ultimate shear load of 114.5 kN corresponding to a mid-span deflection of 13.18 mm. Shear load-mid-span deflection response is shown in Figure 4.25.

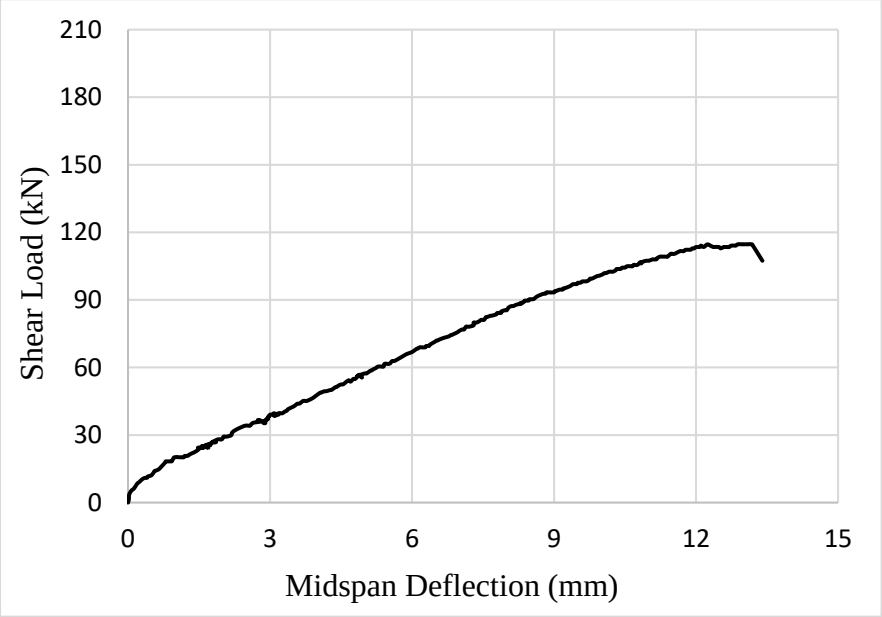

Figure 4.25: Shear load-mid-span deflection curve for beam D-2

It can be observed from Figures 4.26 that the minor hairline cracks start developing in flexural zone at initial stage of loading followed by the development of diagonal cracks in the shear zone of the beam. The beam specimen failed in pure shear with the development of more flexural cracks in the flexural zone. The reason behind more flexural cracks is the higher *a/d* ratio =2.6. In addition, theses flexural cracks were lesser than that of beam D-1 because of higher, ρ.

Figure 4.26: Mode of failure for beam D-2

Figure 4.27 shows the plots of strains in concrete measured during load testing of beam D-2 with the help of strain gauges attached at different locations. Concrete strain at the top of the beam was 0.0017 at the time of failure that is less than crushing strain (0.0033) of the UHPC mixture (1.0% fiber content) obtained from compression stress-strain behavior. This indicates that no crushing of concrete occurred at the top of the beam when beam failed in pure shear diagonally near the support, as shown in Figure 4.26.

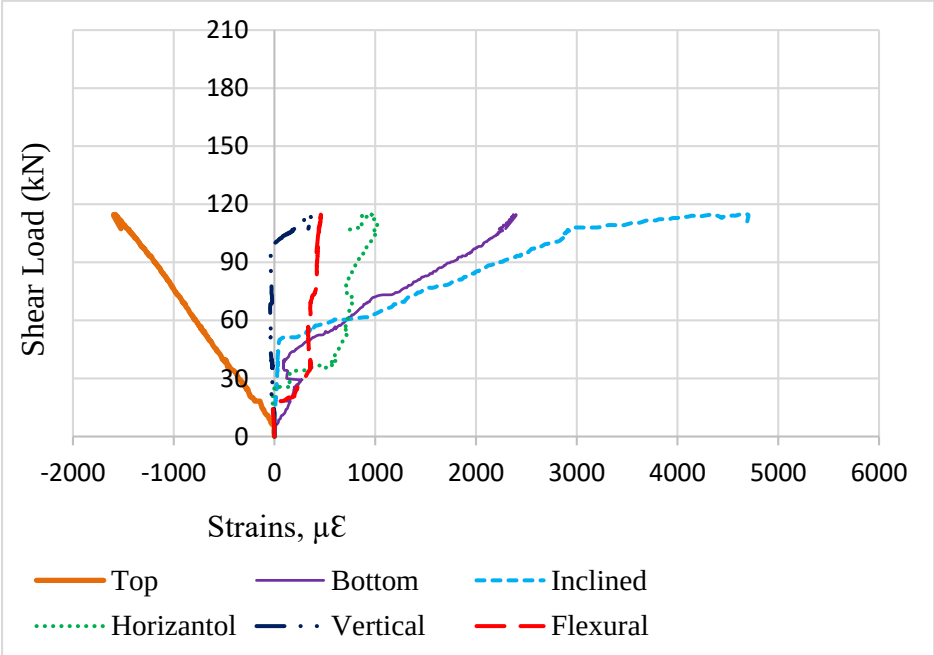

Figure 4.27: Strains in concrete at different locations on the surface of beam D-2

4.2.9. Beam E-1

Beam E-1 cast with 2.0% steel fibers, 3ϕ15mm longitudinal reinforcements in tension zone (ρ=1.935%), 2ϕ15mm longitudinal reinforcements in compression zone, 10 mm @ 370 mm shear reinforcement center-to-center and *a/d* ratio =2.6.

The first crack detected in flexural area at a shear load of 19.5 kN corresponding to a displacement of 0.91 mm. With the increasing load, hairline cracks increased and diagonal cracks appeared at shear zones. Diagonal cracks started at a load of 40 kN corresponding to a displacement of 3.14 mm and propagated to compression zone till failure and beam failed in pure shear at an ultimate shear load of 116 kN corresponding to a mid-span deflection of 15.03 mm. Shear load-mid-span deflection response is shown in Figure 4.28.

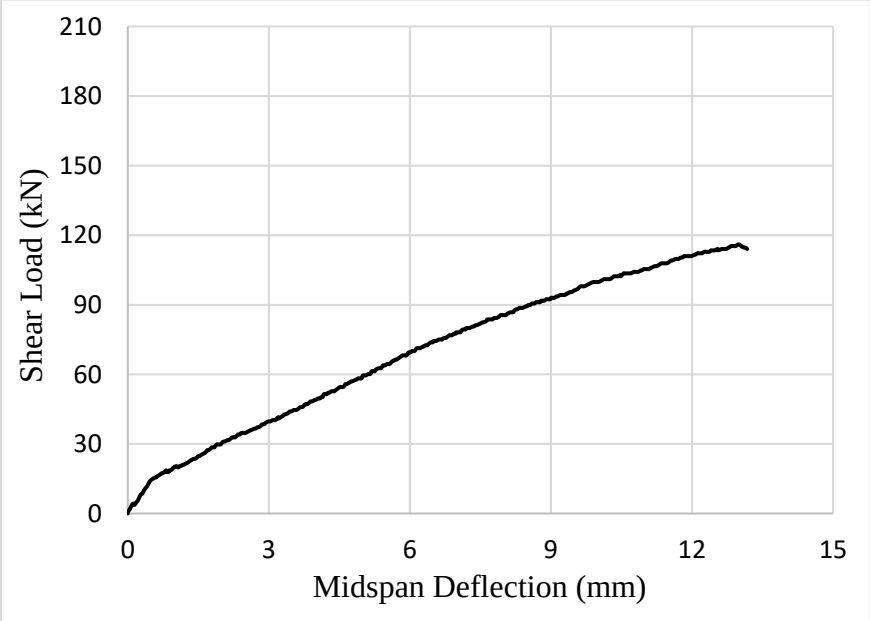

Figure 4.28: Shear load-mid-span deflection curve for beam E-1

It can be observed from Figures 4.29 that the minor hairline cracks developed in flexural zone at an initial stage of loading followed by the development of diagonal cracks in the shear zone of the beam. The beam specimen failed in pure shear with the development of

more flexural cracks in the flexural zone. The reason behind more flexural cracks is the higher *a/d* ratio =2.6. In addition, theses flexural cracks were lesser than that of beam D-1 because of higher fiber content.

Figure 4.29: Mode of failure for beam E-1

Figure 4.30 shows the plots of strains in concrete measured during load testing of beam E-1 with the help of strain gauges attached at different locations. Concrete strain at the top of the beam was 0.0028 at the time of failure that is less than crushing strain (0.0035) of the UHPC mixture (2.0% fiber content) obtained from compression stress-strain behavior. This indicates that no crushing of concrete occurred at the top of the beam when beam failed in pure shear diagonally near the support, as shown in Figure 4.29.

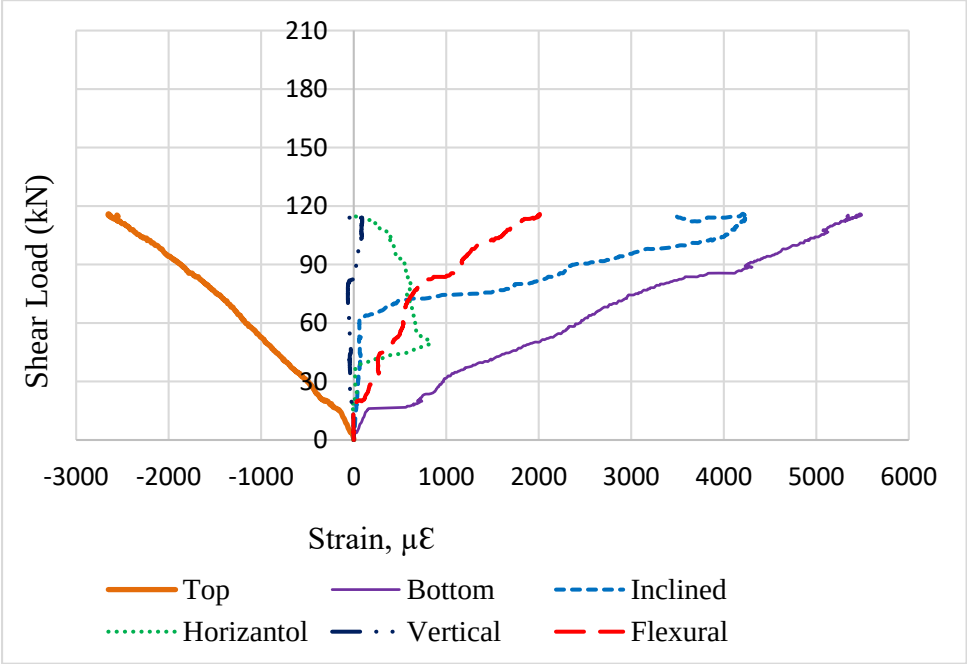

Figure 4.30: Strains in concrete at different locations on the surface of beam E-1

Figure 4.31 shows the plots of strains in longitudinal steel bars at the time of failure. The top and bottom bars had a strain of 0.0028 and 0.0044, respectively. Strains in the longitudinal bars were less than the yielding strain of 0.00694 (for PSB 1080 bars) indicating that they did not yield at the time of shear failure. However, a strain of 0.0059 in stirrups that is more than the yielding strain of 0.0023 (for Grade 60 steel bars) indicated that the stirrups yielded during the shear failure.

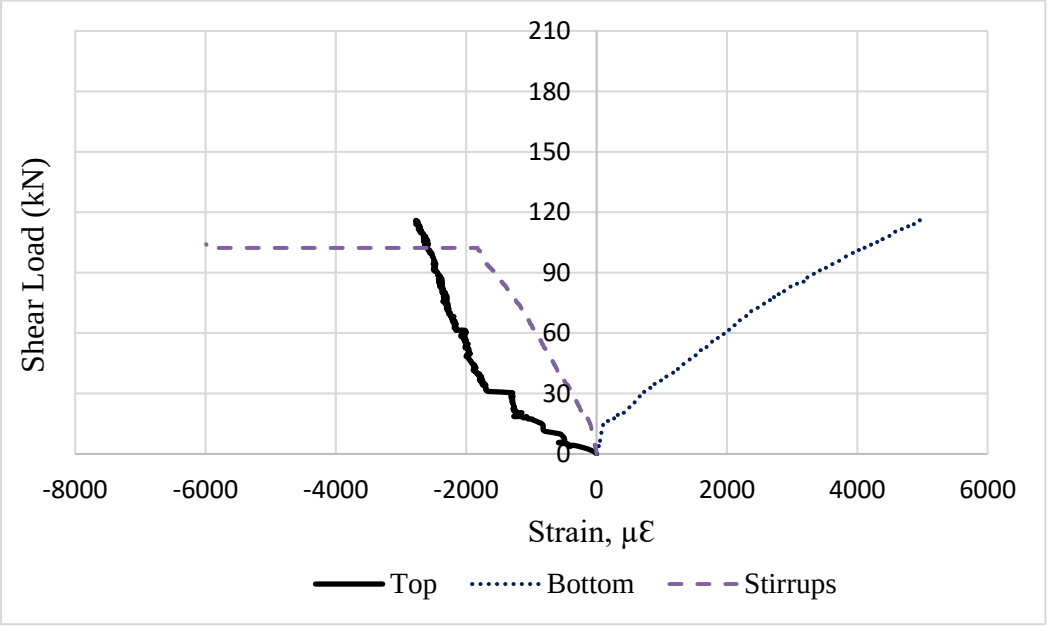

Figure 4.31: Strains in top and bottom longitudinal rebars and in stirrups of beam E-1

4.2.10. Beam E-2

Beam E-2 cast with 2.0% steel fibers, 5ϕ15mm longitudinal reinforcements in tension zone (ρ=3.226%), 2ϕ15mm longitudinal reinforcements in compression zone, 10 mm @ 370 mm shear reinforcement center-to-center and *a/d* ratio =2.6.

The first crack detected in flexural zone at a shear load of 21 kN corresponding to a displacement of 1.98 mm. With the increasing load, hairline cracks increased and diagonal cracks appeared at shear zones. Diagonal cracks started at a load of 53.5 kN corresponding

to a displacement of 5.43 mm and propagated to compression zone till failure and beam failed in pure shear at an ultimate shear load of 125 kN corresponding to a mid-span deflection of 16.18 mm. Shear load-mid-span deflection response is shown in Figure 4.32.

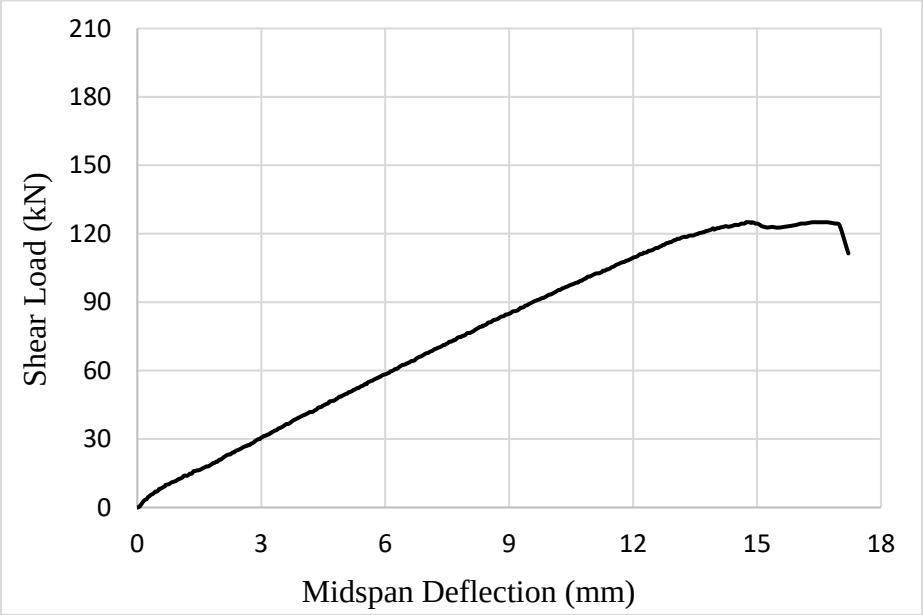

Figure 4.32: Shear load-mid-span deflection curve for beam E-2

It can be observed from Figures 4.33 that the minor hairline cracks start developing in flexural zone at initial stage of loading followed by the development of diagonal cracks in the shear zone of the beam. The beam specimen failed in pure shear with the development of more flexural cracks in the flexural zone. The reason behind more flexural cracks is the higher *a/d* ratio =2.6. In addition, theses flexural cracks were lesser than beam D-2 because of higher fiber content.

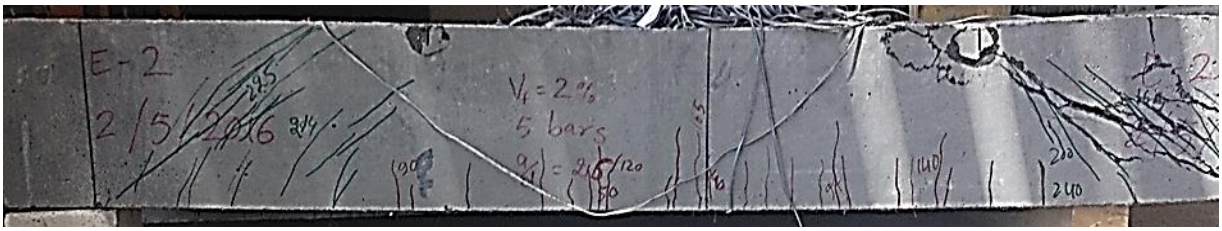

Figure 4.33: Mode of failure for beam E-2

Figure 4.34 shows the plots of strains in concrete measured during load testing of beam E-2 with the help of strain gauges attached at different locations. Concrete strain at the top of the beam was 0.0028 at the time of failure that is less than crushing strain (0.0035) of the UHPC mixture (2.0% fiber content) obtained from compression stress-strain behavior. This indicates that no crushing of concrete occurred at the top of the beam when beam failed in pure shear diagonally near the support, as shown in Figure 4.33.

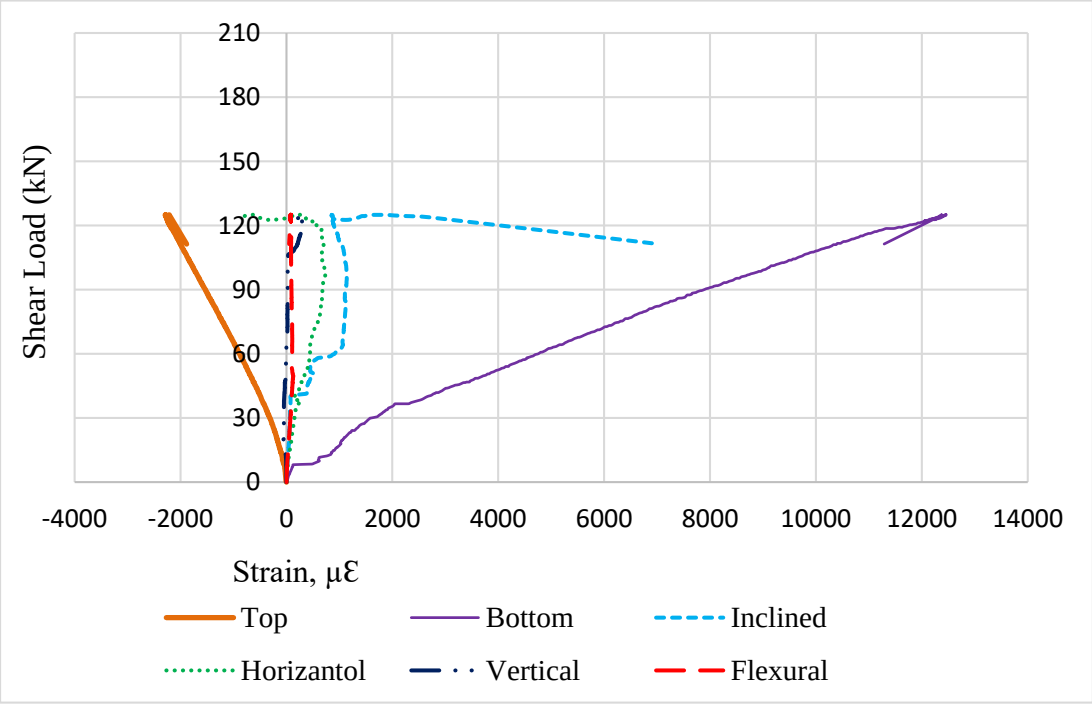

Figure 4.34: Strains in concrete at different locations on the surface of beam E-2

The magnitudes of the shear load capacities and mid-span deflection at different stages (initial cracking, diagonal cracking and ultimate loads), and modes of failure are summarized in Table 4.1:

Table 4.1: Results of four-point loading test on beam specimens

Beam	First Cracking		Diagonal cracking		Ultimate		Modes of Failure
	F_{cr} (kN)	Δ_{fr} (mm)	V_{cr} (kN)	Δ_{cr} (mm)	V_u (kN)	Δ_u (mm)	
A-1	24.0	1.08	59.0	5.10	172.5	21.14	Shear
A-2	28.0	2.08	78.0	7.46	186.0	23.30	Shear
B-1	19.0	1.00	54.5	4.16	147.5	16.1	Shear
B-2	21.5	1.30	57.5	4.93	176.0	18.06	Shear
C-1	20.0	1.46	60.0	5.71	155.5	17.85	Shear
C-2	22.5	2.85	67.5	6.71	182.5	19.86	Shear
D-1	15.0	0.84	41.0	4.56	104.0	14.19	Shear
D-2	18.0	0.92	43.5	3.54	114.5	13.18	Shear
E-1	19.5	0.91	40.0	3.14	116.0	15.03	Shear
E-2	18.0	2.98	51.5	5.43	125.0	16.18	Shear

F_{cr}, first cracking load; Δ_{fr}, mid-span deflection at first cracking; V_{cr}, diagonal cracking load; Δ_{cr}, mid-span deflection at diagonal cracking; V_u, ultimate shear load; Δ_u, ultimate mid-span deflection.

4.3. Effect of the Key Parameters on Shear Behavior of Beams

4.3.1. Effect of Volume Fraction of Steel Fibers (V_f)

A higher fiber content was found to be beneficial against flexural cracking as evident from the comparison of the cracking patterns of beams A-1 and A-2 in Figure 4.35 and beams C-1 and C-2 in Figure 4.36. The beams A-1 and C-1 with 1.0% fibers had relatively more flexural cracks than the beams A-2 and C-2 with 2.0% fibers.

(a)

(b)

Figure 4.35: Comparison of modes of failure for beams; a) V_f=1.0% and; b) V_f=2.0%

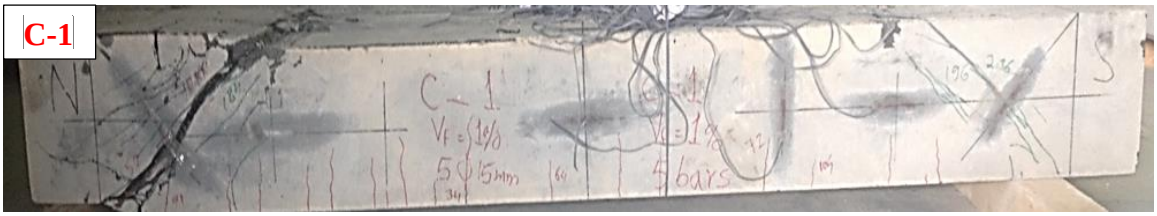

(a)

(b)

Figure 4.36: Comparison of modes of failure for beams; a) V_f=1.0% and; b) V_f=2.0%

The ultimate shear capacity was higher at higher fiber content. Effect of, V_f, on shear load capacities and mid-span deflections was more for beams having lower, ρ, and lower *a/d* ratio as can be seen from Figures 4.37, and 4.38, respectively. It can be observed from Table 4.1 that the shear loads corresponding to the initiation of hairline cracks in the flexural zone, F_{cr}, and initiation of diagonal cracks in shear zone, V_{cr}, are also higher at higher fiber content.

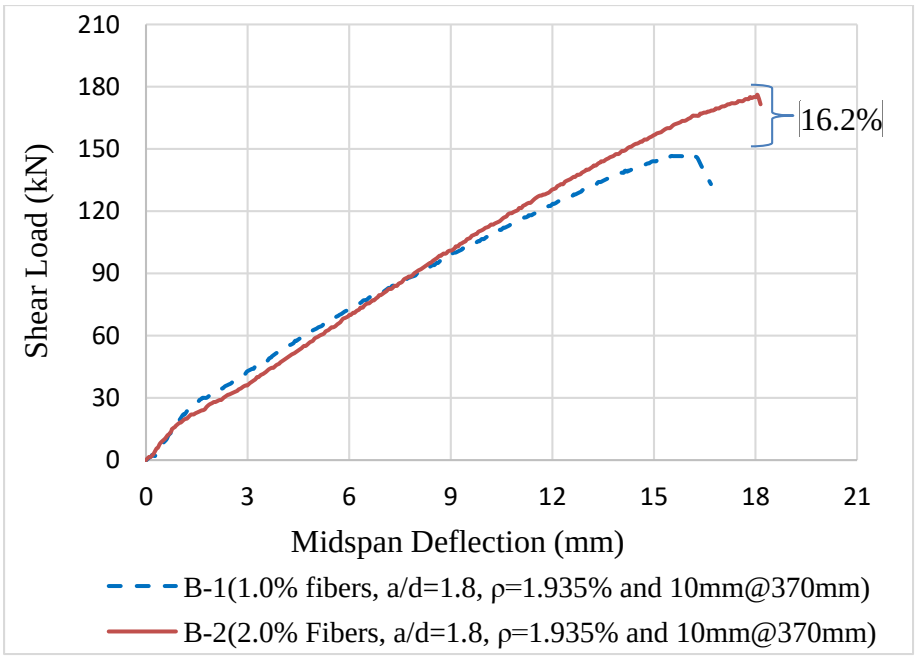

(a)

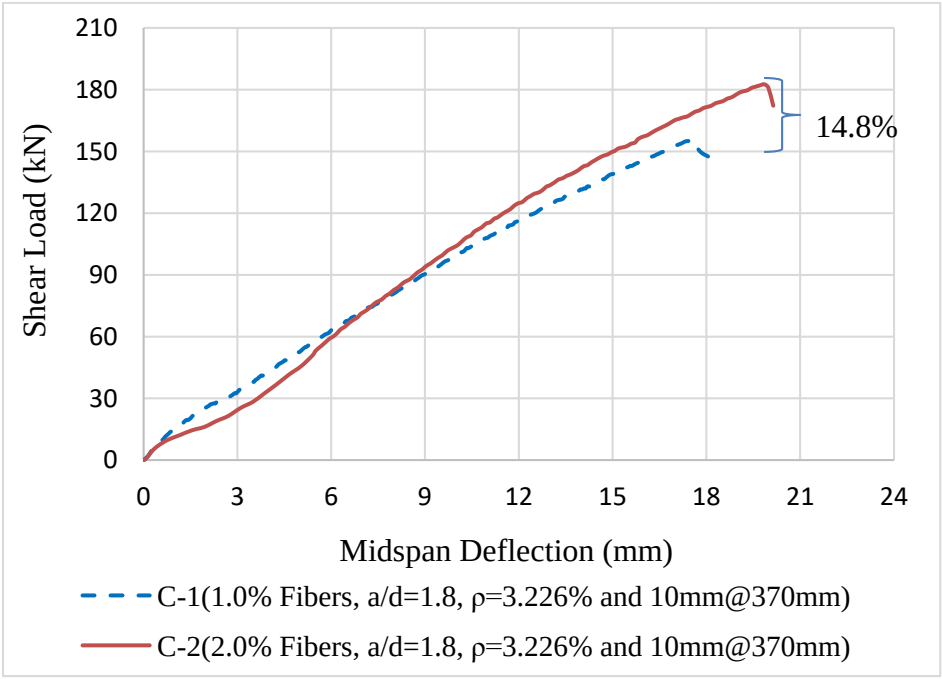

(b)

Figure 4.37: Effect of, V_f, on shear behavior of beams having; a) ρ=1.935%; and b) ρ=3.226%

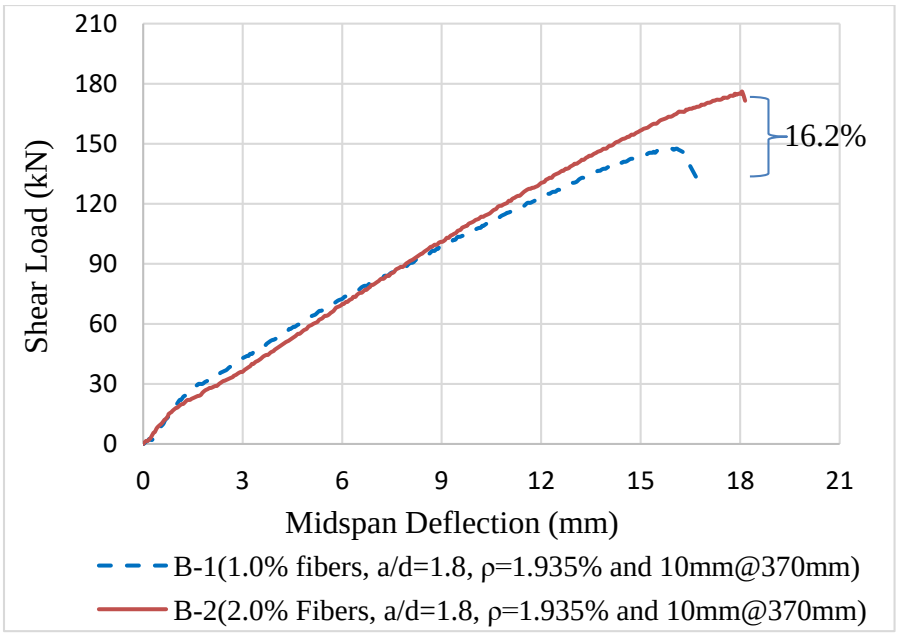

(a)

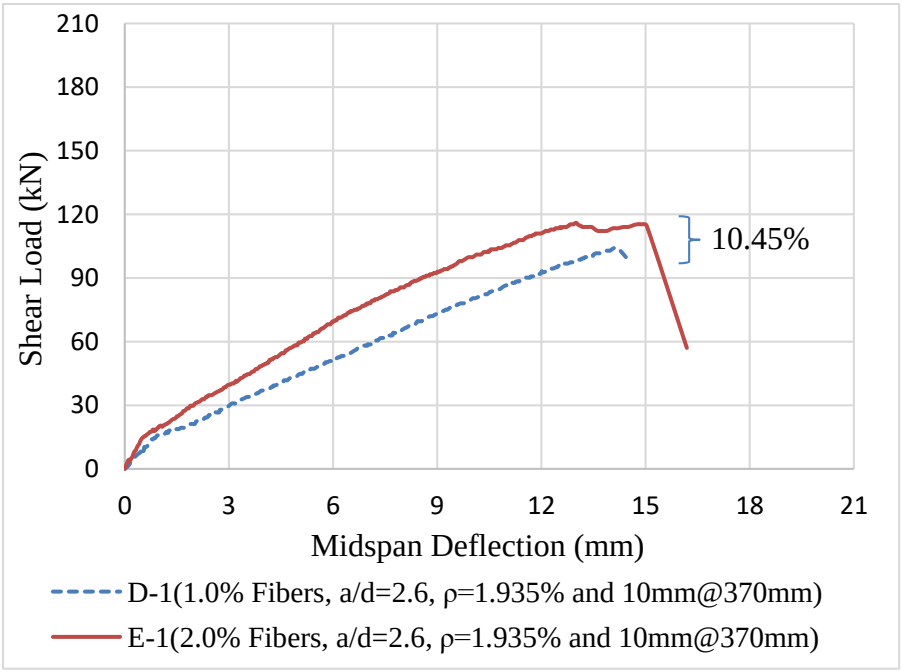

(b)

Figure 4.38: Effect of, V_f, on shear behavior of beams having; a) *a/d*=1.8; and b) *a/d*=2.6

4.3.2. Effect of Shear Span to Effective Depth Ratio (*a/d*)

A lower *a/d* ratio was found to be beneficial against flexural cracking as evident from Figures 4.39 and 4.40. The beams D-1 and D-2 with *a/d*=2.6 had more flexural cracks than the beams B-1 and C-1 with *a/d*=1.8.

(a)

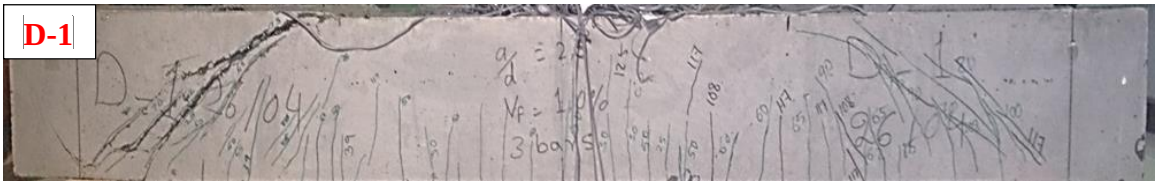

(b)

Figure 4.39: Comparison of modes of failure for beams; a) *a/d*=1.8 and; b) *a/d*=2.6

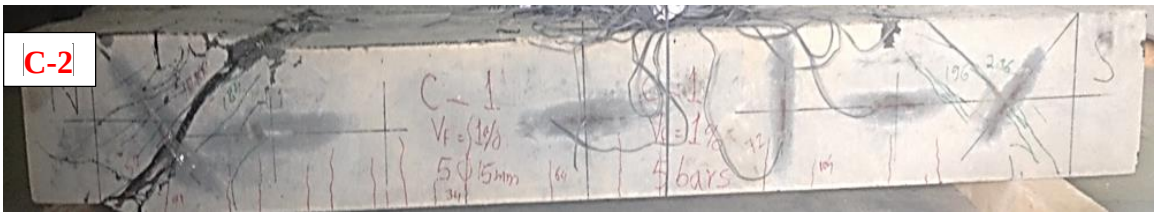

(a)

(b)

Figure 4.40: Comparison of modes of failure for beams; a) *a/d*=1.8 and; b) *a/d*=2.6

Beam specimens belonging to series D and E, with higher *a/d* ratio than beams of series A, B and C, had much lower F_{cr}, V_{cr}, V_u, and ultimate mid-span deflection, Δ_u (Table 4.1).

This indicates a very significant reduction in shear capacity of beams with increase in the *a/d* ratio. The reduction in the shear capacity of the beams with increase in the *a/d* ratio may be attributed to the fact that with increase in the shear span, *a*, at the same effective depth, *d*, the bending moment increases at shear force remains same at a given applied load. Since the depth of neutral axis is much lower than the half of the depth of the beam, both normal and shear stresses developed at the mid-depth of the beam resulting into a compound tensile stress (resultant of normal and shear stresses) in the shear zone (between support and the point of application of the load *P/2*). The increase in the magnitude of compound tensile stress with increase in the bending moment at a higher shear span caused the diagonal cracking at a much lower load. Effect of *a/d* ratio on shear load capacities and mid-span deflections was more for beams having low, ρ, and high, V_f, as shown in Figures 4.41 and 4.42.

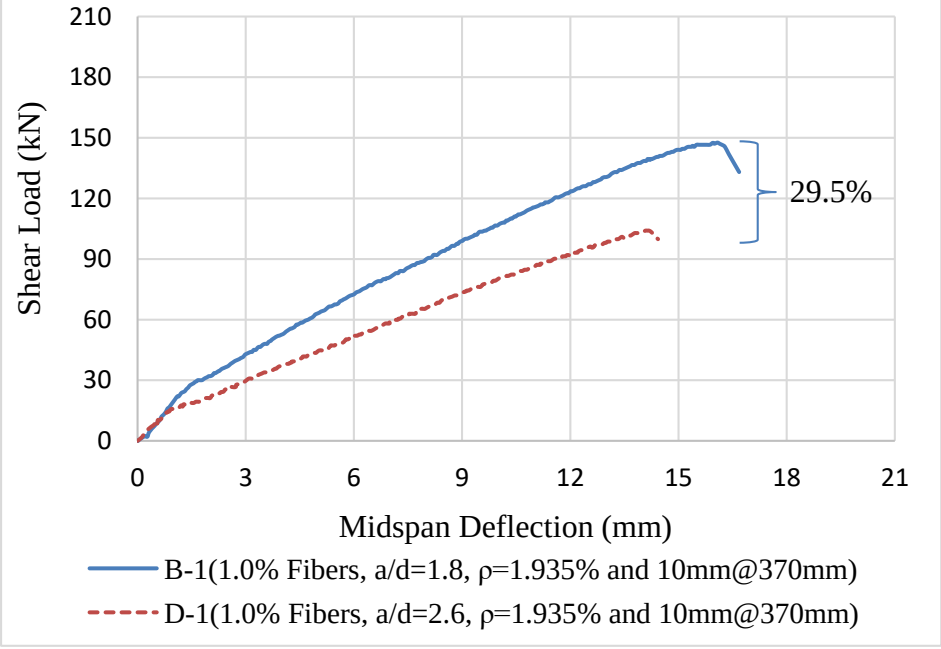

(a)

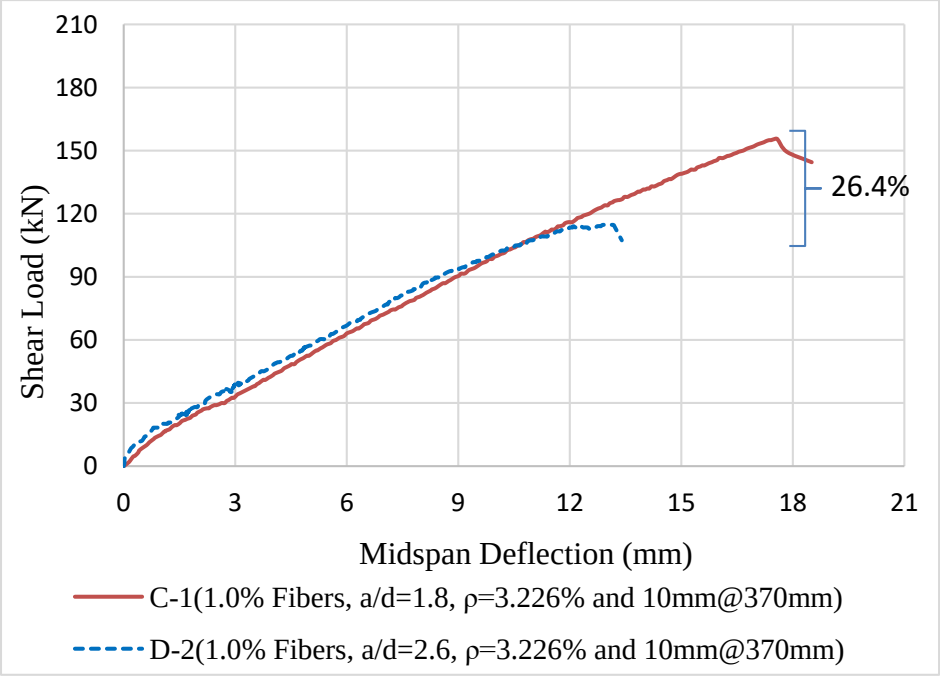

(b)

Figure 4.41: Effect of *a/d* ratio on shear behavior of beams: a)ρ=1.935% and b)ρ=3.226%

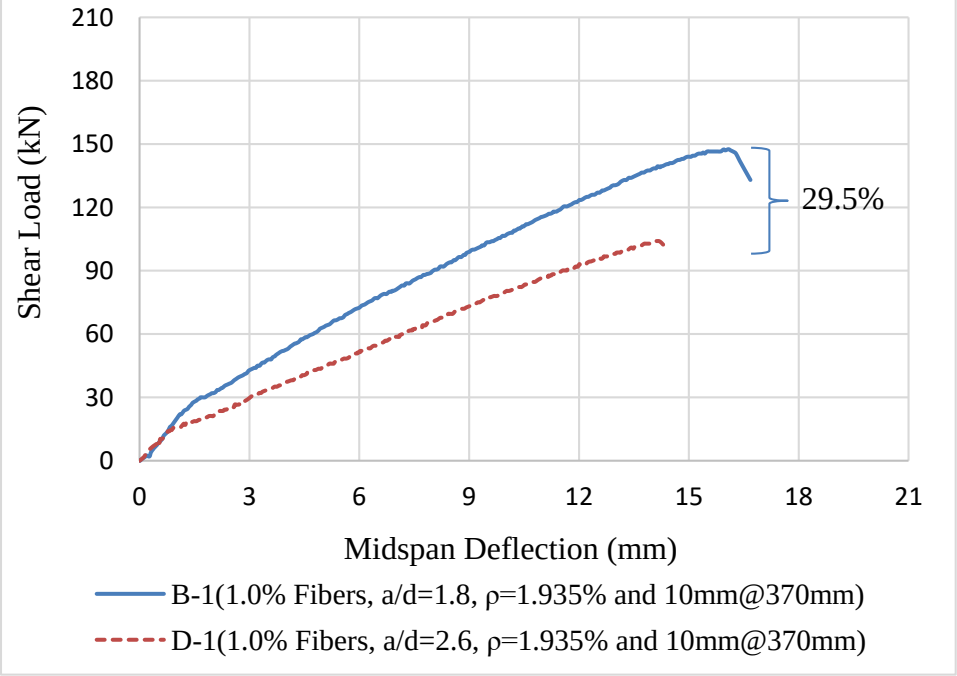

(a)

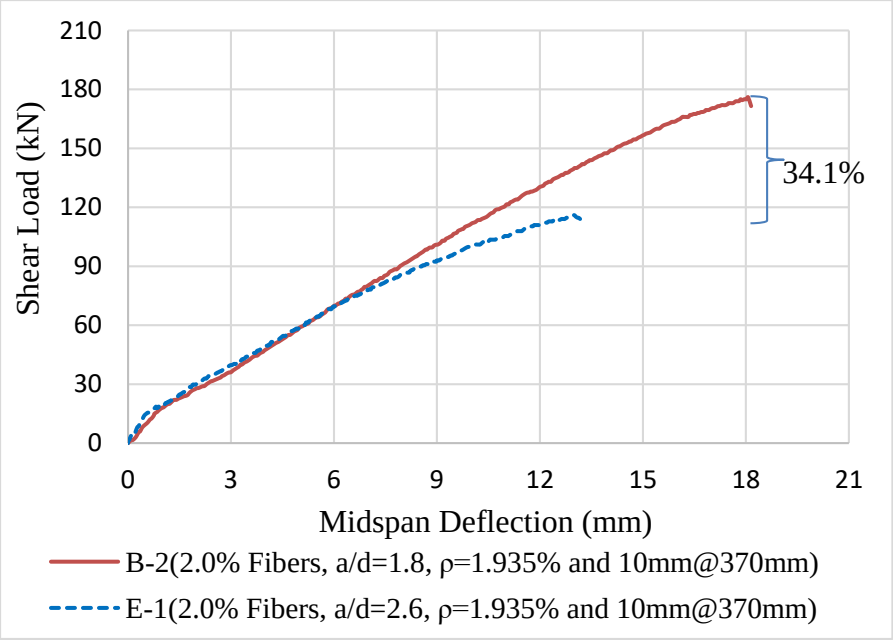

(b)

Figure 4.42: Effect of *a/d* ratio on shear behavior of beams: a) V_f =1.0%; and b) V_f =2.0%

4.3.3. Effect of Percentage of Longitudinal Reinforcement (*ρ*)

A higher percentage of longitudinal reinforcement, ρ, was found to be beneficial against flexural cracking as evident from Figure 4.43. The beam D-1 with ρ=1.935% had more flexural cracks than the beam D-2 with ρ=3.226%.

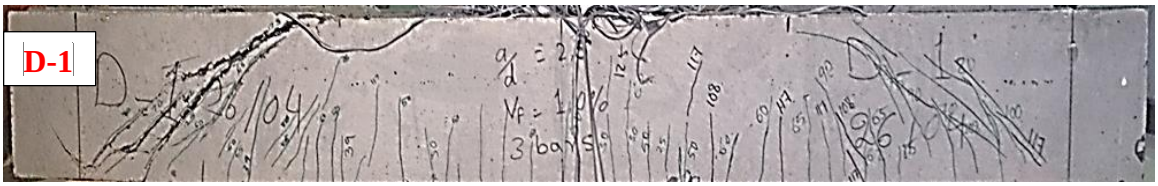

(a)

(b)

Figure 4.43: Comparison of modes of failure for beams; a) ρ=1.935% and; b) ρ=3.226%

The results show an increase in shear load capacities and mid-span deflections with increase in, ρ. Effect of, ρ, on shear load capacities and mid-span deflections was more for beams having lower V_f and higher *a/d* ratio as shown in Figures 4.44 and 4.45. For example, the beams D-1 and D-2 had same higher value of the *a/d* ratio but different percentages of longitudinal reinforcement. The beam D-1 with lower, ρ had a lower neutral axis depth and therefore developed a higher compound tensile stress failing at a lower ultimate load of 104 kN as compared to that of beam D-2 which had higher, ρ and failed at a higher ultimate load of 114.5 kN.

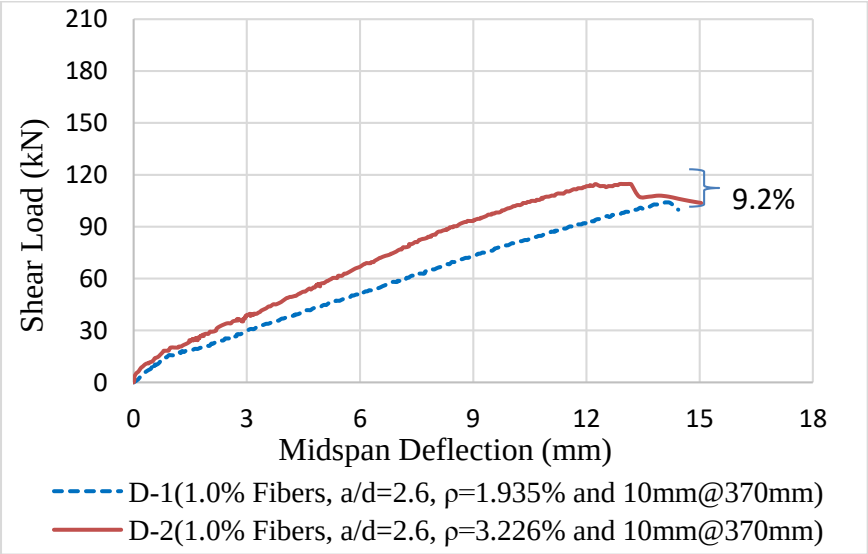

(a)

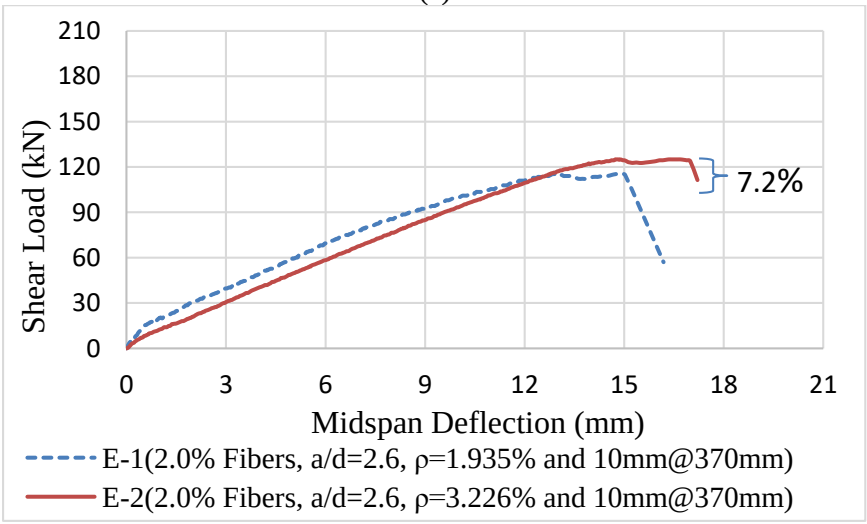

(b)

Figure 4.44: Effect of, ρ, on shear behavior of beams having; a) V_f =1.0%; and b) V_f =2.0%

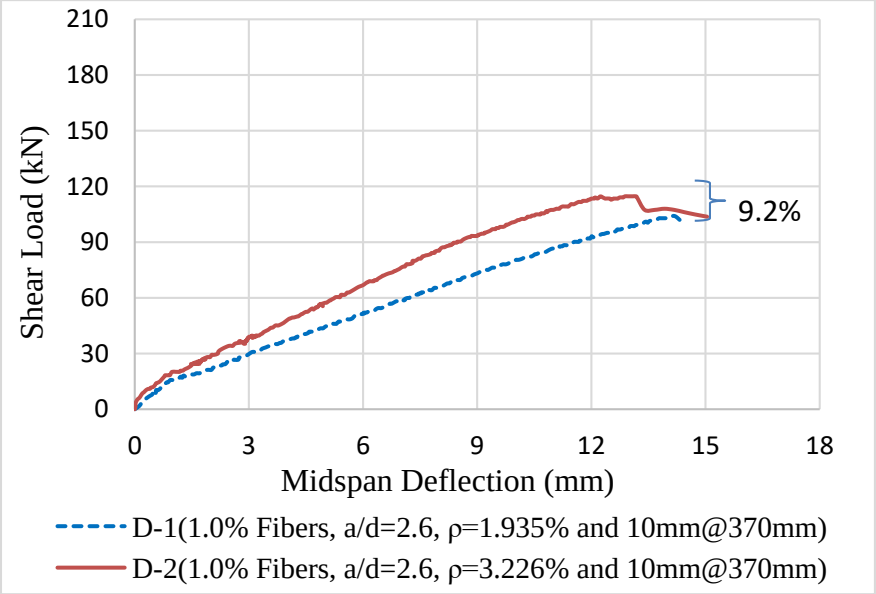

(a)

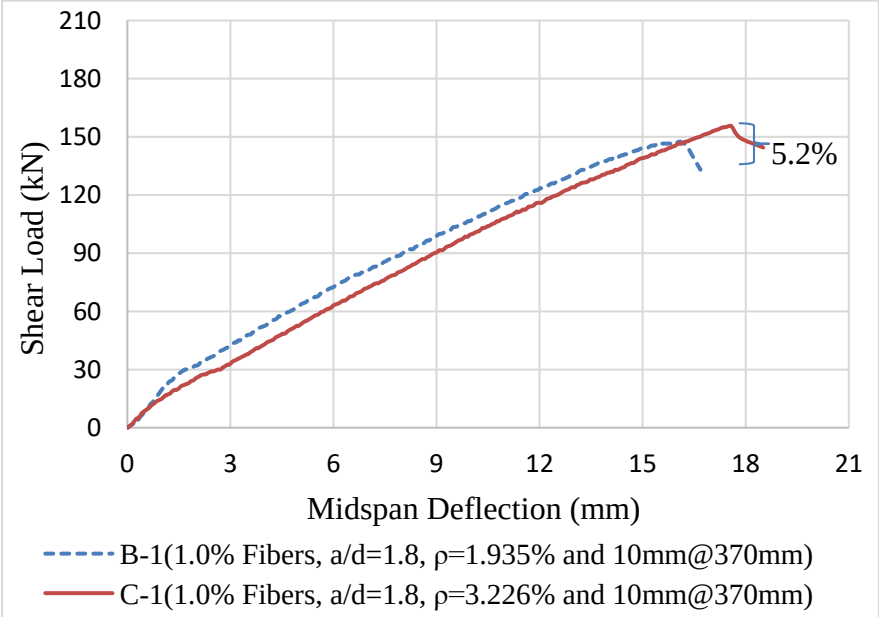

(b)

Figure 4.45: Effect of, ρ, on shear behavior of beams having; a) a/d =2.6; and b) a/d =1.8

4.3.4. Effect of Stirrups Spacing (*s*)

It is clear from Figures 4.46 that a single wide diagonal crack was developed in beams A-1 and A-2 (with stirrup spacing of 200 mm) whereas multiple diagonal cracks with relatively lesser width were developed in all other beams B-1, B-2, C-1, C-2, D-1, D-2, E-1 and E-2 (with stirrup spacing of 370 mm) as shown in Figure 4.47. This can be attributed to the fact that the beams A-1 and A-2 had more shear reinforcement than the other eight beams. Due to more shear reinforcement in beams A-1 and A-2, the load is distributed over a smaller area that resulted into wider and single crack. The reason behind multiple and lesser wide cracks in the rest of eight beams is the distribution of the load to concrete over a wider area due to lesser shear reinforcement.

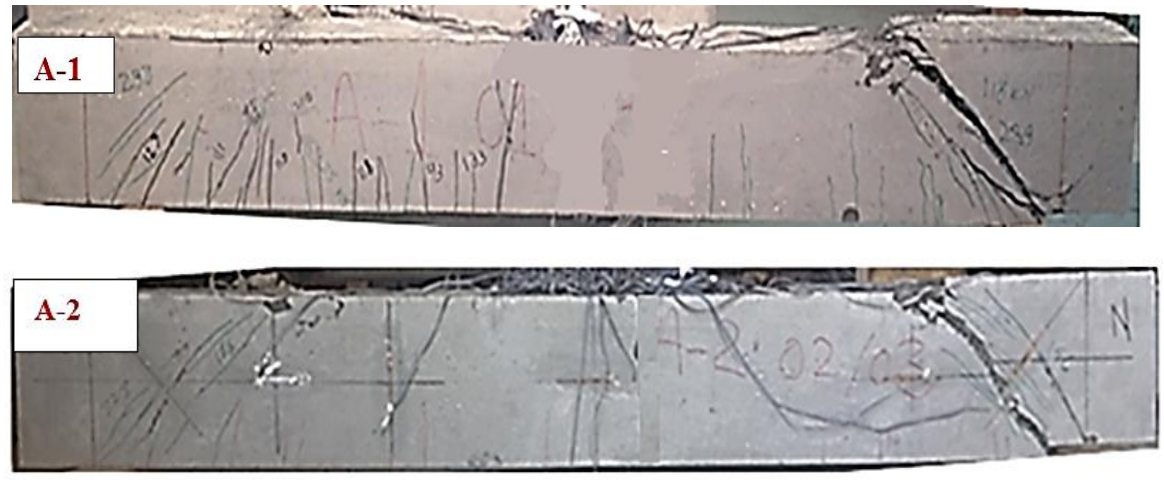

Figure 4.46: Mode of failure for beams A-1 and A-2

Figure 4.47: Mode of failure for beams B-1 and B-2

However, as expected, shear load capacities and mid-span deflections were increased with the decreasing stirrups spacing, *s*. Effect of, *s*, on shear load capacities and mid-span deflections was more for beams having lower, V_f, as shown in Figure 4.48.

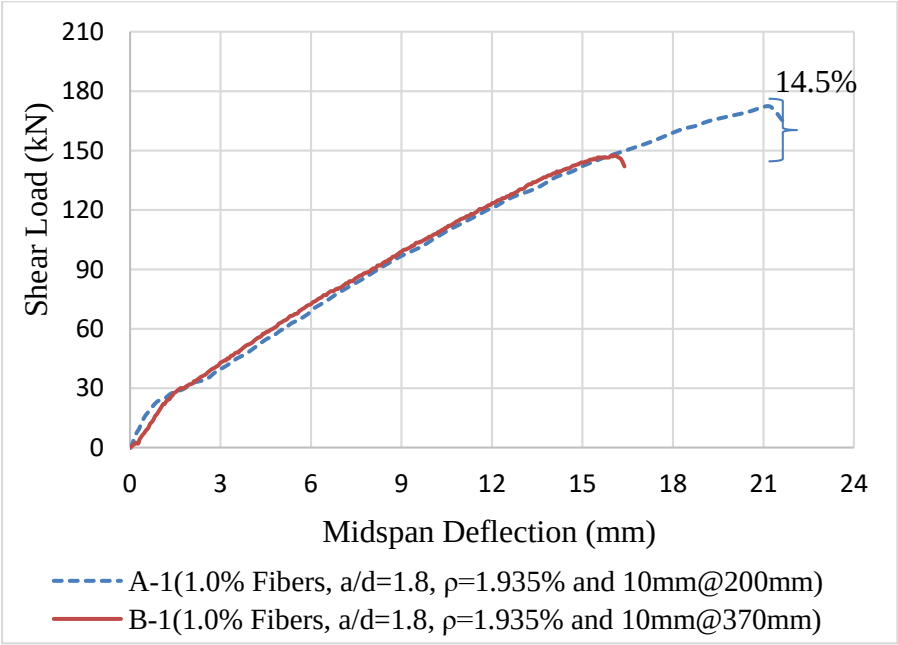

(a)

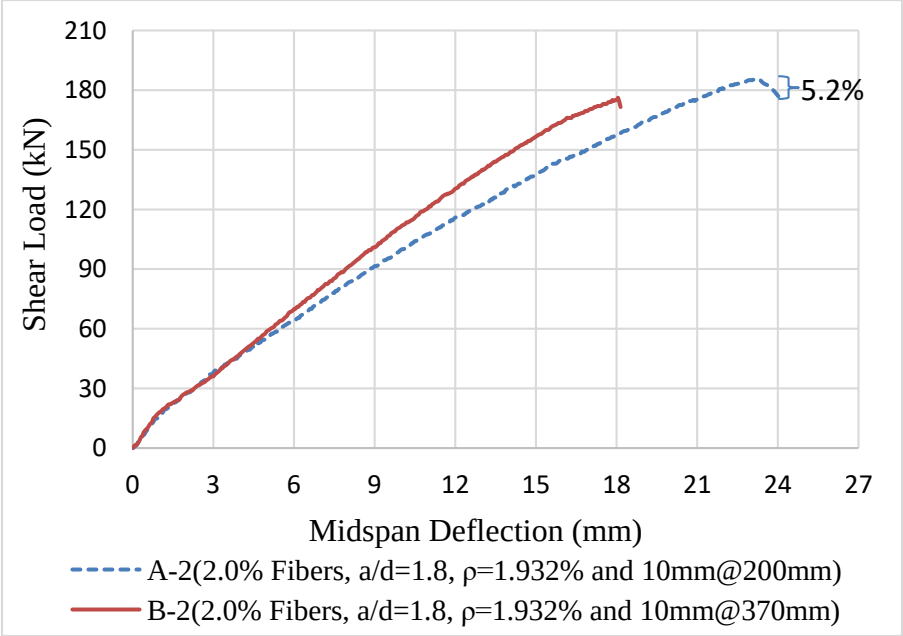

(b)

Figure 4.48: Effect of, *s*, on shear behavior of beams having; a) V_f =1.0%; and b) V_f =2.0%

CHAPTER 5

FINITE ELEMENT MODELING

5.1. General

Numerical modeling of shear behavior of UHPC beams is presented in this chapter. Behavior of UHPC is non-linear and complex, but computer-based finite element packages are able to analyze these complex behaviors. Nonlinear 3-D finite element Modeling (FEM), using the concrete damage plasticity (CDP) model and material properties obtained from uniaxial compressive and tensile laboratory tests, was developed to simulate shear behavior of UHPC beams. For this purpose, a commercial finite element software package ABAQUS 6.13 (a general-purpose analysis software having capability to solve linear and nonlinear problems) was used. The main purpose of FEM was to further improve the understanding of shear behavior of UHPC beams and conduct a parametric study considering the levels of the key parameters beyond the experimental values. Shear load-mid-span deflection relationships and cracking propagation behaviors obtained from FEM were compared with that obtained from the experimental work. Comparison of the results predicted using FEM and the experimental results showed that the FEM is a highly effective and reliable tool to predict the shear behavior of UHPC beams.

5.2. Finite Element Modeling (FEM)

FEM is a powerful numerical tool mostly used to simulate the nonlinear problems of elasticity, solids and structures [42]. FEM presented below describes the simulation of concrete followed by Modeling of reinforcing steel bars and its interaction behavior with

UHPC beams. Dynamic explicit approach is adopted to overcome convergence problems associated with cracking of concrete.

5.2.1. Geometry Model

5.2.1.1. Concrete Model

In order to model the real behavior of UHPC beams, it is recommended that UHPC should be modeled with 8-nodded linear 3-D brick solid element. Each 3-D solid element has 8-nodes and each node has 3 degrees of freedom and provides reliable solution to most applications as shown in Figure 5.1.

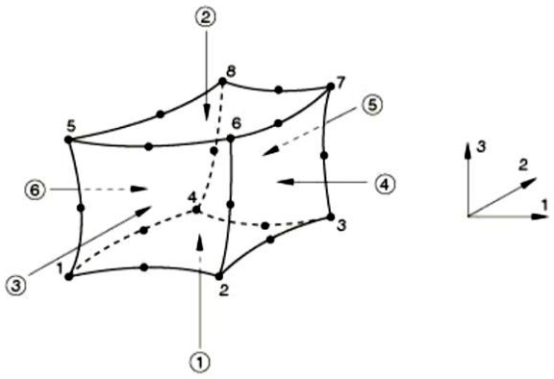

Figure 5.1: 3-D brick, 8-nodded element

Steel plates having dimensions of 50 × 100 × 150 mm and using 8-nodded linear 3-D brick solid element were modeled and implemented at the supports and loading points to avoid stress concentrations problems and equally distribute the loads on the loaded area.

5.2.1.2. Steel Reinforcement Rebars Model

The longitudinal and stirrups bars were modeled by using 2-nodded linear 3-D truss elements, as the longitudinal and stirrups bars will only carry the axial forces induced from

loading. Each element has 2-nodes with 3 degrees of freedom in the nodal *x*, *y* and *z* directions with no bending of the elements, as shown in Figure 5.2.

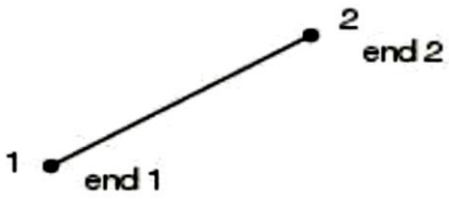

Figure 5.2: 2-nodded linear 3-D truss element

5.2.2. Boundary Condition and Loading

Displacement boundary conditions were applied at supports and loads acting points to constrain the model for getting a unique solution and to act in the same way as experimental beam. Supports are considered as a roller (U_y is restrained) and a pin (U_x, U_y and U_z are restrained) in the same way as experimental beam. The load was applied as a vertical displacement at two loading points (at distance 328.5 mm from each support for *a/d* ratio = 1.8 and at 474.5 mm from each support for *a/d* ratio = 2.6). Loading and boundary conditions profile are shown in Figure 5.3.

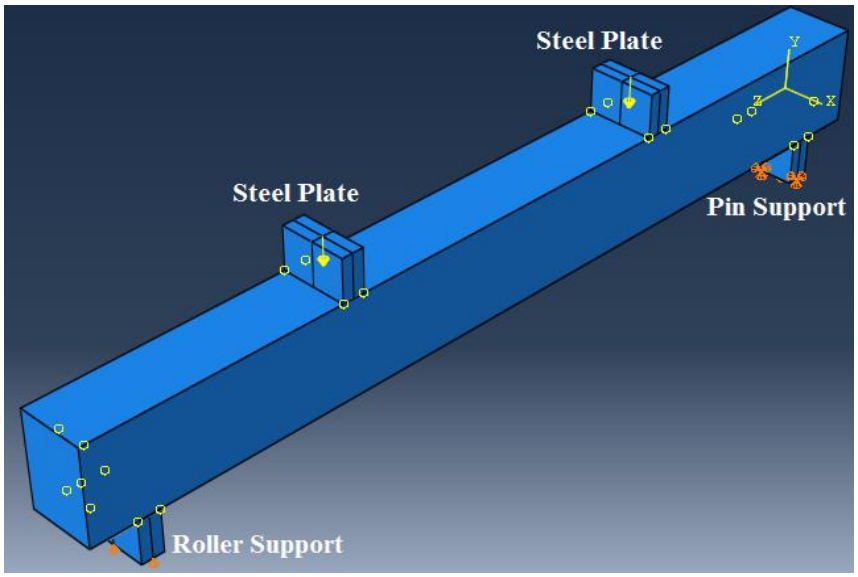

Figure 5.3: Loading and boundary conditions profile

5.2.3. Model Constraints

A certain number of constraints were created to model the UHPC beam specimens. These constraints defined the interactions between the various parts of the model.

5.2.3.1. Tie Constraint

The contact between UHPC beam and steel plates was defined by using the tie constraint. Steel plate surfaces were selected as master type because of their hardness and UHPC beam surfaces were selected as salve type.

5.2.3.2. Embedded Region Constraint

For the interaction between steel reinforcement bars and UHPC, embedded region constraints were applied. In this constraint, steel reinforcement bars and stirrups were selected as embedded region while UHPC as host region. The constraint used the geometric relationship between the nodes of the embedded elements and the host elements.

5.2.4. Meshing Elements

In order to get accurate results from FEM, all the elements were meshed with the same size to ensure that each two different materials share the same nodes. The mesh element for Modeling of concrete and steel plates is (25 mm), 8-nodded linear brick. This element type can be used for both linear and complex non-linear analysis involving contact, plasticity and large deformations. 2-nodded linear truss element used to mesh both longitudinal steel reinforcement bars and stirrups. The meshed UHPC beam is shown in Figure 5.4.

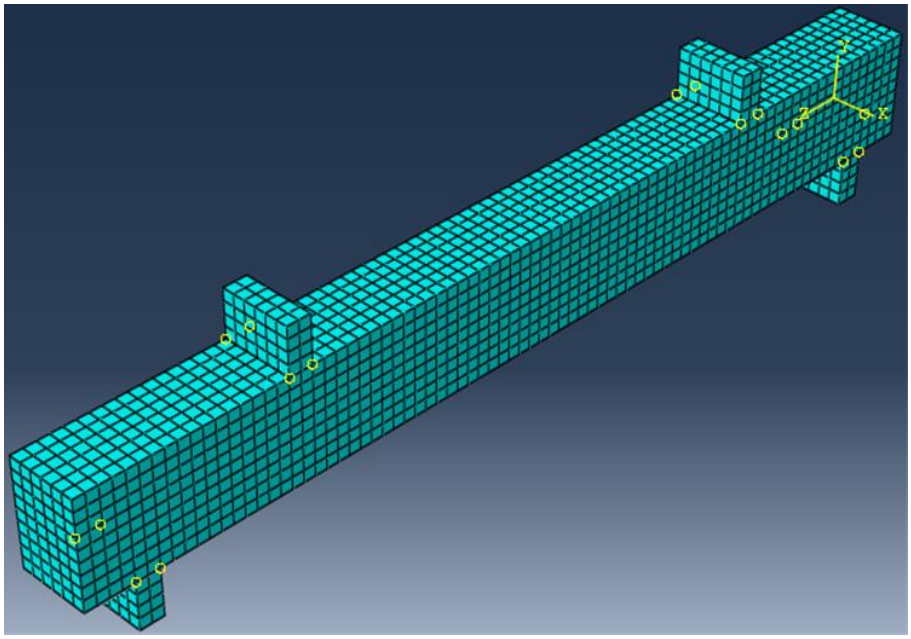

Figure 5.4: Discretized beam using the 3-D stress 8-nodded elements

5.2.5. Materials Model

5.2.5.1. Concrete Damage Plasticity (CDP) Model

To simulate quasi-brittle nature of reinforced concrete, various conceptual models are available in literature such as discrete crack model, smeared crack model, inner softening band etc. In this study, CDP model has been utilized for UHPC, which is a constitutive model available in non-linear finite element software ABAQUS.

The CDP model is primarily intended to provide a general capability for the analysis of concrete or other quasi-brittle materials, such as rock, mortar and ceramics structures under static, cyclic and dynamic loading. CDP model describes the inelastic and fracture behavior of concrete by the concept of isotropic damage elasticity in combination with isotropic compressive and tensile plasticity. It allows strain hardening in compression, strain softening in tension, and uncoupled damage initiation and accumulation in tension and compression. The CDP model assumes that both tensile cracking and compressive crushing

of concrete is characterized by damage plasticity. The CDP parameters considered in the FEM are summarized in Table 5.1.

Table 5.1: CDP parameter for material definition of concrete

Parameter	Value	Description
$\psi(\circ)$	36	Dilation angle
$\in$	0.1	Eccentricity
$\frac{\sigma_{b0}}{\sigma_{c0}}$	1.16	The ratio of biaxial compressive ultimate strength to uniaxial ultimate compressive strength
k	0.667	The ratio of the second stress invariant on the tensile meridian
μ	0	Viscosity parameter

Model Code of fib for concrete structures [43] was adopted as this model has advanced parameters to control ascending as well as post-peak behavior of stress-strain curve for concrete. The compressive stress-strain relationship is as follow:

$$\frac{\sigma_c}{f_{cm}} = -\left(\frac{k\cdot\eta-\eta^2}{1+(k-2)\cdot\eta}\right)$$

Where:

$$\eta = \frac{\in_c}{\in_{c1}}$$

$$k = \frac{E_{ci}}{E_{c1}}$$

f_{cm} is the concrete compressive strength, $\in_c$ is the concrete compressive strain; $\in_{c1}$ is the strain at maximum compressive stress; E_{ci} is the modulus of elasticity at 28 days; E_{c1} is the secant modulus and k, is the plasticity number.

Stress-strain relation with the related parameters is shown in Figure 5.5:

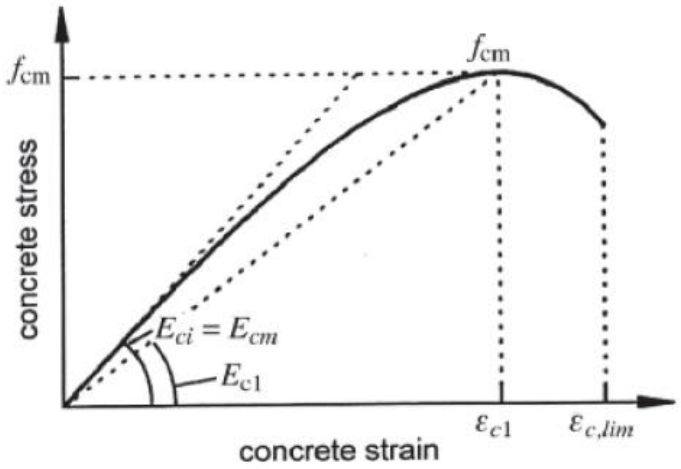

Figure 5.5: Compressive stress-strain relationship

Following bilinear stress-strain relationship was used for tensile behavior of concrete:

$$\sigma_{ct} = E_{ci} \ \in_{ct} \quad \text{for} \quad \sigma_{ct} \leq 0.9 f_{ctm}$$

$$\frac{\sigma_{ct}}{f_{ctm}} = \left(1 - 0.1 \frac{0.00015 - \in_{ct}}{0.00015 - 0.9 \frac{f_{ctm}}{E_{ci}}} \right) \quad \text{for} \quad 0.9 f_{ctm} \leq \sigma_{ct} \leq f_{ctm}$$

Where; $\in_{ct}$, is the tensile strain, σ_{ct} is the tensile stress, and f_{ctm} is the tensile strength.

Tensile stress-strain relation with the related parameters is shown in Figure 5.6:

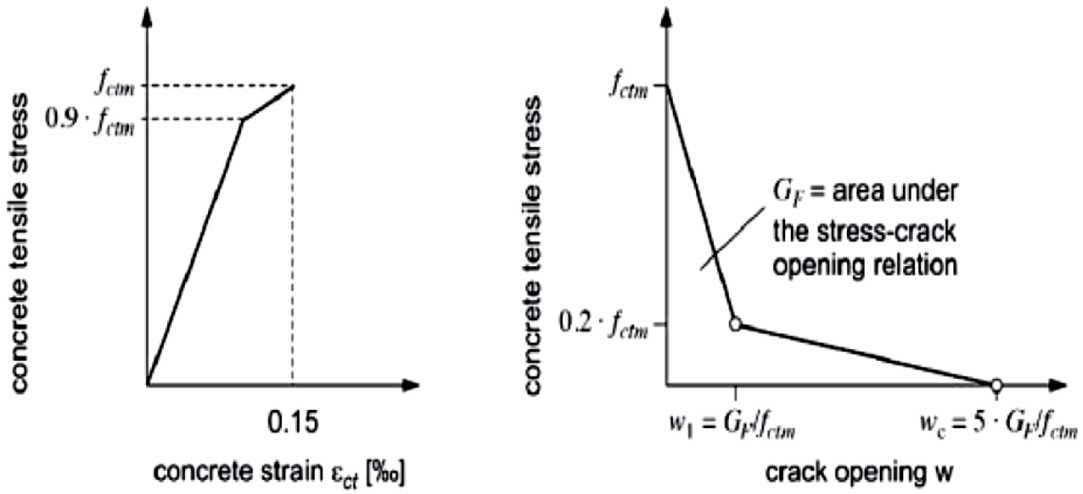

Figure 5.6: Tensile stress-strain relationship

Concrete compression damage parameters which was used in model are as below [44]:

$$d_c = 1 - \frac{\sigma_c E_c^{-1}}{\in_c^{pl} \left(\frac{1}{b_c} - 1 \right) + \sigma_c E_c^{-1}}$$

where:

d_c = Concrete compression damage parameter; σ_c = compressive Stress; E_c = modulus of elasticity of concrete; $\in_c^{pl}$ = plastic strain corresponding to compressive strength, b_c = constant ranges, $0 < b_c < 1$.

Figure 5.7 shows the physical interpretation of compression damage parameter in defining stiffness after damage in non-linear part of stress-strain curve of concrete in uniaxial compression.

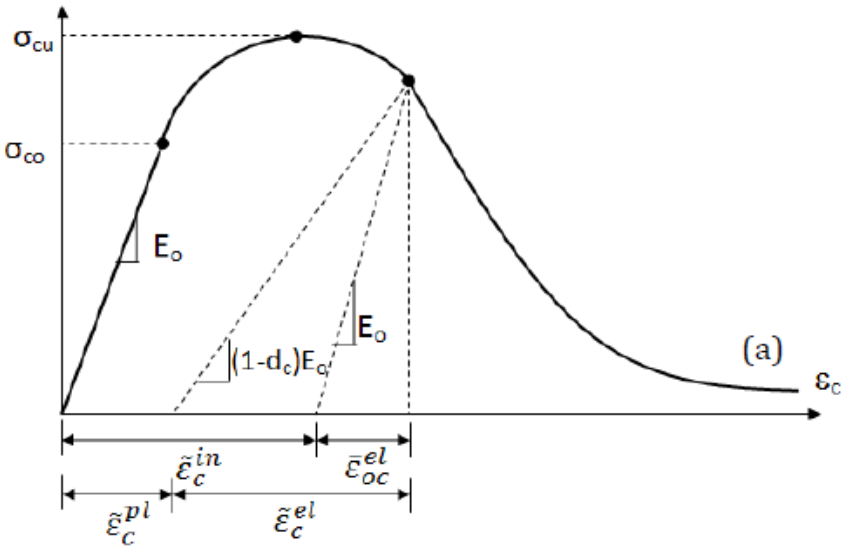

Figure 5.7: Behavior of Concrete under Uniaxial Compression

Concrete tensile damage parameters which was used in model are as below [44]:

$$d_t = 1 - \frac{\sigma_t E_c^{-1}}{\in_t^{pl} \left(\frac{1}{b_t} - 1 \right) + \sigma_t E_c^{-1}}$$

Where:

d_t = concrete tension damage parameter; σ_t = tensile stress; E_c = modulus of elasticity of concrete; $\in_t^{pl}$ = plastic strain corresponding to tensile strength, b_t = constant ranges $0 < b_t < 1$.

Tensile response of concrete can be characterized by concrete damage plasticity model in Figure 5.8.

The mechanical properties of UHPC such as uniaxial compression and tensile stress-strain behavior, modulus of elasticity (47000 MPa) and Poisson's ratio (0.15) were obtained experimentally from cylinder and dog-bone uniaxial test specimens. Compressive stress

versus plastic strain behavior and tensile stress versus plastic strain behavior of UHPC used in the present FEM are shown in Figures 5.9 and 5.10, respectively.

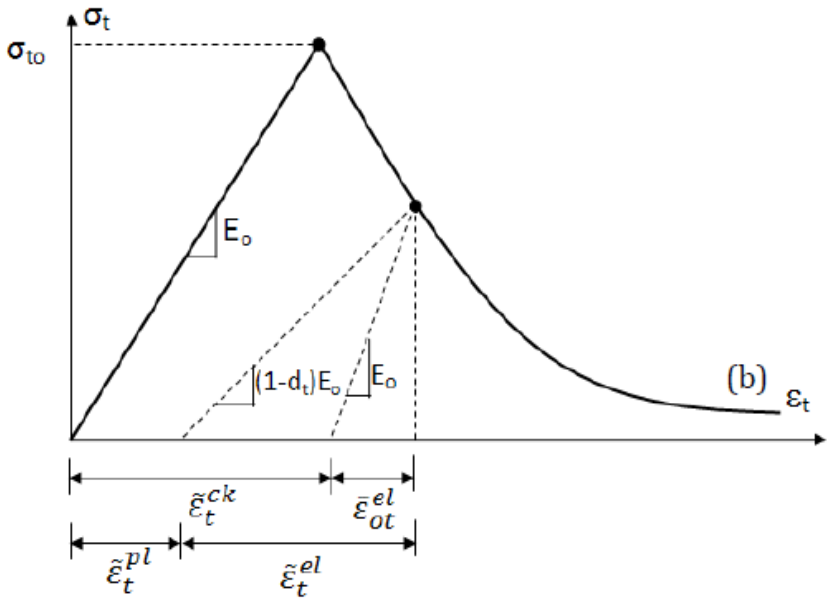

Figure 5.8: Behavior of Concrete under Uniaxial Tension

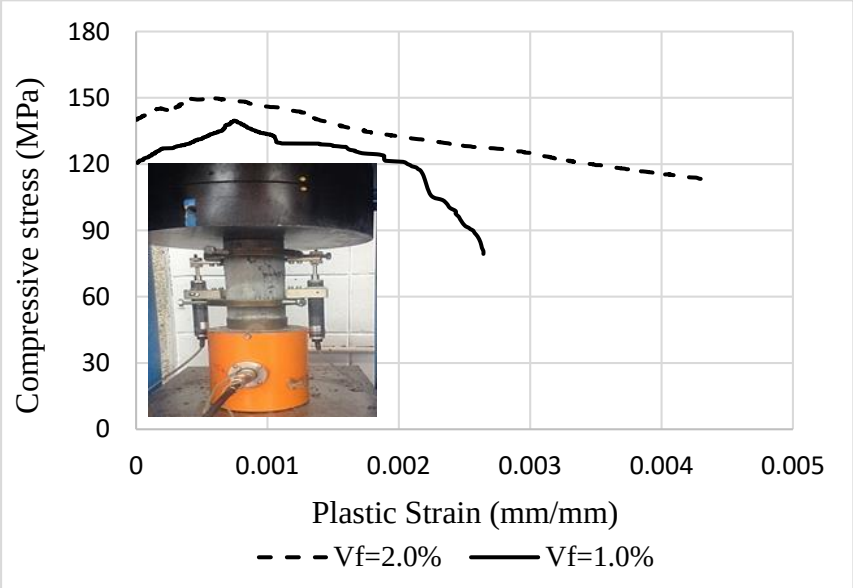

Figure 5.9: Uniaxial compression stress-plastic strain curves

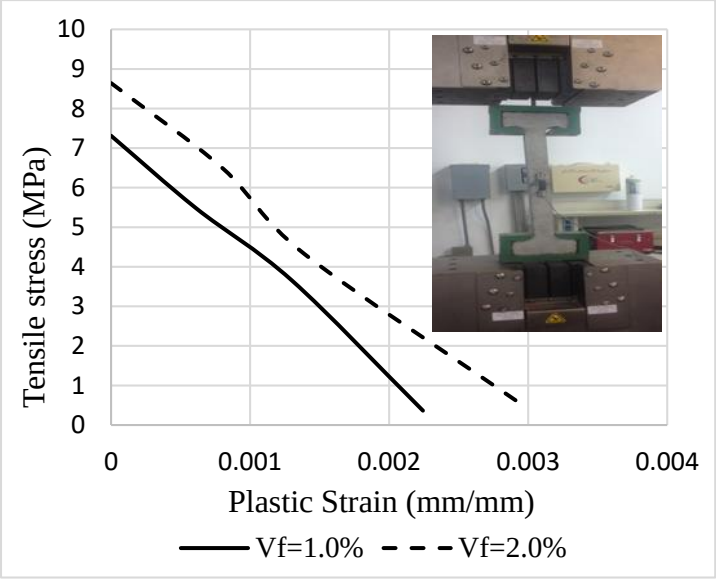

Figure 5.10: Uniaxial tensile stress-plastic strain curves

5.2.5.2. Steel Reinforcing Bars Model

Material behavior of steel reinforcement bars is defined by an elastic-perfectly plastic relationship whose parameters were obtained by experimental testing as shown in Figure 5.11. The input parameters used to define the behavior of both high-strength and normal-strength steel bars are summarized in Table 5.2.

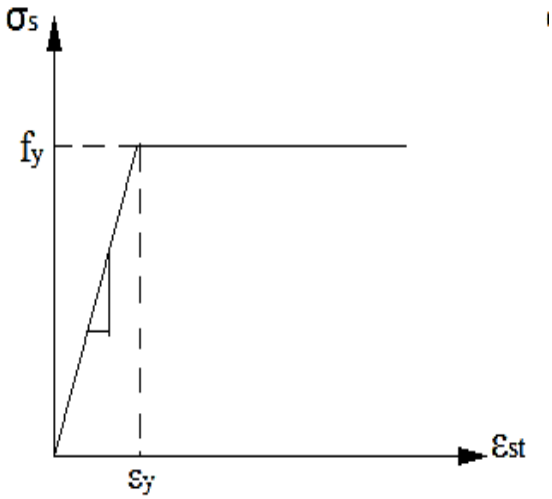

Figure 5.11: Behavior of steel reinforcing bars in tension

Tensile stress versus plastic strain behavior of both high-strength and normal-strength steel rebars used in the present FEM are shown in Figures 5.12 and 5.13, respectively.

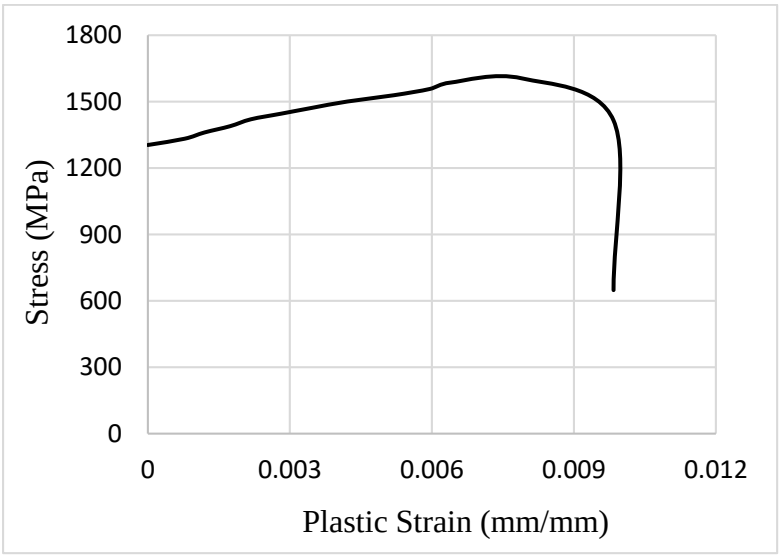

Figure 5.12: Uniaxial tensile stress-plastic strain curves for high-strength steel bars

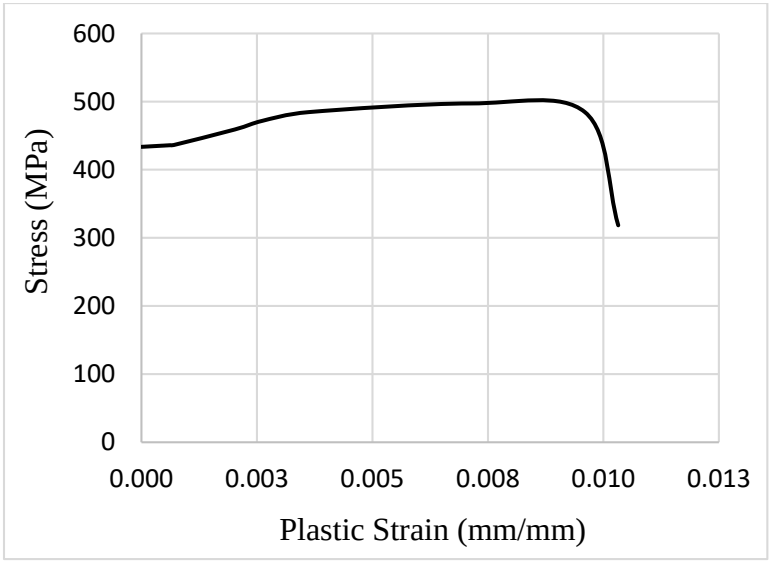

Figure 5.13: Uniaxial tensile stress-plastic strain curves for normal-strength steel bars

Table 5.2: Input parameters of steel bars

Modulus of elasticity (MPa)	2×10^5
Poisson's ratio	0.3
Mass density (ton/mm^3)	7.85×10^{-9}
Yield stress of high-strength steel bars (MPa)	1320
Yield stress of normal-strength steel bars (MPa)	430

5.3. Validation of the Developed FEM

5.3.1. General

The FEM developed, as described in the previous section, was compared with the experimental results presented in Chapter 4. This comparison was to validate the competency of FEM to envisage the failure shear load, mode of failure and overall shear behavior of UHPC beams.

Shear load-mid-span deflections response from FEM were compared with the experimental results for all the UHPC beam specimens. The shear load-mid-span deflection predicted by the FEM was generally similar to the experimental data. However, the FEM shear load-mid-span deflection response has a minor difference in terms of stiffness and mid-span deflection at ultimate load. After initial cracking, FEM shear load-mid-span deflection curves are stiffer than that obtained through experiments. There could be many reasons behind higher stiffness in FEM. The most important reason is the development of micro cracks due to dry shrinkage, handling of concrete, environmental effects etc. in case of the experiments. FEM does not include such micro cracks in the simulations. The shear load-mid-span deflection characteristic for all the beams was linear up to approximately 90% of

the ultimate load, and then the mid-span deflection increased with increasing cracking widths until failure.

Similar cracking propagation was observed in FEM as captured during the experimental study. Similar to experimental work, first cracks detected at flexural zones. With the increasing load, cracks increased and became deeper in both shear and flexural zones. The failure type for all the beam specimens was found as splitting failure. The diagonal crack formed in both shear spans and extended from support towards the loading plates. This continued until diagonal cracks reached about 90% of the overall depth of the beam followed by the failure.

5.3.2. Beam A-1

Ultimate shear load for beam A-1, predicted by FEM, is 178 kN at a mid-span deflection of 20.03 mm against their respective experimental values of 172.5 kN and 21.14 mm. Prediction of shear load-mid-span deflection response for beam A-1 using the developed FEM is in perfect match with that of the experimental results. Shear load-mid-span deflection response predicted by FEM along with experimentally obtained curve for beam A-1 is shown in Figure 5.14.

FEM predicted similar cracking propagation for beam A-1 as captured during the shear load experiment for beam A-1, as shown in Figure 5.15.

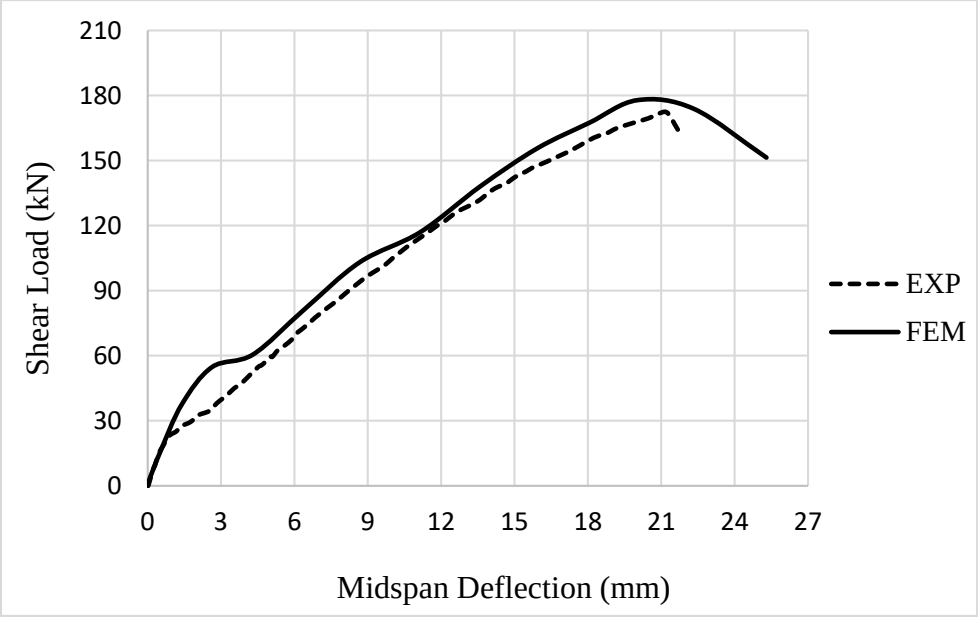

Figure 5.14: Shear load-mid-span deflection curves from EXP and FEM for beam A-1

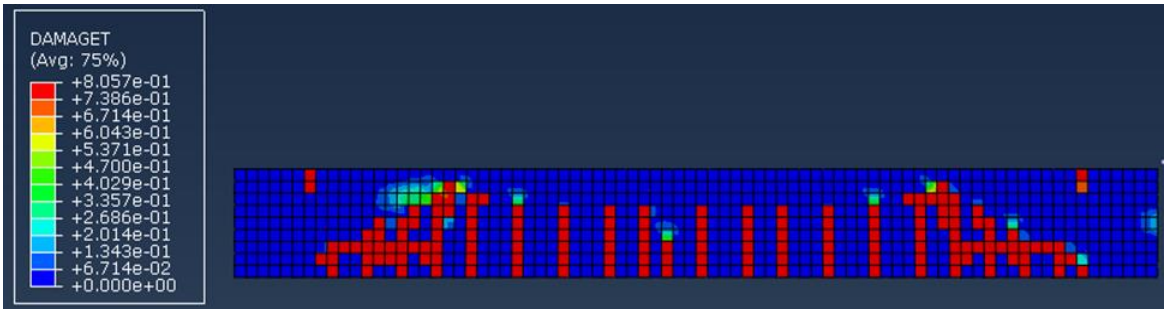

(a)

(b)

Figure 5.15: Cracking pattern of beam A-1 observed from a) FEM; and b) Experiment

5.3.3. Beam A-2

Ultimate shear load of beam A-2, predicted by FEM, is 185 kN at a mid-span deflection of 21.77 mm against their respective experimental values of 178.5 kN and 23.3 mm. A narrow difference between the predicted and experimental values of ultimate shear load and mid-

span deflection indicates a good agreement. Shear load-mid-span deflection response predicted by FEM along with experimentally obtained curve for beam A-2 is shown in Figure 5.16.

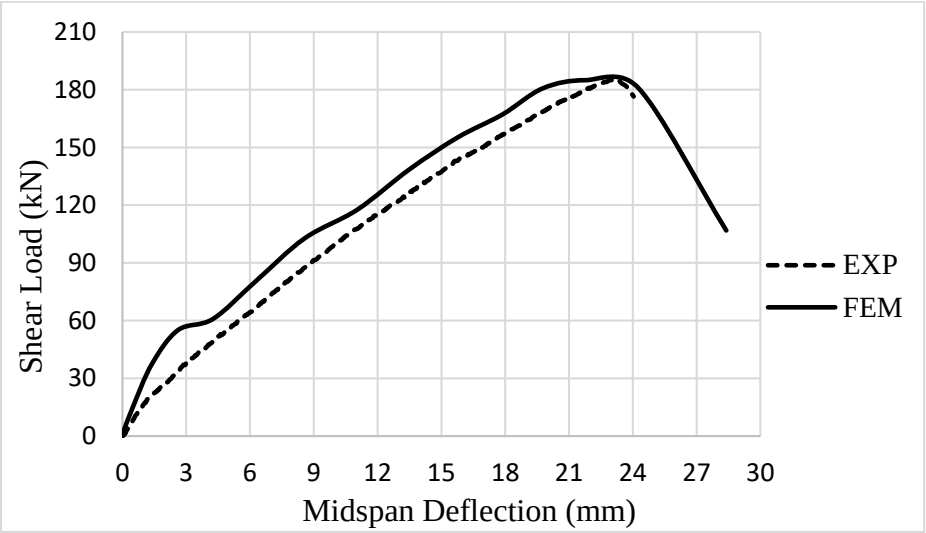

Figure 5.16: Shear load-mid-span deflection curves from EXP and FEM for beam A-2

Cracking propagation generated by FEM for beam A-2 was observed similar to that captured during the experimental study on the same beam, as shown in Figure 5.17.

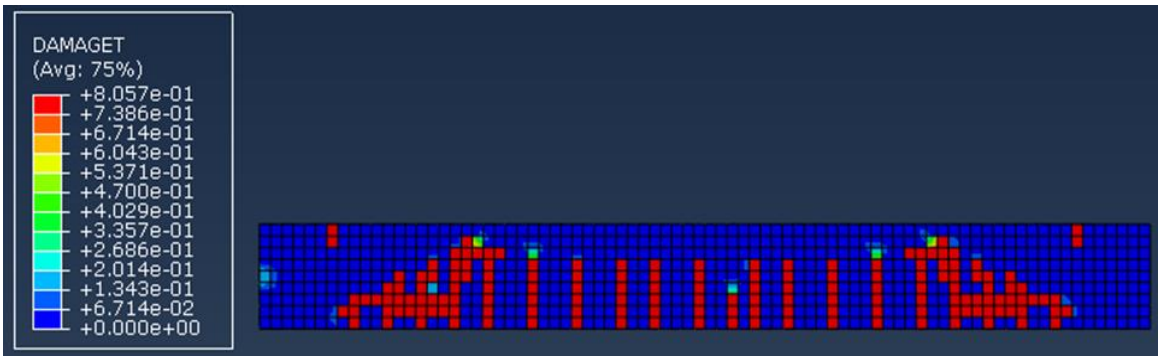

(a)

(b)

Figure 5.17: Cracking pattern of beam A-2 observed from a) FEM; and b) Experiment

5.3.4. Beam B-1

Ultimate shear load of beam B-1, predicted by FEM, is 155.5 kN at a mid-span deflection of 16.17 mm against their respective experimental values of 147.5 kN and 16.10 mm. The predicted and experimental results are in a good agreement. Shear load-mid-span deflection response predicted by FEM along with experimentally obtained curve for beam B-1 is shown in Figure 5.18. Cracking propagation for beam B-1 was obtained using FEM is similar to that captured during the experimental study, as shown in Figure 5.19.

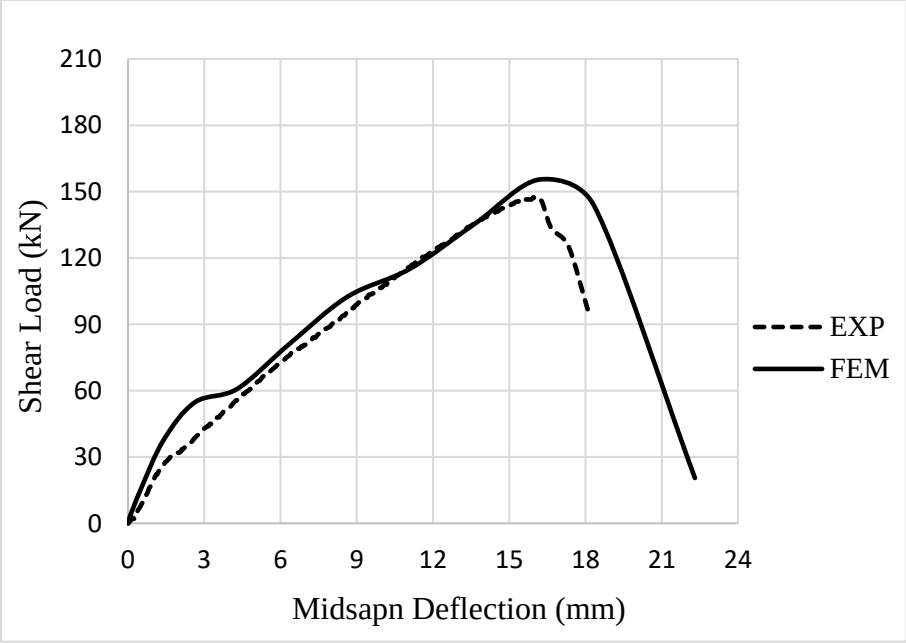

Figure 5.18: Shear load-mid-span deflection curves from EXP and FEM for beam B-1

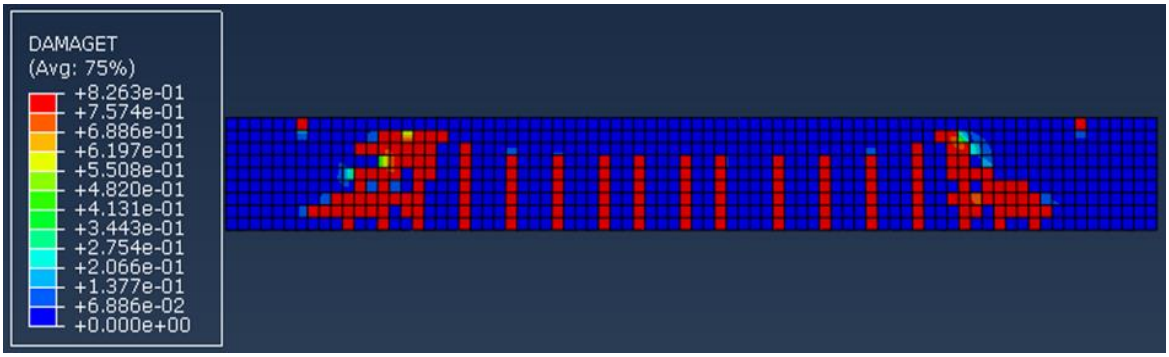

(a)

(b)

Figure 5.19: Cracking pattern of beam B-1 observed from a) FEM; and b) Experiment

5.3.5. Beam B-2

Ultimate shear load of beam B-2, predicted by FEM, is 177.1 kN at a mid-span deflection of 20.11 mm against their respective experimental values of 176 kN and 18.06 mm. Shear load-mid-span deflection response predicted by FEM along with experimentally obtained curve for beam B-2 is shown in Figure 5.20.

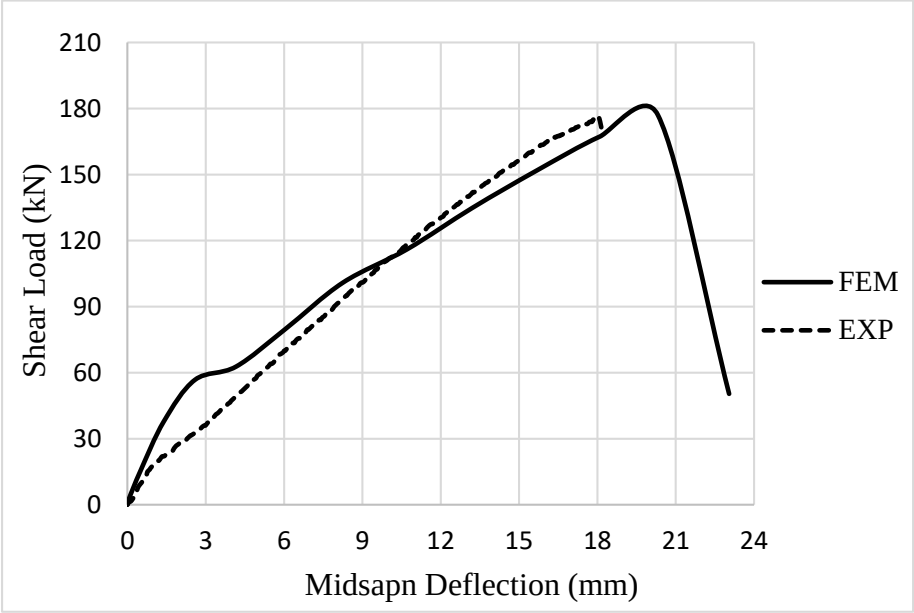

Figure 5.20: Shear load-mid-span deflection curves from EXP and FEM for beam B-2

Cracking propagation for beam B-2 was obtained using FEM is similar to that captured during the experimental study, as shown in Figure 5.21.

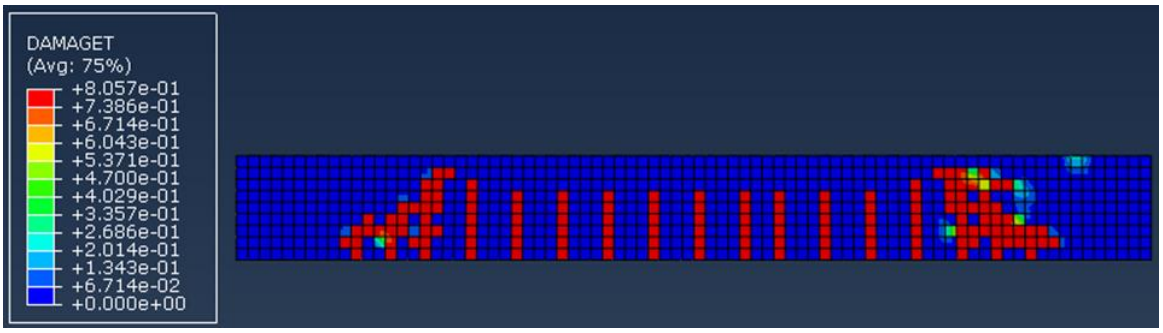

(a)

(b)

Figure 5.21: Cracking pattern of beam B-2 observed from a) FEM; and b) Experiment

5.3.6. Beam C-1

Ultimate shear load of beam C-1, predicted by FEM, is 152 kN at a mid-span deflection of 18.17 mm against their respective experimental value of 155.5 kN and 17.85 mm. Shear load-mid-span deflection response predicted by FEM along with experimentally obtained curve for beam C-1 is shown in Figure 5.22.

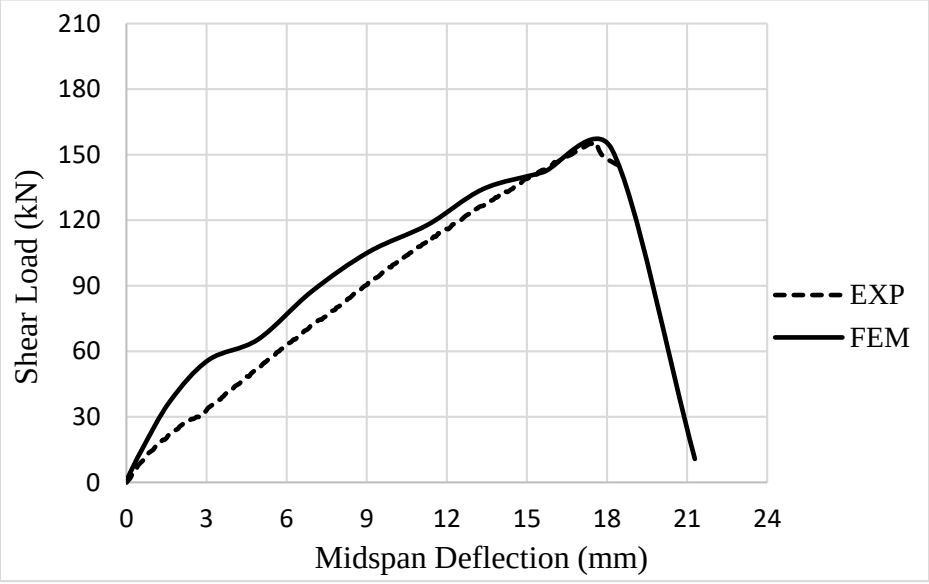

Figure 5.22: Shear load-mid-span deflection curves from EXP and FEM for beam C-1

Cracking propagation for beam C-1 was obtained using FEM is similar to that captured during the experimental study, as shown in Figure 5.23.

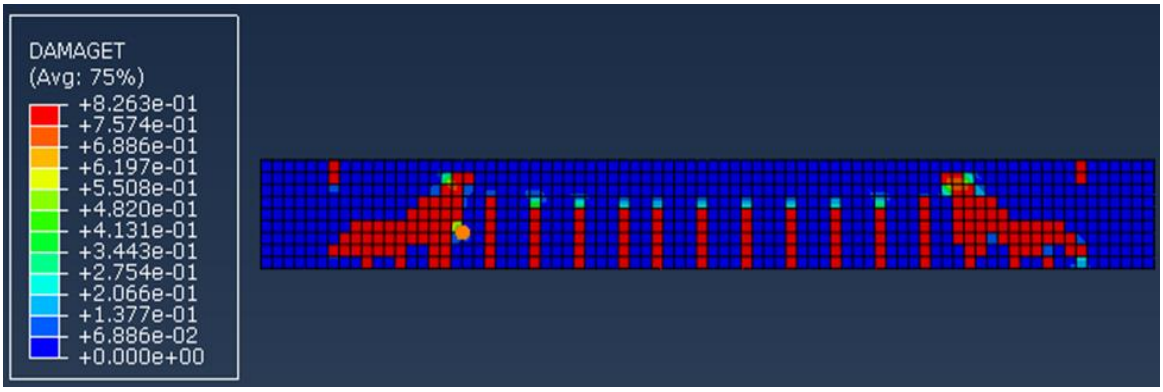

(a)

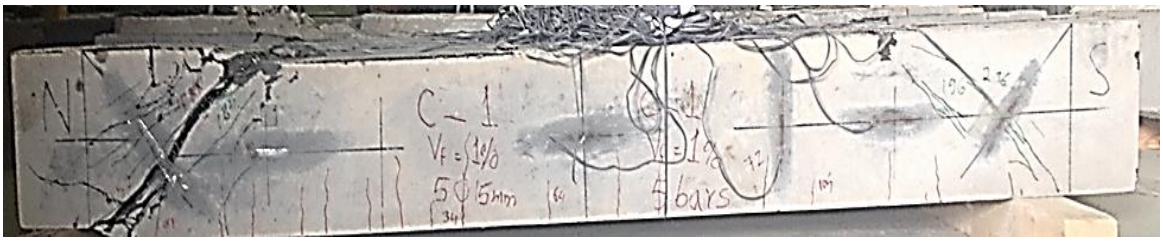

(b)

Figure 5.23: Cracking pattern of beam C-1 observed from a) FEM; and b) Experiment

5.3.7. Beam C-2

Ultimate shear load of beam C-2, predicted by FEM, is 185.14 kN at a mid-span deflection of 20.03 mm against their respective experimental values of 182.5 kN and 19.86 mm. Shear load-mid-span deflection response predicted by FEM along with experimentally obtained curve for beam C-2 is shown in Figure 5.24. Cracking propagation for beam C-2 was obtained using FEM is similar to that captured during the experimental study, as shown in Figure 5.25.

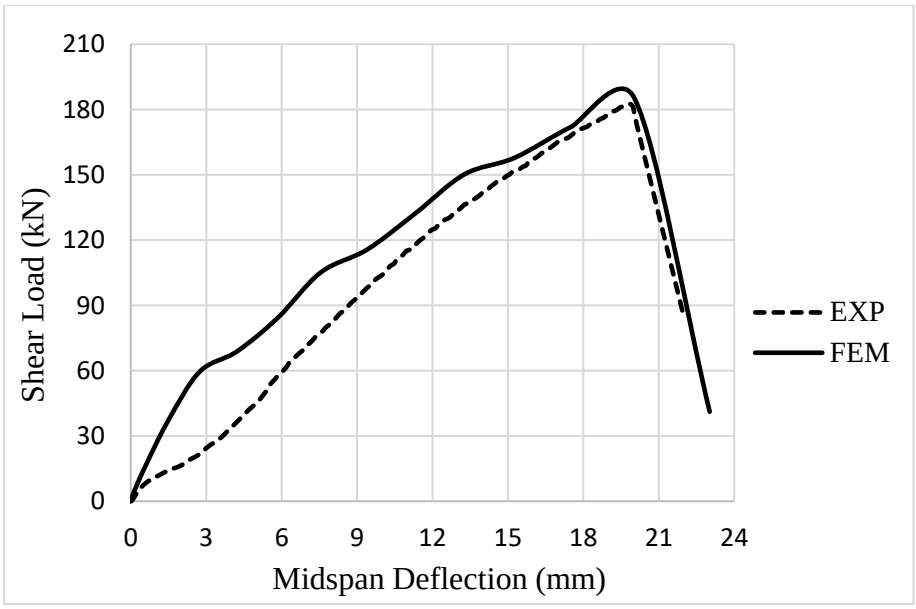

Figure 5.24: Shear load-mid-span deflection curves from EXP and FEM for beam C-2

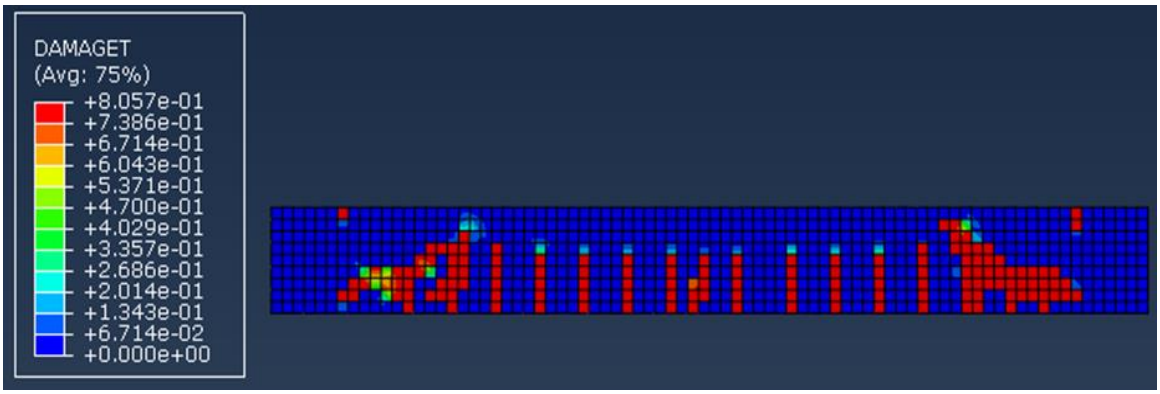

(a)

(b)

Figure 5.25: Cracking pattern of beam C-2 observed from a) FEM; and b) Experiment

5.3.8. Beam D-1

Ultimate shear load of beam D-1, predicted by FEM is 101 kN at a mid-span deflection of 18.0 mm against their respective experimental values of 104 kN and 14.19 mm. It is to be

noted that although the predicted and experimental values of ultimate shear load are in good agreement, there is a significant difference between the predicted and experimental values of the mid-span deflection. This may be due to some error in measuring the mid-span deflection experimentally. Shear load-mid-span deflection response predicted by FEM along with experimentally obtained curve for beam D-1 is shown in Figure 5.26.

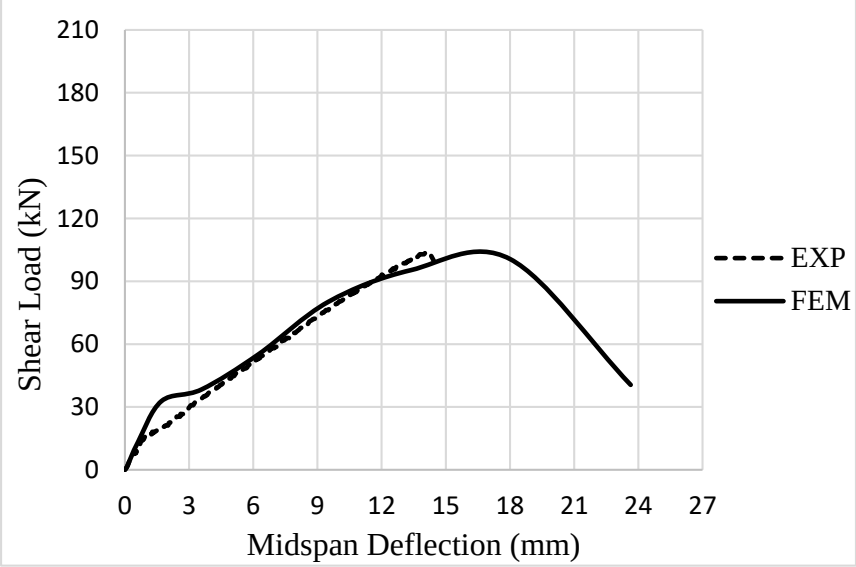

Figure 5.26: Shear load-mid-span deflection curves from EXP and FEM for beam D-1

Cracking propagation for beam D-1 was obtained using FEM is similar to that captured during the experimental study, as shown in Figure 5.27.

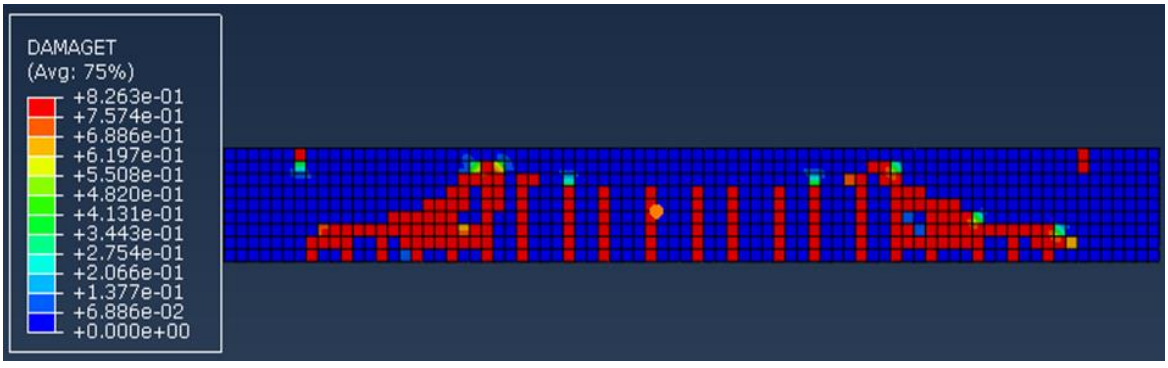

(a)

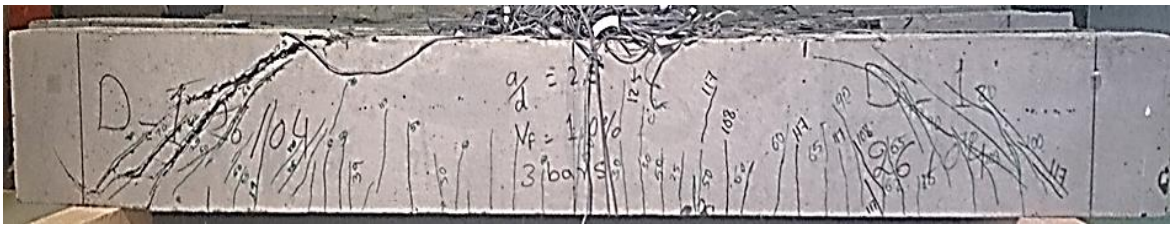

(b)

Figure 5.27: Cracking pattern of beam D-1 observed from a) FEM; and b) Experiment

5.3.9. Beam D-2

Ultimate shear load of beam D-2, predicted by FEM, is 116.81 kN at a mid-span deflection of 14.17 mm against their respective experimental values of 114.5 kN and 13.18 mm. Shear load-mid-span deflection response predicted by FEM along with experimentally obtained curve for beam D-2 is shown in Figure 5.28.

Cracking propagation for beam D-2 was obtained using FEM is similar to that captured during the experimental study, as shown in Figure 5.29.

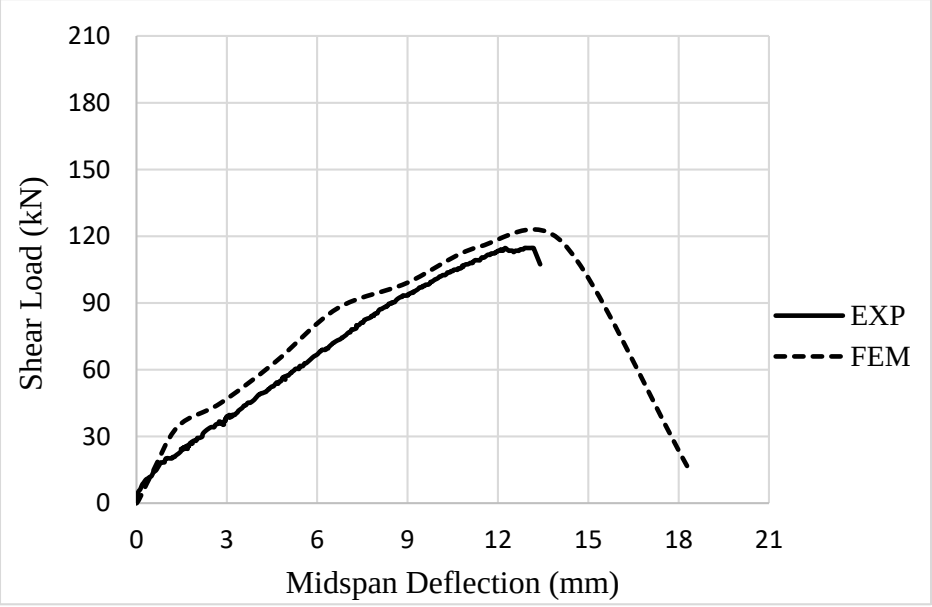

Figure 5.28: Shear load-mid-span deflection curves from EXP and FEM for beam D-2

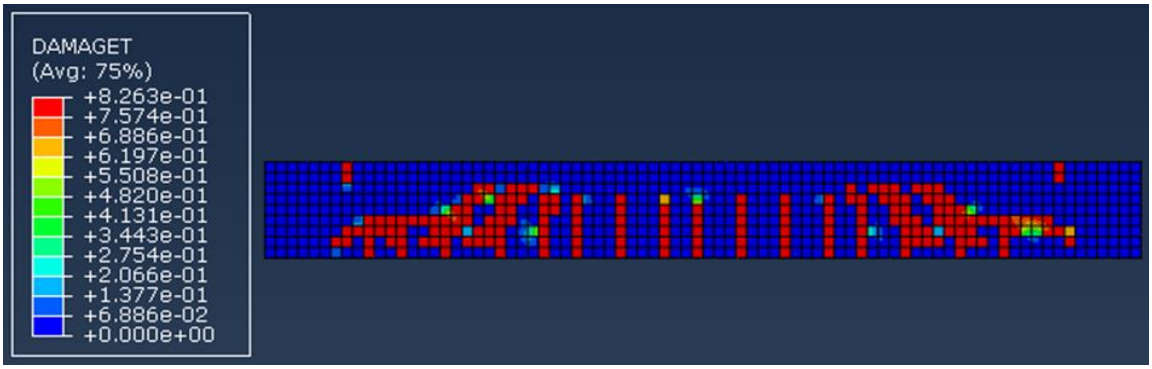

(a)

(b)

Figure 5.29: Cracking pattern of beam D-2 observed from a) FEM; and b) Experiment

5.3.10. Beam E-1

Ultimate shear load of beam E-1, predicted by FEM. is 110.81 kN at a mid-span deflection of 15.19 mm against their respective experimental values of 116 kN and 13.01 mm. Shear load-mid-span deflection response predicted by FEM along with experimentally obtained curve for beam E-1 is shown in Figure 5.30.

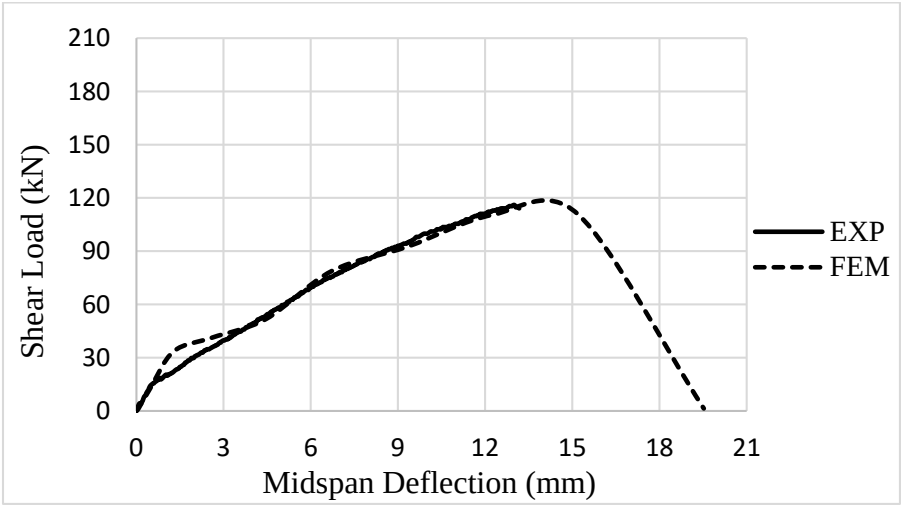

Figure 5.30: Shear load-mid-span deflection curves from EXP and FEM for beam E-1

Cracking propagation for beam E-1 was obtained using FEM is similar to that captured during the experimental study, as shown in Figure 5.31.

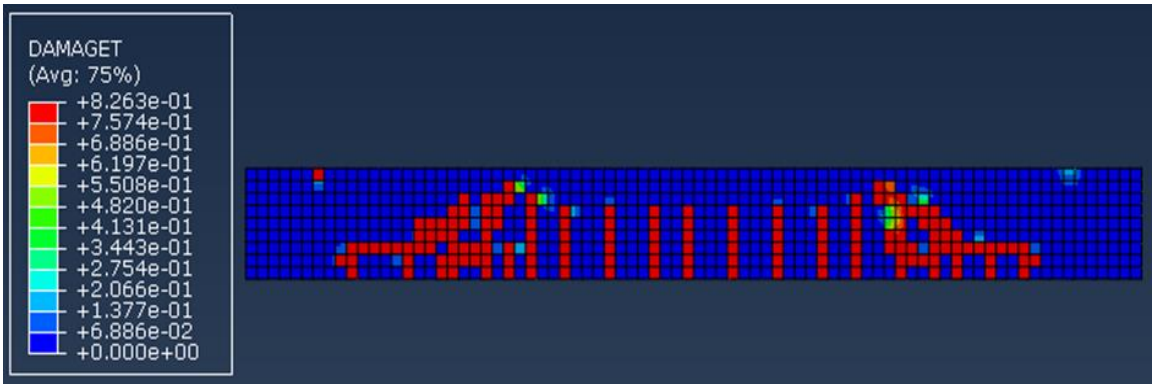

(a)

(b)

Figure 5.31: Cracking pattern of beam E-1 observed from a) FEM; and b) Experiment

5.3.11. Beam E-2

Ultimate shear load of beam E-2, predicted by FEM, is 130.61 kN at a mid-span deflection of 16.01 mm against their respective experimental value of 125 kN and 16.18 mm. Shear load-mid-span deflection response predicted by FEM along with experimentally obtained curve for beam E-2 is shown in Figure 5.32. Cracking propagation for beam E-2 was obtained using FEM is similar to that captured during the experimental study, as shown in Figure 5.33.

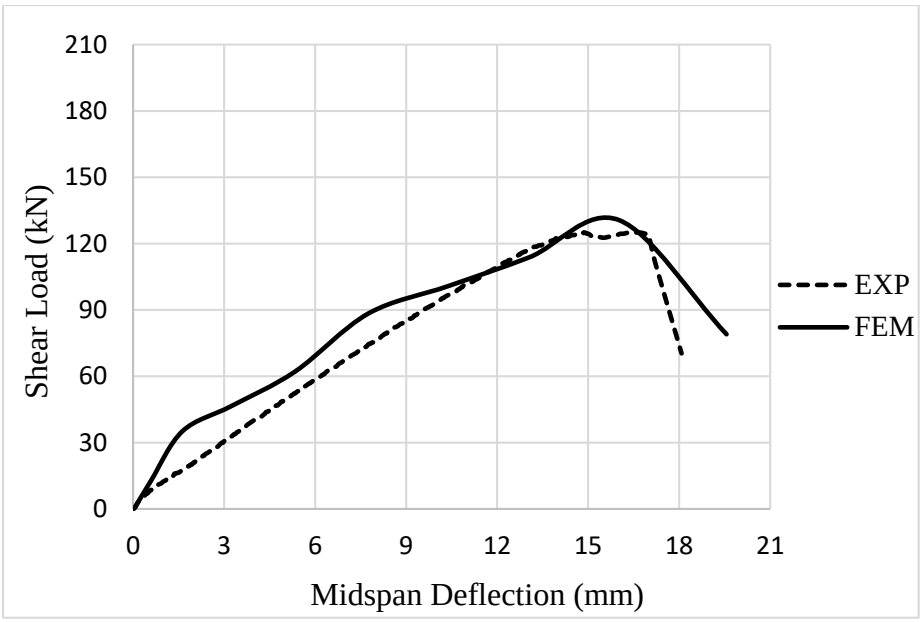

Figure 5.32: Shear load-mid-span deflection curves from EXP and FEM for beam E-2

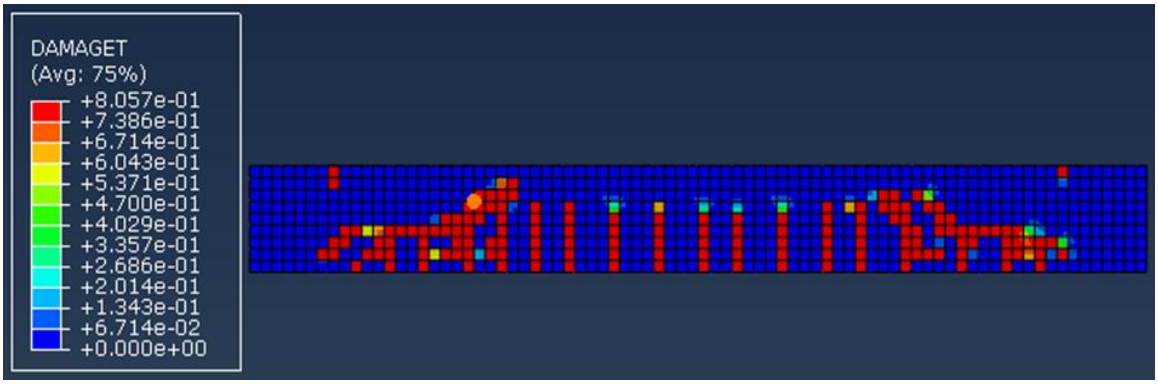

(a)

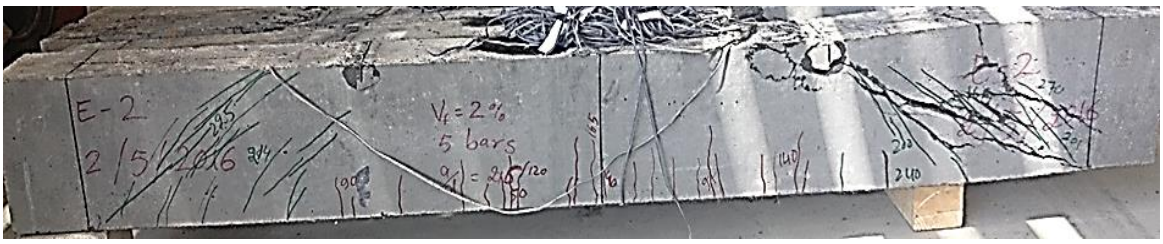

(b)

Figure 5.33: Cracking pattern of beam E-2 observed from a) FEM; and b) Experiment

Table 5.3 shows the summary of FEM and experimental results and their comparison.

Table 5.3: Summary of FEM and experimental results

Beam	Experimental		FEM		Experimental/FEM		Modes of Failure
	V_u (kN)	Δ_u (mm)	V_u (kN)	Δ_u (mm)	V_u (Exp./FEM)	Δ_u (Exp./FEM)	
A-1	172.50	21.14	178.00	20.02	0.97	1.06	Pure shear
A-2	185.50	23.30	185.00	21.78	1.00	1.06	
B-1	147.50	16.10	155.50	16.17	0.95	0.99	
B-2	176.00	18.06	177.10	20.11	0.99	0.89	
C-1	155.50	17.58	152.00	18.17	1.02	0.96	
C-2	182.50	19.86	185.14	20.43	0.98	0.99	
D-1	104.00	14.19	101.00	18.00	1.02	0.78	
D-2	114.50	13.18	116.82	14.17	0.98	0.92	
E-1	116.00	15.03	110.81	15.19	1.05	0.86	
E-2	125.00	16.18	130.61	16.01	0.96	1.05	
Average					**0.993**	**0.956**	

5.4. Parametric Study

Using the developed FEM, the parametric study was performed to further understand the shear behavior of UHPC beams and evaluate the contribution of the extended levels of the volume fraction of steel fibers, V_f, a/d ratio, percentage of longitudinal reinforcement, ρ, and stirrups spacing, s, beyond the experimental limitation. For the parametric study, 18 combinations of the four key parameters were considered, as listed in Table 5.4.

Table 5.4: Cases for parametric study

No	*a/d*	ρ (%)	V_f (%)	*s* (mm)
Variation of V_f				
1	1.8	1.935	**1**	370
2	1.8	1.935	**1.5**	370
3	1.8	1.935	**2**	370
Variation of *a/d*				
4	**1.4**	1.935	1	370
5	**1.8**	1.935	1	370
6	**2.2**	1.935	1	370
7	**2.6**	1.935	1	370
8	**3.0**	1.935	1	370
9	**3.4**	1.935	1	370
Variation of ρ				
10	1.8	**1.29**	1	370
11	1.8	**1.935**	1	370
12	1.8	**2.58**	1	370
13	1.8	**3.226**	1	370
Variation of *s*				
14	1.8	1.935	1	**100**
15	1.8	1.935	1	**200**
16	1.8	1.935	1	**300**
17	1.8	1.935	1	**400**
18	1.8	1.935	1	**500**

5.4.1. Effect of Volume Fraction of Steel Fibers

Three levels of the V_f, were consider to examine its effect on the shear behavior of the UHPC beams using the developed model. Plots of the results obtained through the FEM for three different V_f, are shown in Figures 5.34 and 5.35. It can be observed from Figures

5.34 and 5.35 that the ultimate shear capacity and mid-span deflection of beam increase with increase in the V_f. Similar effects of V_f, on shear capacity and mid-span deflection of UHPC beams were indicated by the experimental results.

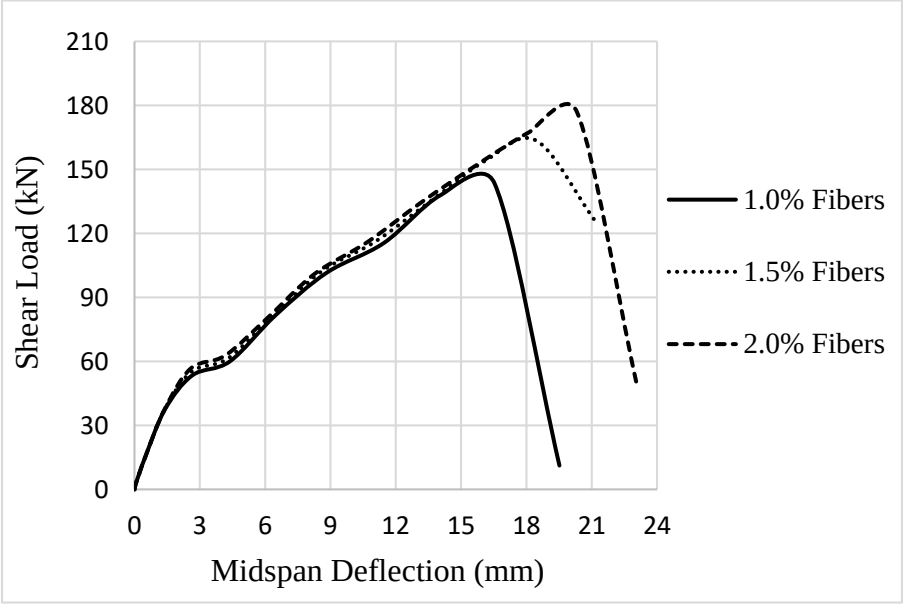

Figure 5.34: Shear load-mid-span deflection curves for different values of V_f

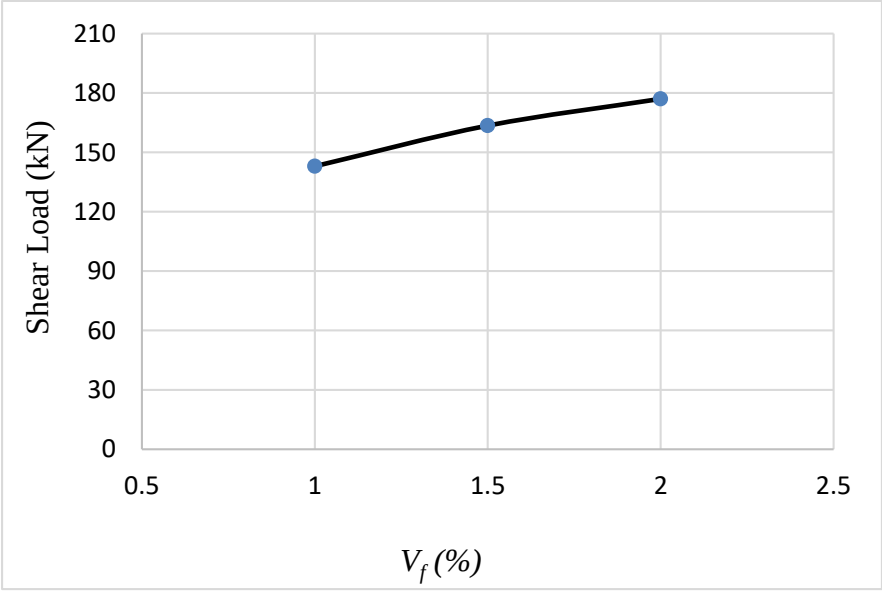

Figure 5.35: Variation of ultimate shear capacity with V_f

5.4.2. Effect of Shear Span to Effective Depth Ratio

To examine the effect of *a/d* ratio on the shear behavior of the beams using the FEM, seven different levels of *a/d* ratio were considered and the shear load versus mid-span deflection results were obtained and plotted, as shown in Figures 5.36 and 5.37. It can be observed from Figures 5.36 and 5.37 that the ultimate shear capacity as well as mid-span deflection of the beams decreases very significantly with increase in the *a/d* ratio. Similar effect of the *a/d* ratio was noticed from the experimental results. It can be further noted from the crack pattern generated by the FEM that the modes of failure changed from shear to almost flexure-shear at high value of *a/d* ratio, as shown in Figure 5.38.

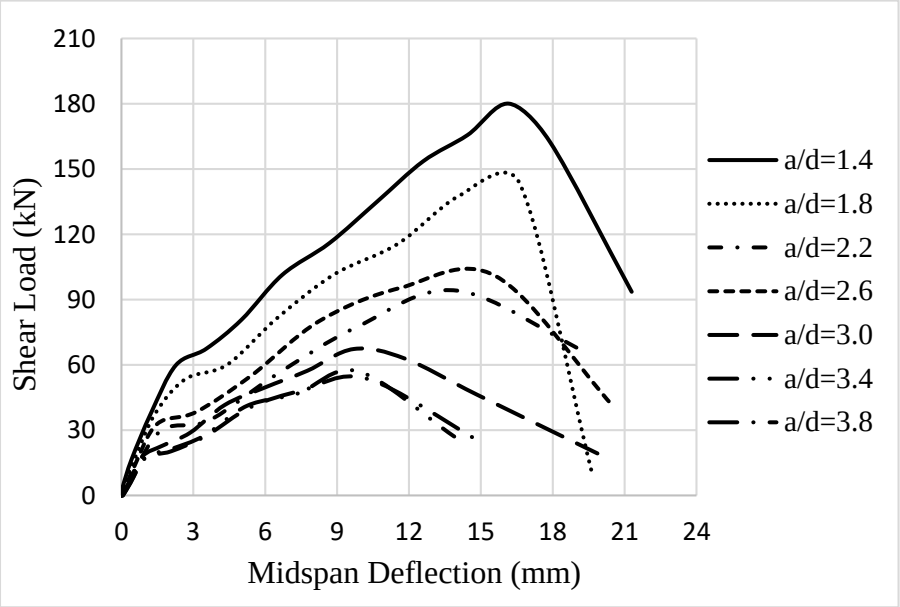

Figure 5.36: Shear load-mid-span deflection curves for different value of *a/d* ratio

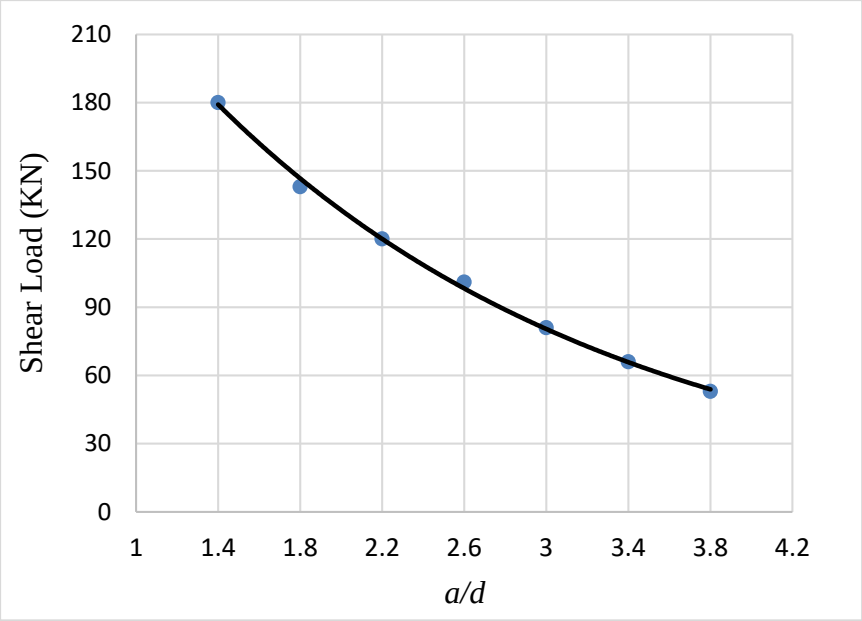

Figure 5.37: Variation of ultimate shear capacity with *a/d* ratio

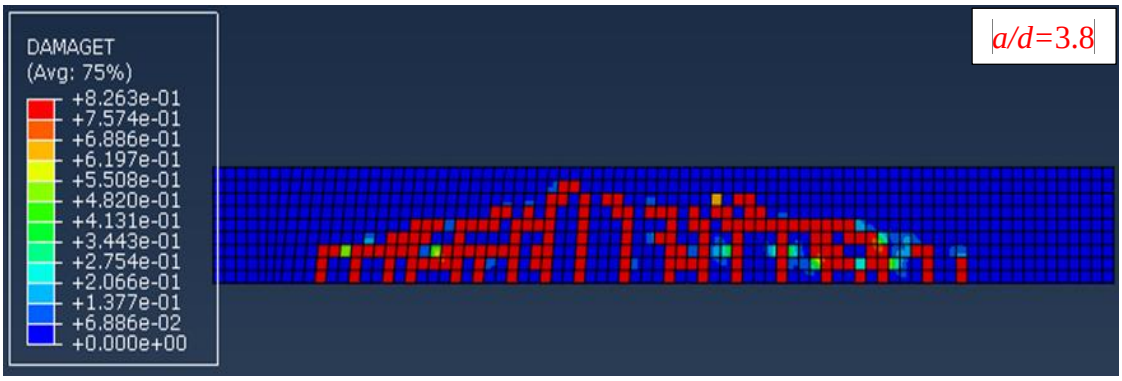

(a)

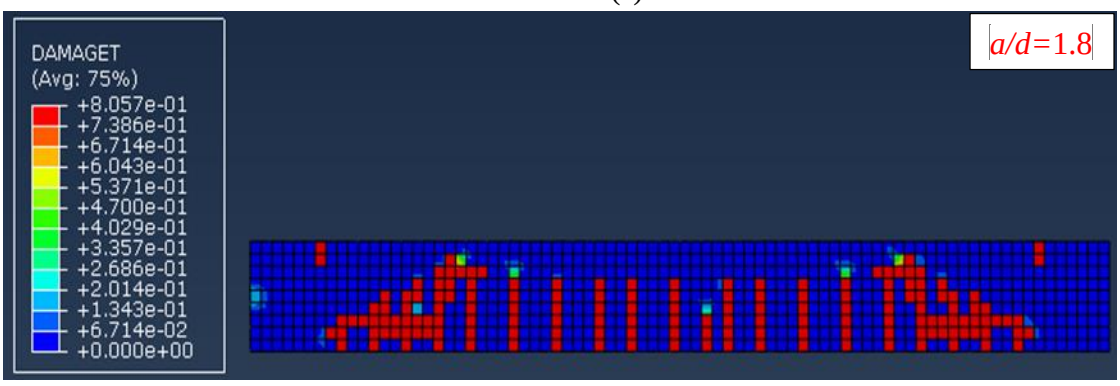

(b)

Figure 5.38: Comparison of modes of failure for beams having; a) *a/d*=3.8; and b) *a/d*=1.8

5.4.3. Effect of Percentage of Longitudinal Reinforcement

To evaluate the effect of, ρ using the FEM, four different levels of ρ were considered. Results pertaining to shear load versus mid-span deflection relationship, obtained through FEM were plotted, as shown in Figures 5.39 and 5.40. It can be seen from Figures 5.39 and 5.40 that the effect of ρ on ultimate shear capacity of beams is insignificant. It can be observed from the crack pattern generated by the FEM that the flexural cracks were deeper in the beams having lower, ρ than beams having higher, ρ, as shown in Figure 5.41.

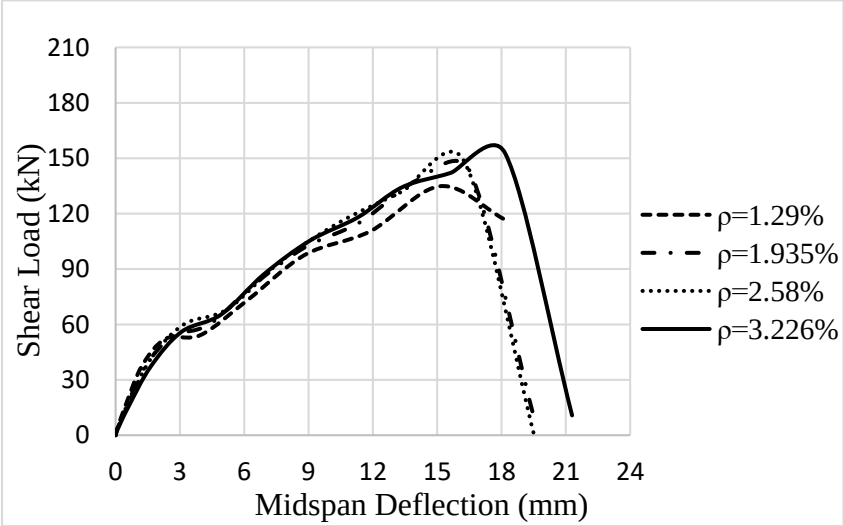

Figure 5.39: Shear load-mid-span deflection curves for different value of ρ

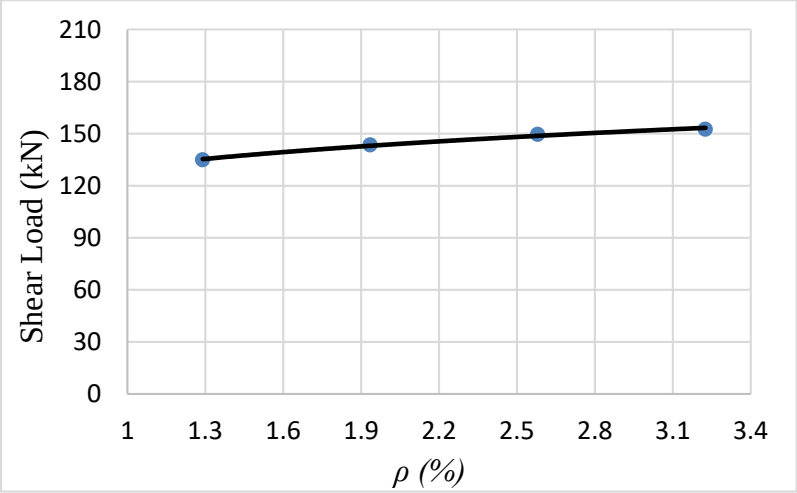

Figure 5.40: Variation of ultimate shear capacity with ρ

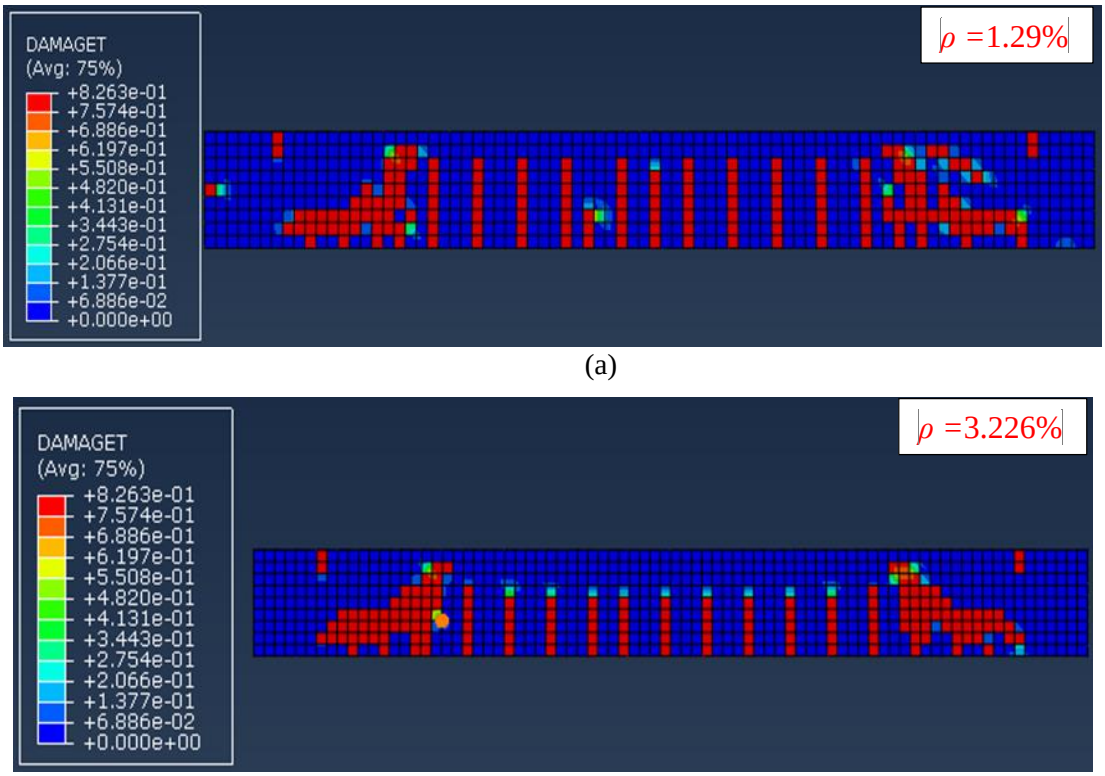

Figure 5.41: Comparison of modes of failure for beams with: a) ρ=1.29%; and b) ρ=3.226%

5.4.4. Effect of Stirrups Spacing

Beam specimens with five different stirrups spacing have been simulated and analyzed using FEM to investigate the effect of, *s*, on shear behavior of the beams. The FEM results show that ultimate shear capacity and mid-span deflection increased with the decrease in the *s*, as shown in Figures 5.42 and 5.43.

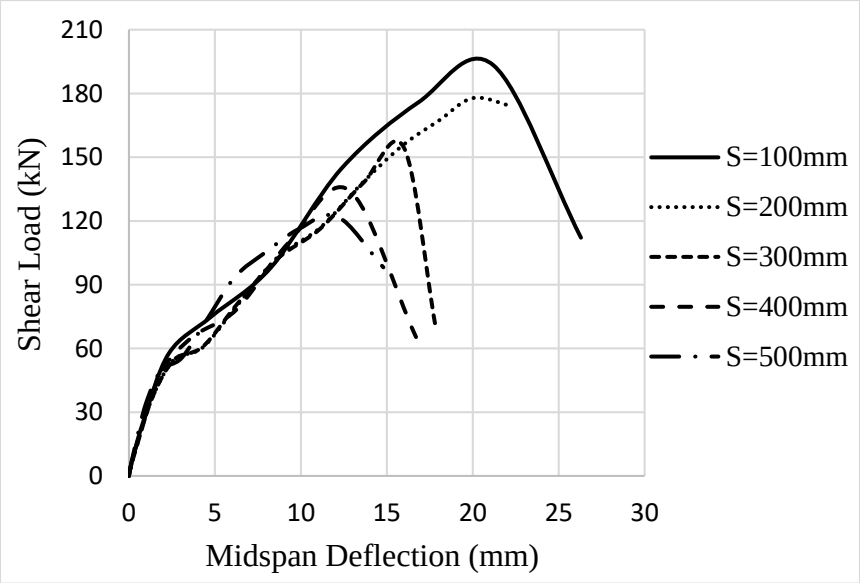

Figure 5.42: Shear load-mid-span deflection curves for different value of *s*

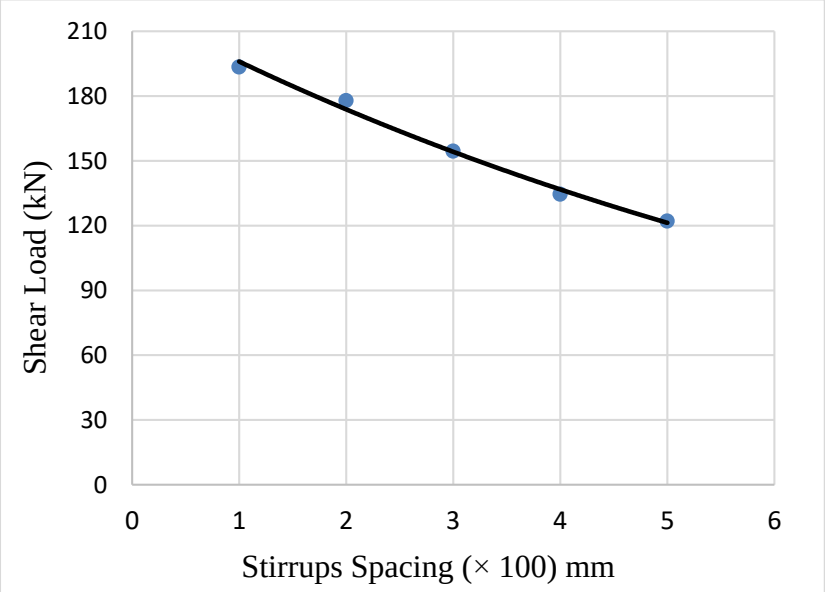

Figure 5.43: Variation of ultimate shear capacity with *s*

CHAPTER 6

DEVELOPMENT OF SHEAR CAPACITY EQUATION FOR UHPC BEAMS USING EXPERIMENTAL DATA

6.1. General

Several empirical and analytical equations are available in the literature to estimate the shear capacity of concrete beams. However, most of the shear capacity equations in literature are to predict shear capacity of normal, high-strength or fiber reinforced concrete beams. Limited study has been conducted to derive equation for prediction of the shear capacity of UHPC beams.

In this chapter, firstly, statistical analysis of the experimental data generated under the present work was conducted using analysis of variance (ANOVA). The results of ANOVA enabled to identify the levels of significance of each of the four key factors (*a/d* ratio, V_f, *s*, and ρ) affecting the shear behavior of the UHPC beams. An attempt was made to best-fit an equation in terms of the key factors that can be used to predict shear capacity of UHPC beams.

6.2. Analysis of Variance (ANOVA) of Experimental Data

In the previous chapters, the effects of *a/d* ratio, ρ, *s*, and V_f on the ultimate shear capacity of beams (V_u) were discussed in semi-qualitative terms. However, there is need to employ inferential statistics tools to quantify the real level of significance of these factors. For this

purpose, ANOVA was conducted. The test response was the shear capacity of the beam, V_u.

The experimental values of V_u, as given in Table 4.1, were used to conduct ANOVA. The results of ANOVA are presented in Table 6.1. It can be clearly observed from Table 6.1 that the strongest determinant of V_u is the *a/d* at 100% confidence level. In addition, V_f and, *s*, had the next significant effect on the shear capacity of the beam at 99.6% and 98.2% confidence levels respectively. However, there is no statistical justification to accept that, ρ, has a significant effect on the beam shear capacity, even though a previous semi-qualitative judgment would suggest some levels of importance. This is because the corresponding *P*-value is larger than 0.05, the level usually employed as the limit of rejecting a null hypothesis. The null hypothesis in the case is that ρ has insignificant effect on the shear capacity of the beam.

Table 6.1: Results of ANOVA for the experimental values of V_u

Variation Source	**DF**	**Adj SS**	**Adj MS**	***F*-Value**	***P*-Value (α = 0.05)**	**Significance criteria P < 0.05**
a/d	1	5151.1	5151.13	164.97	0	Highly significant
V_f	1	810	810	25.94	0.004	Highly significant
s	1	375.4	375.45	12.02	0.018	Significant
ρ	1	153.1	153.12	4.9	0.078	Insignificant
Error	5	156.1	31.22			
Total	9	8719.6				

6.3. Best-Fitting Proposed Shear Capacity Equation

Using the experimental data generated under the present work, an attempt is made to best-fit an equation to predict shear capacity of UHPC beams in terms of *a/d* ratio, V_f, s, and, ρ. For this purpose, firstly, the equation for shear capacity of concrete (V_c) given by ACI318-14 [45] for normal concrete was modified to include the effect of steel fibers in shear capacity of UHPC. Then the modified equation for V_c was best-fitted using least squares method.

The ultimate shear capacity of a reinforced concrete beam with shear stirrups is given as:

$$V_u = V_s + V_c \tag{6.1}$$

Where, V_s is the shear capacity of the stirrups and V_c is the shear capacity of concrete.

The equation for V_s is given as:

$$V_s = \frac{A_s \cdot f_y \cdot d}{s} \tag{6.2}$$

Where;

A_s = cross-section area of stirrups

f_y = yield strength of stirrups

d = effective depth of the beam

s = stirrups spacing

Shear capacity of the normal concrete without steel fibers, as given by ACI318-14 [45], is as follows:

$$V_c = \left[0.16\lambda\sqrt{f_c'} + 17\rho_w \frac{V_u d}{M_u} \right] b_w \cdot d \tag{6.3}$$

Where:

f_c' = compressive strength of concrete (MPa)

λ = modification factor

b_w = width of the beam

ρ_w = ratio of longitudinal reinforcement

M_u = ultimate moment capacity (M_u/V_u is shear span)

Eq. 6.3 for V_c of a normal concrete was modified as follows to suit the V_c for UHPC having steel fibers:

$$V_c = \left[A \cdot \sqrt{f_c'} + B \cdot \rho \frac{d}{a} + C \cdot F_1^D \left(\frac{d}{a} \right)^E \right] \cdot b \cdot h \tag{6.4}$$

$$F_1 = \frac{l_f}{d_f} \cdot V_f \cdot \alpha$$

l_f = length of steel fibers

d_f = diameter of steel fibers

V_f = volume fraction of steel fibers in percentage

α = bond factor (for straight steel fibers = 0.5)

a = shear span

ρ = ratio of longitudinal reinforcement

b = width of the beam

h = overall depth of the beam

A, *B*, *C*, *D*, and *E* are the empirical constants. These empirical constants were determined by best-fitting the experimental data, presented in Table 6.2, in the proposed Eq. 6.4 using the least squares method with the help of *Excel Solver*.

Table 6.2: Input data for best-fitting of the proposed equation for V_u

Beam	f'_c **(MPa)**	***a/d***	V_f **(%)**	ρ **(%)**	***s*** **(mm)**	V_u **(kN)**	$V_c = V_u - V_s$ **(kN)**
A-1	145	1.8	1.0	1.935	200	172.5	96.6
A-2	150	1.8	2.0	1.935	200	185.5	110.1
B-1	145	1.8	1.0	1.935	370	147.5	106.5
B-2	150	1.8	2.0	1.935	370	176.0	135.0
C-1	145	1.8	1.0	3.226	370	155.5	114.5
C-2	150	1.8	2.0	3.226	370	182.5	142.0
D-1	145	2.6	1.0	1.935	370	104.0	63.0
D-2	145	2.6	1.0	3.226	370	114.5	73.5
E-1	150	2.6	2.0	1.935	370	116.0	75.0
E-2	150	2.6	2.0	3.226	370	125.0	84.0

The proposed equation for V_c after substituting the best-fitted values of empirical constants *A*, *B*, *C*, *D*, and *E* in Eq. 6.4 is as follows:

$$V_c = \left[0.35\sqrt{f'_c} + 132\rho\frac{d}{a} + 14F_1^{5.8}\left(\frac{d}{a}\right)^{1.1} \right] \cdot b \cdot h \qquad (R^2 = 0.94) \qquad (6.5)$$

The proposed equation for ultimate shear capacity of UHPC beam with stirrups, V_u, is given as:

$$V_u = \left[0.35\sqrt{f_c'} + 132\rho\frac{d}{a} + 14F_1^{5.8}\left(\frac{d}{a}\right)^{1.1} \right] \cdot b \cdot h + \frac{A_s \cdot f_y \cdot d}{s} \tag{6.6}$$

The experimental values of V_u and the values of V_u predicted using proposed Eq. 6.6 are presented in Table 6.3. The deviation of experimental and predicted values of V_u in a very narrow range, as shown in Table 6.3, and a very high value of R^2 = 0.94 indicate a high degree of fit of Eq. 6.6.

Table 6.3: Comparison of experimental and predicted values of V_u

Beam	**V_u (kN)**		**Deviation (%)**
	Experimental	**Predicted using best-fitted Eq. 8**	
A-1	172.5	176	-2.0
A-2	185.5	197	-6.2
B-1	147.5	141	4.4
B-2	176.0	162	8.0
C-1	155.5	158	-1.6
C-2	182.5	179	1.9
D-1	104.0	103	1.0
D-2	114.5	110	3.9
E-1	116.0	117	-0.9
E-2	125.0	125	0.0

The experimental values of V_u reported in literature [9, 24, 30, 31] is compared with the values of V_u predicted by the proposed Eq. 6.6, as shown in Table 6.4.

Table 6.4: Comparison of V_u reported in literature with the values of V_u predicted by Eq. 6.6

Researcher	f'_c (MPa)	a/d	V_f (%)	ρ (%)	V_u (kN)		Deviation (%)
					Researcher experimental value	Value predicted by proposed model	
Son et al. [24] (without shear stirrups)	100	2	2.00	0.0316	493	393	-25.00
	200	2	2.00	0.0316	568	495	-14.00
Gustafsson and Noghabai [9] (without shear stirrups)	114	3.3	1.00	0.0446	290	276.2	-5.00
	124	3.3	1.00	0.0446	300	284.2	-5.56
	109	3.3	0.50	0.0446	230	273.4	15.88
	109	3.3	0.75	0.0446	265	286.5	7.52
	97	2.9	1.00	0.0306	370	484.2	23.58
	102	2.9	1.00	0.0306	325	493.0	34.07
	94	2.9	0.50	0.0306	260	482.0	46.05
	80	2.9	0.75	0.0306	340	485.9	30.03
Kwak, et al. [30] (without shear stirrups)	64	2	0.50	0.0152	157	119.3	-31.46
	69	2	0.75	0.0152	170	129.1	-31.66
	64	3	0.50	0.0152	96.5	108.7	11.13
	69	3	0.75	0.0152	106.5	116.1	8.47
	64	4	0.50	0.0152	75.5	103.3	27.11
	69	4	0.75	0.0152	85.5	109.6	21.89
	31	2	0.50	0.0152	126.5	92.7	-36.23
	31	3	0.50	0.0152	80.0	82.0	2.82
	31	4	0.50	0.0152	62.5	76.7	18.47
Lim and Hong [31] (with shear stirrups)	167	3	1.50	0.08	347	356.8	2.74
	167	3	1.50	0.08	449	440.5	-1.93
	167	3	1.50	0.08	501	482.4	-3.86
	167	3	1.50	0.08	603	566.1	-6.52

The experimental values of V_u reported in literature [9, 24, 30, 31] is compared with the values of V_u predicted by the proposed Eq. 6.6, as shown in Table 6.4. It can be observed from Table 6.4 that in some cases a wider variation of experimental and predicted values is noticed in the case of the studies conducted by first three researchers [9, 24, 30] without shear stirrups. However, in case of fourth researcher [31], who conducted research with stirrups and concrete compressive strength very close to the present study, the maximum variation between experimental and predicted values is only around 7.0%. This indicates that the proposed Eq. 6.6 can be used for shear design with a fair degree of accuracy for UHPC with compressive strength of around 150 MPa and in presence of shear stirrups.

CHAPTER 7

CONCLUSIONS AND RECOMMENDATIONS

7.1. Conclusions

Following conclusions can be drawn based on the experimental results, finite element modeling, statistical analysis and the proposed best-fitted equation for shear capacity of the UHPC beams:

1. All beams failed in pure shear confirming the adequacy of the design of beam specimens. Longitudinal steel bars did not yield at the time of failure because of less strain than their yielding strain, however, stirrups yielded because more strains recorded for stirrups than their yielding strain. Concrete crushing was not obtained at the top of UHPC beams because of less strain recorded in concrete at the time of failure than crushing strains.
2. The beams with more stirrups (i.e., lower spacing of stirrups) failed with the formation of single but wider diagonal cracks. On the other hand, beams with less stirrups failed with the formation of multiple but thin diagonal cracks. However, in case of more stirrups the shear load capacity and mid-span deflection of UHPC beams was higher.
3. Shear load capacity and mid-span deflection increased with the increase in volume fraction of steel fibers. The cracking of concrete in flexural zone decreased with the increase in the fiber content.
4. At a higher shear span to effective depth (a/d) ratio, the shear load capacity and mid-span deflection were found to be lower. The decrease in shear load capacity and mid-

span deflection with increase in *a/d* ratio was more at a lower percentage of longitudinal reinforcement.

5. Shear load capacity slightly increased with the increase in percentage of longitudinal reinforcement.
6. Finite element Modeling incorporating the concrete damage plasticity model for concrete was found to be capable of capturing shear behavior of UHPC beams in the same way as that through experimental investigation. However, shear load versus mid-span deflection curves obtained through FEM are found to be somewhat stiffer than that plotted using experimental data because of micro cracks in concrete due to shrinkage, handling, etc. in experimentally tested beams, which were not considered in FEM.
7. Since the results obtained through FEM developed in the present work are in good agreement with experimental results, therefore, it can be used as a reliable and effective tool to study the shear behavior of UHPC beams.
8. ANOVA results showed that *a/d* ratio, V_f, and stirrups spacing have significant effect on shear load capacity, however, percentage of longitudinal reinforcement has insignificant effect on shear load capacity of UHPC beams.
9. The proposed Eq. 6.6 for shear load capacity can be used for designing the UHPC for shear with a fair degree of accuracy for UHPC with compressive strength of around 150 MPa and in presence of shear stirrups.

7.2. Recommendations

1. The effect of types, shapes and sizes of steel fibers on shear behavior of UHPC beams should be investigated.

2. Size of the UHPC beams is also one of the critical factor for shear behavior of UHPC, therefor it also need to be studied.

References

1. Rossi, P., D. Daviau-Desnoyers, and J.-L. Tailhan, Probabilistic Numerical Model of Cracking in Ultra-High Performance Fibre Reinforced Concrete (UHPFRC) Beams Subjected to Shear Loading, 2016.
2. Russell, H.G. and B.A. Graybeal, Ultra-high performance concrete: A state-of-the-art report for the bridge community. 2013.
3. Ferrier, E., et al., Mechanical behaviour of ultra-high-performance short-fibre-reinforced concrete beams with internal fibre reinforced polymer bars. Composites Part B: Engineering, 2015. 68: p. 246-258.
4. Meng, W. and K.H. Khayat, Experimental and Numerical Studies on Flexural Behavior of Ultra-High-Performance Concrete Panels Reinforced with Embedded Glass Fiber-Reinforced Polymer Grids. Transportation Research Record: Journal of the Transportation Research Board, 2016 (2592): p. 38-44.
5. Farnam, Y., S. Mohammadi, and M. Shekarchi, Experimental and numerical investigations of low velocity impact behavior of high-performance fiber-reinforced cement based composite. International Journal of Impact Engineering, 2010. 37 (2): p. 220-229.
6. Issa, M.A. and H.A. Abdalla, Structural behavior of single key joints in precast concrete segmental bridges. Journal of Bridge Engineering, 2007. 12(3): p. 315-324.
7. Arnold, S., et al., A test method and deterioration model for joints and cracks in concrete slabs. Cement and concrete research, 2005. 35(12): p. 2371-2383.

8. Son, J., B. Beak, and C. Choi, Experimental Study on Shear Strength for Ultra-High Performance Concrete Beam, in 18th International Conference on Composites Materials (ICCM. 2011: Jeju Island, Korea.
9. Gustafsson, J. and K. Noghabai, Steel fibers as shear reinforcement in high strength concrete beams. Nordic Concrete Research-Publications-, 1999. 22: p. 35-52.
10. Mansur, M., K. Ong, and P. Paramasivam, Shear strength of fibrous concrete beams without stirrups. Journal of Structural Engineering, 1986. 112(9): p. 2066-2079.
11. Demir, A., H. Öztürk, and G. Dok, 3D Numerical Modeling of RC Deep Beam Behavior by Nonlinear Finite Element Analysis. Disaster Science and Engineering, 2016. 2(1): p. 13-18.
12. Schramm, N. and O. Fischer, Investigations on the Shear Behavior of Bridge Girders made of Normal and Ultra-high Performance Fiber-Reinforced Concrete. Procedia Engineering, 2016. 156: p. 411-418.
13. Graybeal, B., Finite Element Analysis of UHPC: Structural Performance of an AASHTO Type II Girder and a 2nd-Generation Pi-Girder. 2010.
14. Chen, L. and B.A. Graybeal, Modeling structural performance of ultrahigh performance concrete I-girders. Journal of Bridge Engineering, 2011. 17(5): p. 754-764.
15. Al-Azzawi, A.A., A.S. Ali, and H.K. Risan, Behavior of ultra high performance concrete structures. ARPN Journal of Engineering and Applied Sciences, 2011. 6(5): p. 95-109.

16. Mahmud, G.H., Z. Yang, and A.M. Hassan, Experimental and numerical studies of size effects of Ultra High Performance Steel Fibre Reinforced Concrete (UHPFRC) beams. Construction and Building Materials, 2013. 48: p. 1027-1034.
17. TELLEEN, K., et al. Experimental investigation into the shear resistance of a reinforced UHPFRC web element. in 8th fib PhD Symposium in Kgs. Lyngby, Denmark. 2010.
18. Kirllos Wahba, B.E., Toronto, Mechanical and Structural Properties of Ultra High Performance Fiber Reinforced Concrete, in Civil Engineering. 2012, Ryerson: Ontario, Canada.
19. Karmout, M., Mechanical Properties of Ultra High Performance Concrete Produced in Gaza Strip, in Civil Engineering. 2009, T he Islamic University of Gaza: Gaza.
20. Fehling, E., et al., Ultra-high Performance Concrete UHPC: Fundamentals, Design, Examples. 2014: John Wiley & Sons.
21. Schmidt, M. and E. Fehling, Ultra-high-performance concrete: research, development and application in Europe. ACI Special publication, 2005. 228: p. 51-78.
22. Neville, A., Properties of Concrete Fifth and Final Edition. 2011.
23. Graybeal, B.A., Material property characterization of ultra-high performance concrete. 2006.
24. Son, J., B. Beak, and C. Choi, Experimental Study on Shear Strength for Ultra-High Performance Concrete Beam, 2011.

25. Baby, F., et al., Shear resistance of ultra high performance fibre-reinforced concrete I-beams. 2010, Jeju, Korea. p. 1411-1417.

26. Hegger, J. and G. Bertram, Shear carrying capacity of ultra-high performance concrete beams. Tailor Made Concrete Structures. Walraven & Stoelhorst. London, 2008: p. 341-7.

27. Voo, Y.L., W.K. Poon, and S.J. Foster, Shear strength of steel fiber-reinforced ultrahigh-performance concrete beams without stirrups. Journal of structural engineering, 2010. 136(11): p. 1393-1400.

28. Awadallah, Z.H., et al., Some Parameters Affecting Shear Behavior of High Strength Fiber Reinforced Concrete Beams Longitudinally Reinforced with BFRP Rebars. 2014.

29. Ciprian, Ţ., et al., Ultra High Performance Fiber Reinforced Concrete "I" Beams Subjected to Shear Action, 2011.

30. Kwak, Y.-K., et al., Shear strength of steel fiber-reinforced concrete beams without stirrups. ACI Structural Journal, 2002. 99(4): p. 530-538.

31. Lim, W.-Y. and S.-G. Hong, Shear Tests for Ultra-High Performance Fiber Reinforced Concrete (UHPFRC) Beams with Shear Reinforcement. International Journal of Concrete Structures and Materials, 2016: p. 1-12.

32. Mahmood, M.S., Finite Element Analysis of Shear Deficient Large Size Reinforced Concrete Beams, 2009.

33. Graybeal, B., Ultra-high performance concrete: A state-of-the-art report for the bridge community. FHWA, US Department of Transportation, Report No. FHWA-HRT-13-060, 2013.

34. Chen, L. and B.A. Graybeal, Modeling structural performance of second-generation ultrahigh-performance concrete pi-girders. Journal of Bridge Engineering, 2011. 17(4): p. 634-643.

35. Ambily, P., et al., Experimental and analytical investigations on shear behaviour of reinforced geopolymer concrete beams. International Journal of Civil & Structural Engineering, 2011. 2(2): p. 682-697.

36. Abed, F.H., A. Al-Rahmani, and A.H. Al-Rahmani. Finite element simulations of the shear capacity of GFRP-reinforced concrete short beams. in Modeling, Simulation and Applied Optimization (ICMSAO), 2013 5th International Conference on. 2013. IEEE.

37. Narayanan, R., and Darwish, I.Y.S,. Use of steel fibers as shear reinforcement ACI Structural Journal 1987. 84(3): p. 216-227.

38. Wasan, I. and Y. Khalil Tayfur, Flexural Strength of Fibrous Ultra High Performance reinforced concrete beams. ARPN Journal of Engineering and Applied Sciences, 2013. 8(3): p. 200-14.

39. ASTM, C., 39, Standard test method for compressive strength of cylindrical concrete specimens. ASTM International, 2001.

40. ASTM, C., 469-94. Standard Test Method for Static Modulus of Elasticity and Poisson's Ratio of Concrete in Compression, American Society for Testing and Materials, West Conshohocken, PA, 1994.

41. ASTM, C., 1018:'Standard Test Method for Flexural Toughness and First-Crack Strength of Fiber-Reinforced Concrete (Using Beam With Third-Point Loading). American Society of Testing Materials, USA, 1997.

42. Ferrier, E., P. Labossière, and K. Neale, Modeling the bending behaviour of a new hybrid glulam beam reinforced with FRP and ultra-high-performance concrete. Applied Mathematical Modeling, 2012. 36(8): p. 3883-3902.

43. Structure, f.M.C.f.C., International Federation for Structural Concrete (fib). 2010. 1.

44. Birtel, V. and P. Mark. Parameterised finite element Modeling of RC beam shear failure. in ABAQUS Users' Conference. 2006.

45. Institute, A.C., Building code requirements for structural concrete (ACI 318-05) and commentary (ACI 318R-05). 2004: American Concrete Inst.

Vitae

Name:	**Sifatullah Bahij**
Nationality:	Afghan
Date of Birth:	15th of April, 1989
Email:	sifatullah.bahij@gmail.com
Address:	Qale-Nazir, 5th District, Kabul, Afghanistan

Academic Background:

M.Sc. in Civil Engineering-Materials and Structures

(Aug 2014 – Dec 2016)

Civil & Environmental Engineering Department, King Fahd University of Petroleum & Minerals, Dhahran, Saudi Arabia.

Thesis: Study on shear behavior of ultra-high performance concrete (UHPC) beams.

B.Sc. in Civil Engineering (Aug 2007 – Feb 2012)

Civil and Industrial Construction Department, Construction Faculty, Kabul Polytechnic University, Afghanistan.

Final Year Project: Architectural and structural design of 9-storey residential building in Kabul, Afghanistan.